ACTA UNIVERSITATIS SZEGEDIENSIS

ACTA MINERALOGICA-PETROGRAPHICA

Tomus XXXIV

SZEGED, HUNGARIA

1993

NOTE TO CONTRIBUTORS

General

The Acta Mineralogica—Petrographica publishes original studies on the field of geochemistry mineralogy and petrology, first of all studies of Hungarian researchers, papers resulted in by cooperation of Hungarian researchers and those of other countries and, in a limited volume, papers from abroad on topics of global interest.

Manuscripts should be written in English and submitted to the Editor-in-chief, Institute of Mineralogy, Geochemistry and Petrography, Attila József University, H-6701 Szeged, Pf. 651 Hungary.

The authors are responsible for the accuracy of their data, references and quotations from other sources.

Manuscript

Manuscripts should be typewritten with double spacing, 25 lines on a page and space for 50 letter, in a line. Each new paragraph should begin with an indented line. Underline only words that should be typed in italics.

Manuscripts should generally be organized in the following order:

Title
Name(s) of author(s) and their affiliations, in foot-note the address of the author to whom the correspondence should be sent.
Abstract
Introduction
Methods, techniques, material studied, description of the area investigated, etc.
Results
Discussion or conclusions
Acknowledgement
Explanation of plates (if any)
Tables
Captions of figures (drawings, photomicrographs, etc.)

Abstract

The abstract cannot be longer than 500 words.

Tables

The tables should be typewritten on separate sheets and numbered according to their sequence in the text, which refers to all tables.

The title of the table as well as the column headings must be brief, but sufficiently explanatory.

The tables generally should not exceed the type-area of the journal, i.e. 12.5x18.5 cm. Foldouts can only exceptionally be accepted.

(continuation on the inner side of verso)

ACTA UNIVERSITATIS SZEGEDIENSIS

ACTA MINERALOGICA-PETROGRAPHICA

Tomus XXXIV

SZEGED, HUNGARIA

1993

HU ISSN 0365—8066
HU ISSN 0324—6523

SERIES NOSTRA AB INSTITUTIS MINERALOGICIS, GEOCHIMICIS PETROGRAPHICIS UNIVERSITATUM HUNGARICUM ADIUVATUR

Nota

Acta Miner. Petr., Szeged

Szerkeszti

SZEDERKÉNYI TIBOR

a szerkesztőbizottság tagjai

KUBOVICS IMRE
EGERER FRIGYES
SZŐŐR GYULA
KLEB BÉLA

Kiadja

a József Attila Tudományegyetem Ásványtani, Geokémiai és Kőzettani Tanszéke
H-6722 Szeged, Egyetem u. 2—6

Kiadványunk címének rövidítése
Acta Miner. Petr., Szeged

SOROZATUNK A MAGYARORSZÁGI EGYETEMEK ROKON TANSZÉKEINEK TÁMOGATÁSÁVAL JELENIK MEG

CONTENTS

Acta Mineralogica-Petrographica, Szeged, XXXIV, 5—6, 1993

STANDARDISATION OF POLYTYPE SUFFIXES

E. H. NICKEL*

Vice-Chairman, I. M. A. Commission on New Minerals and Mineral Names
Division of Mineral Products, CSIRO

The Commission on New Minerals and Mineral Names (CNMMN) of the International Mineralogical Association has published guidelines on a number of matters dealing with mineralogical nomenclature including polytype nomenclature (e.g. NICKEL and MANDARINO 1987). In essence, polytypes are distinguished by alphanumeric symbols appended to the root name and joined to it by a hyphen. The numeric part of the symbol represents the layering periodicity, and the alphabetic part, rendered in italic print, represents the crystallographic system. For example, wurtzite 4*H* is a hexagonal wurtzite polytype with a periodicity of 4 times the c-dimension of the wurtzite parent.

Prior to the publication of these guidelines, various other polytype symbols had been used in the mineralogical literature and, in an effort to standardise polytype nomenclature, members of the CNMMN decided that previous usage should be brought into conformity with current practice, which follows recommendations of the International Union of Crystallography (GUINIER *et al.*, 1984). Polytype names in the literature that require changing are as follows:

Original Name	**Present Name**	**Reference**
Anandite-2*Or*	Anandite-2*O*	FILUT *et al.* (1958)
Gageite-1 *TC*	Gageite-1*A*	FERRARIS *et al.* (1987)
Hilgardite-1 *TC*	Hilgardite-1*A*	GHOSE (1985)
Hilgardite-3 *TC*	Hilgardite-1*A*	GHOSE (1985)
Pyrophyllite-1 *TC*	Pyrophyllite-1*A*	WARDLE BRINDLEY (1972)
Sapphirine-1 *TC*	Sapphirine-1*A*	MERLINO (1973)
Tyretskite-1 *TC*	Tyretskite-1*A*	GHOSE (1985)
Wollastonite-1*T*	Wollastonite-1*A*	HENMI *et al.* (1978)
Wollastonite-3*T*	Wollastonite-3*A*	HENMI *et al.* (1983)
Wollastonite-4*T*	Wollastonite-4*A*	HENMI *et al.* (1983)
Wollastonite-5*T*	Wollastonite-5*A*	HENMI *et al.* (1983)
Wollastonite-7*T*	Wollastonite-7*A*	HENMI *et al.* (1978)

It is quite likely that the mineralogical literature contains additional examples of polytype symbols that do not confirm to the recommended usage. Such names should also be revised to bring them into conformity. The recommended alphabetic

* Wembley, WA 6014. Australia

symbols are as follows: cubic, **C**; hexagonal, **H**; rhombohedral, **R**; trigonal, **T**; tetragonal, **Q** (for quadratic); **O**; monoclinic, **M**; and triclinic, **A** (for anorthic).

REFERENCES

FERRARIS, G., MELLINI, M., MERLINO, S. (1987); Electron-diffraction and electron-microscopy study of balangeroite and gageite: Crystal structures, polytypism, and fibre texture. American Mineralogist **72**, 382—391.

FILUT, M. A., RULE, A. C., BAILEY, S. W. (1985): Crystal structure refinement of anandite — 2Or, a barium- and sulfur-bearing trioctahedral mica. American Mineralogist **70**, 1298—1308.

GHOSE, S. (1985): A new nomenclature for the borate minerals in the hilgardite ($Ca_2B_5O_9ClH_2O$) — tyretskite ($Ca_2B_5O_9OH.H_2O$) group. American Mineralogist **70**, 636—637.

GUINER, A. *et al.* (1984): Nomenclature of polytype structures. Report of the International Union of Crystallography Ad-Hoc Committee on the Nomenclature of Disordered, Modulated and Polytype Structures. Acta Crystallographica, **A40**, 399—404.

HENMI, C., KUSACHI, I., KAWAHERA, A., HENMI, K. (1978): 7*T* wollasonite from Fuka, Okayama Prefecture. Mineralogical Journal **9**, 169—181.

HENMI, C., KAWAHARA, A., HENMI, K., KUSACHI, I., TEKEUCHI, Y. (1983): The 3*T*, 4*T* and 5*T* polytypes of wollastonite from Kushiro, Hiroshima Prefecture, Japan. American Mineralogist **68** (1983), 156—163.

MERLINO, S. (1973): Polymorphism in sapphirine, Contributions to Mineralogy and Petrology **41**, 23—29.

NICKEL, E. H., MANDARINO, J. A. (1987): Procedures involving the IMA Commission on New Minerals and Mineral Names, and guidelines on mineral nomenclature. Mineralogy and Petrology **37**, 157—179. (Also published in other mineralogical, journals).

WARDLE, R., BRINDLEY, G. W. (1972): The crystal structures of pyrophyllite, 1Tc, and of its dehyroxylate. American Mineralogist **57**, 732—750.

Manuscript received, 11 May, 1993

Acta Mineralogica-Petrographica, Szeged, XXXIV, 7—19, 1993

MG-MINERALS OF RECENT HYDROTHERMAL FORMATIONS OF THE CU-PORPHYRIC MINERALISATION AT RECSK, HUNGARY

J. KISS, M. JÁNOSI*

Department of Mineralogy, Eötvös Loránd University

ABSTRACT

A great variety of minerals precipitated from thermal waters (35—44 °C) were observed in the drifts of the copper-porphyritic skarn ore deposit at Recsk. Beside calcite-aragonite and various salts with different solubility, the Mg-minerals (nesquehonite—dypingite—hydromagnesite—giorgiosite-northupite—astrakhanite— /vanthoffite; langbeinite/ —epsomite—palygorskite) have outstanding importance at this locality. The present work focussed on the study and interpretation of the hydrothermal formation of the Mg-minerals otherwise known as hypergenitic evaporites.

AUSZUG

In den Stollen des porphyrischen-skarn Cu-Erzlagers in Recsk ist eine ausserordentlich grosse Variation von hydrothermalen (35—44 °C) Mineralienabsonderungen vorhanden. Unter den Kalzit-Aragonit-, und anderen Mineralsalzen von veränderlicher Lösbarkeit spielen die Magnesiumminerale (Nesquehonit—Dypingit—Hydromagnesit—Giorgiosit—Northupit—Astrakhanit— /Vanthoffit; Langbeinit/— Epsomit—Palygorskit) eine beachtliche Rolle. In dieser Arbeit wird die hydrothermale Entstehung dieser, von anderen Lokalitäten meistens als hypergen-evaporitischen Phasen beschriebenen Mg-Mineralien untersucht und erklärt.

INTRODUCTION AND REVIEW OF CHEMICAL AND PHYSICAL CIRCUMSTANCES

As the Au-enargite and luzonite deposits of Recsk became barren, in the vicinity a new and intense exploration campaigne was initiated by KISVARSÁNYI, G., KISS, J. in 1953—55 years. As a result, several new ore deposits were discovered; polymetallic ore formations ($PbS—CuFeS_2—FeS_2$) in the Middle-Mátra Mts. (Parádsasvár), Au-Mo(Re) containing Cu-porphyritic mineralisations, $CuFeS_2—FeS_2$ skarn formations and a $ZnS—PbS—CuFeS_2$ polymetallic ore deposit in the deep drillings of the Recsk area going down to over 1200 m. The later mineralisation are associated with Paleogene—Eocene ($Sr^{87}—Sr^{85}$=0.705/0.708) contaminated (dioritic-andesitic) magmatic intrusions (endo-skarn), metasomatic contact of Permain-Triassic limestone and dolomite (grossularite-hybschite-andradite-diopside-pyroxmangite-epidote-actinolite-tremoli te -antigorite-wollastonite-quartz-calcite exoskarn) as well as their calcareous foliated rocks respectively. A substantial portion of these deposits has not been limited yet towards the depth yielding an estimated exploitable mineral stock of well over 100 million tons (mean values = 1.30 to 1.70 % Cu).

* H—1088 Budapest, Múzeum krt. 4/a, Hungary

Thermal springs, also utilized as curative waters, of the near and far vicinity of Recsk (Bükkszék 37 °C, Demjén 69 °C) and a great number of methan-radon containing alkaline hydrocarbonic thermal water occurrences at Mátraderecske, Mátraballa, Parádfürdő and Parádsasvár indicated, that intensive hydrothermal activity should be expected during the mining process of the aforementioned mineral deposits. (Several thermal water wells, some of them extremely (80—90 °C) hot, are known in the Pannonian Basin and also a 180 °C hot saline-carbon-dioxid steam outburst was found near Fábiánsebestyén, *(Fig. 1a)*.

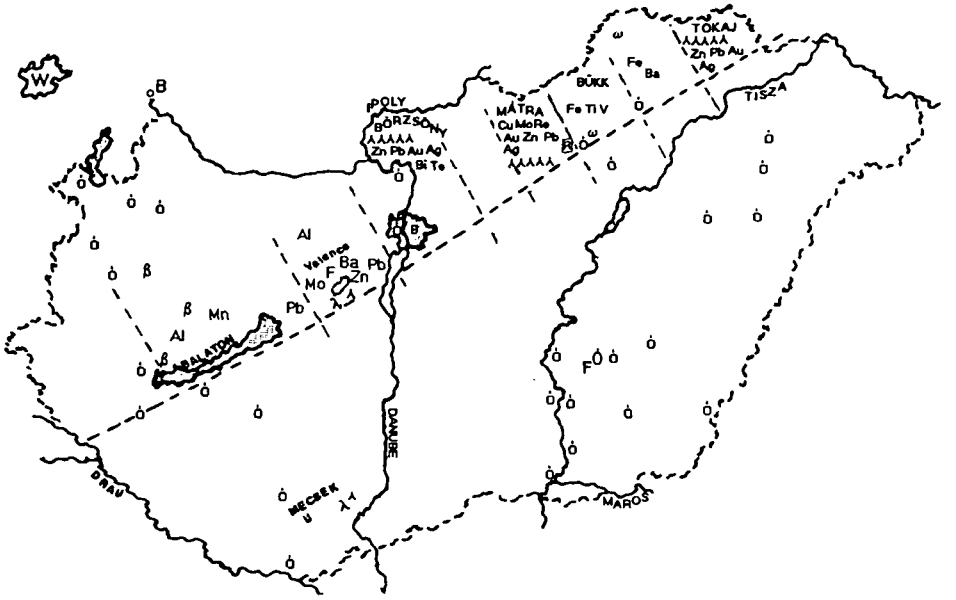

Fig. 1-a. A sketch of metallogeny of Hungary showing several important thermal water wells and springs.
Legend: R: Recsk, λ: granite, ω: gabbro, wehrlite, β: basalt, α: andesite, ó: thermal waters, FÓ: Fábiánsebestyén well with 180 °C water

In two of the drifts driven into the ore deposit, 690 and 890 m below the sea-level respectively, gaseous (CO_2-methan) thermal water (35—44 °C) outbursts occur with various water production. A study of their chemical composition and of their spectacular mineral precipitations might yield valuable data for the interpretation of the hydrothermal process.

The chemical composition and the temperature of these thermal waters are obviously affected by the lithological environment (e.g. water from limestone-dolomitic rock is rich in Mg—Ca—Cl, while those coming through volcanic and skarn formation skarn formations have higher alkali ($Na^+ > K^+$) and trace element (Pb—Zn—Cu) content). Table 1. summarizes the chemical composition of these waters, the maximum and minimum ionic concentrations (a), their mean values (b) and the gross ion content (x).

An active hydrothermal solution is a pH 6.4—7.8 system with major Na—Ca—Mg chloro-hydrocarbonatic-sulphatic, and minor K^+—NH_4^+—Fe^{2+} content. Besides free CO_2 it may also contain methane and radon gases.

Thermal waters of the deeper drifts (-890 m) have higher mean Ca^{2+}—Fe^{2+}—NH_4^+ and SO_4^{2-} ion content, while on the upper levels (-690 m), due to the mineral

TABLE 1

Chemical composition of the epithermal soutions at the –690 m and – 890 m levels

Sample (No)	T	Gallery (m)		Cation	Anion	pH	Ca^{2+}	Mg^{2+}	Fe^{2+}	NH_4^+	Na^+	K^+	$(HCO_3)^-$	$(SO_4)^{--}$	Cl^-
				mg/l			mg/l								
1-44 (29)	35—44 °C	-690	(a)	3010-6662	5319-12106	6.4-7.5	76-5900	164-717	0.0-0.20	18.0-110	1800-3600	10-193	48.8-5392	138-1085	195-11920
			(b)	3526.6	7302.8										
			(b)	10829.4 (x)		6.8	590	265.3	0.08	75.1	2465	107	3545	927	2792
47-71 (18)	35—44 °C	-890	(a)	3700-6440	4105-9153	6.5-7.8	40-664	14.6-551	0.0-0.20	14.5-65.8	3000-5400	118-145	1756-5051	420-768	1580-4600
			(b)	4764.04	7097.1										
	(57 °C)		(b)	11861.1 (x)		7.3	290	306.2	0.03	35.9	3970	127	3626	564	2910

a = Deviation; b = Mean; (x) = Σ ion

precipitations in the course of the 200 meters long migration, the water is a relatively dilute Na^+—Mg^{2+}—K^+ chloro-hydrocarbonic and sulphatic solution. The Br content of the surface occurrences is 11.5 mg/l.

The dripstone formations precipitating from these waters transform in a relatively short time the mining tunnels into "caves of the fairy tales". These dripstone precipitations are usually rich in forms; there are stalagmites, stalactites, ooides, oolites, pisolites, coral and cole-flower-like bizarre clusters and coatings. The precipitations larger in size have rhythmic band-like structure. Some of their inner layers are brownish-black coloured by mineral oil derivatives (hydrocarbons) while the surface is sometimes yellowish-red (goethite-"hydrogoethite") or green, greenish-blue (malachite-brochantite-atacamite-spangolithe).

Similarly to the chemical composition of the thermal waters, the mineral composition and the paragenetic sequence of the dripstones of the deeper (-890 m) and upper (-690 m) drifts are different (Table 2). On the basis of their mineral composition the dripstones could be divided into nine groups and within these

/a/ on the upper levels (-690 m) the calcite-aragonite composition with minor Mg-mineral constituents is characteristic

TABLE 2

Paragenetic sequence of the dripstones minerals at the -690 m and -890 m levels

GALLERY	PARAGENESIS
-690 m	PRINCIPAL MINERALS: [Calcite > Aragonite] > Gypsum > NaCl >(Nesquehonite>>Thenardite > Northupite > Dypingite, α Sulfur
	ACCESSORY MINERALS: Arcanite, Brochantite, Botallackite, Burkeite, Giorgiosite, Hidromagnesite, Mirabilite, Metathenardite, Glaserite, Palygorskite, (Parasepiolite), Saponite (x), Sepiolite (x), Tschermigite, (?= Antigorite (x), Glauberite, Hydrohalite, Kaolinite (x), Zeolithe (x)
-890 m	PRINCIPAL MINERALS: Nesquehonite > (Dypingite-NaCl) > Northupite + (Aragonite > Calcite) > Thenardite > Astrakhanite (Blödite)>(Gypsum + α Sulfur)
	ACCESSORY MINERALS: Arcanite, Atacamite, Brochantite, Botallackite, Chalcantite, Cristobalite (x), Epsomite, Gaylussite, Goldichite, Hydrogoethite, Langbeinite, (Parasepiolite) (x), Pirssonite, Saponite (x), Sepiolite (x), Spangholite, Stevensite? (x), Syngenite, Vanthoffite
	Botallackite= $Cu_2(OH)_3Cl$, Burkeite= $Na_6[CO_3(SO_4)_2]$, Goldichite= $KFe(SO_4)_2.4H_2O$ Spangolithe= $Cu_6Al[(OH)_{12}Cl,SO_4].3H_2O$?=Alunite, Dickite, Hexahidrite, Eriochalcite= $CuCl_2.H_2O$ (x) = Insoluble remain in acid

/b/ the aragonite-calcite dripstones of the deeper drifts may be characterized by more intense Mg-mineral (nesquehonite-dypingite-northupite-astrakhanite) precipitations. Considerably less frequent is the occurrence of NaCl-thenardite-gypsum and alpha-sulphur precipitations.

The present study focuses particularly on the Mg-minerals because of their special mineral paragenetic importance. These minerals are:

Nesquehonite	$MgCO_3.3H_2O$
Dypingite	$Mg_5[(OH)_2(CO_3)_4].5H_2O(8H_2O)$
Hydromagnesite	$Mg_5[(OH)(CO_3)_2]_2.4H_2O$
Giorgiosite	$Mg_5(CO_3)_4(OH)_2.5H_2O$
Northupite	$Na_3Mg[Cl(CO_3)_2]$
Astrakhanite (Blödite)	$Na_2Mg(SO_4)_2.4H_2O$
Vanthoffite	$Na_6Mg(SO_4)_4$
Langbeinite	$K_2Mg_2(SO_4)_3$
Epsomite	$MgSO_4.7H_2O$
Palygorskite	$(Mg,Al)_2[(OH)Si_4O_{10}].4H_2O$
Sepiolite	$Mg_4[(OH)_2Si_6O_{15}].6H_2O$
(Parasepiolite)	
Saponite	$(Mg>Fe)_3(O.5Ca,Na)0.33$ $[(OH)_2(Al,Si)_4O_{10}].x(H_2O)$

Nesquehonite ($MgCO_3.3H_2O$)

The nesquehonite is the most frequent Mg-mineral of the thermal waters at Recsk. Its several generational appearances can be traced as follows:

/a/ in the ooides it appears in the form of lathy crystals with radial ordering (400—500 μm). On its upgrown crystals terminating forms can also be recognized *(Plate I. Figs.1, 2)*,

/b/ on the surface of aragonite-calcite dripstones it forms powder-like but nodular coatings,

/c/ the single phase Ne ooides are sometimes terminated by a dypingite band sharply separated from the nesquehonite bulk *(Plate I. Fig 3)*,

/d/ the crystallites of the wheat-white powder-like nesquehonite grains and spores are idiomorphic-hypidiomorphic needle-like accicular formations *(Plate I-II, Figs. 4, 5)* here and there holey skeleton crystals *(Plate II, Fig.6)*,

/e/ crystallites showing signs of recrystallization or resolution according to the pattern of decrescence can often be observed *(Plate II, Fig.7)*. Under laboratory conditions at room temperatures in distilled water a sample consisting of Ne>Dy (-890 m) transformed into pure dypingite in seven days. This recrystallization into dypingite goes together with the appearance of pseudohexagonal-monoclinic (orthorhombic?) crystallites. It is possible that the morphology of the dypingite phase formed by the recrystallization of the nesquehonite is significantly different from that of the primary modification:

$$5(MgCO_3.3H_2O)+xH_2O=Mg_5[(CO_3)_4(OH)_2].5H_2O(8H_2O)+(H_2O+CO_2)+xH_2O$$

According to the literature, nesquehonite primarily is a crack filling mineral of serpentinized alkali magmatites; sometimes appears as thin layers in asbestos, magnesite and coal-antracite deposits; precipitations of saline lakes or disseminations and crack fillings in dolomites of tropical territories.

Dypingite [$Mg_5(CO_3)_4(OH)_2.5H_2O(8H_2O)$]

Fig. 1-b. Microphotograph of a nesquehonite (Ne) ooide with dypingite (Dy) crystallites on its surface

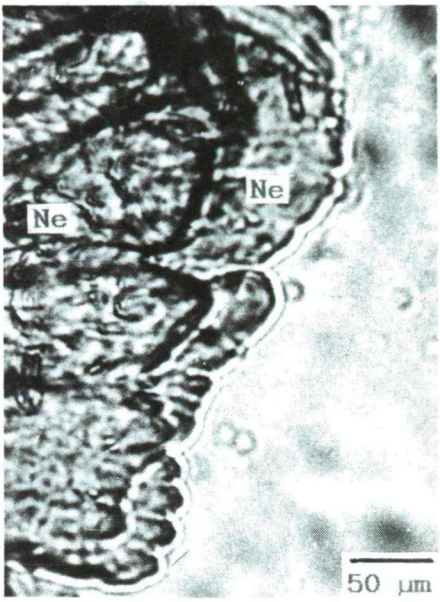

Fig. 2. Microphotograph of the cross section of a nesquehonite (Ne) pisolite. Several hypidiomorphic crystals are overgrown on each other in a layer-like manner.

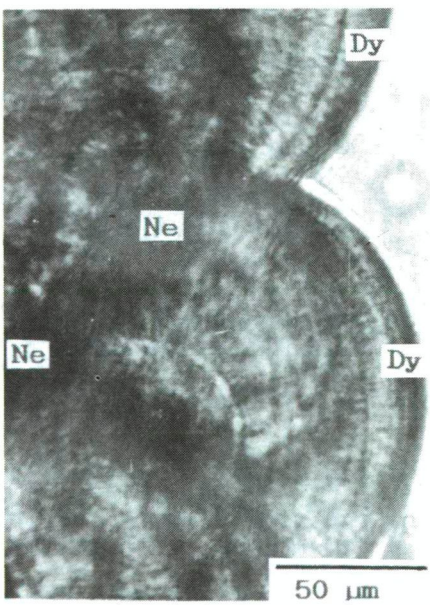

Fig. 3. Microphotograph of a nesquehonite (Ne) — dypingite pisolite. The rhythmic band-like texture is mainly nesquehonite, the outer surface layer is dypingite

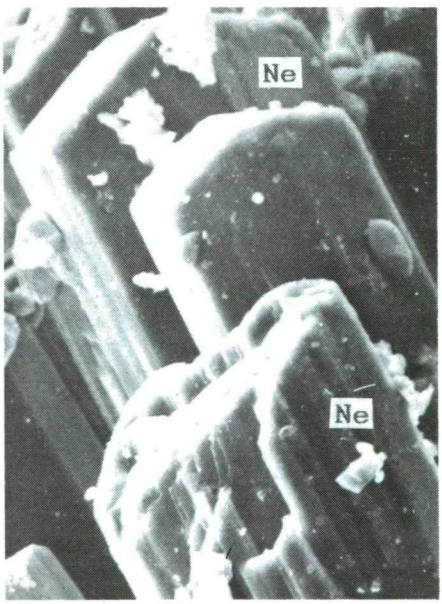

Fig. 4. SEM picture of idiomorphic nesquehonite (Ne) crystallites [(011), (010), (110)]. The grains on their surface with anhedral morphology are supposedly hydromagnesite.

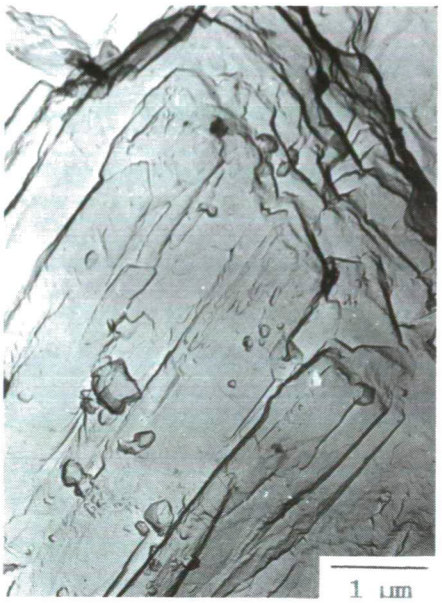

Fig. 5. TEM photograph of a nesquehonite (Ne) ooide.

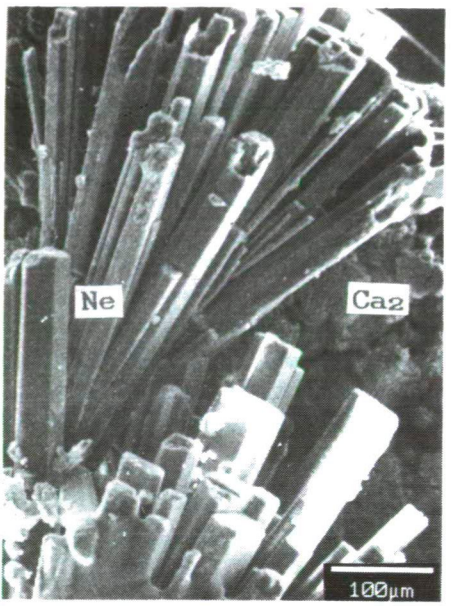

Fig. 6. SEM photograph of upgrown idiomorphic nesquehonite crystallites and skeleton crystals on the surface of an aragonite dripstone.

Fig. 7. TEM photograph showing the resorption-recrystallization formations of the single phase nesquehonite (Ne).

Fig. 8. TEM photograph of dypingite crystallites terminated by (hk0) (hkl) planes. Some clusters of alpha-sulfur (S) can also be seen.

Several generational appearances of dypingite can be recognized at Recsk *(Plate I, Figs. 1 and 3)* as follows:

/a/ the dypingite forming the outer layer of some nesquehonite ooides *(Plate I, Fig. 3)* is a primary formation,

/b/ the pseudomorphic dypingite after nesquehonite is of epigene origin,

/c/ fine needle-like accicular upgrown crystallites on the surface of nesquehonite-aragonite *(Plate II, Fig.8)*,

/d/ dypingite phase identified within some nesquehonite ooides by X-ray diffraction, TEM and SEM.

The dypingite was first described from a magnesite deposit (Dyping-dal, Snarum, Norway) together with hydrotalcite $[Mg_6Al_2(OH)_2(CO_3).4H_2O]$, marassite $[Mg_6Al_2(OH)_2(CO_3).4H_2O]$, szájbelyite $[Mg_2(B_2O_5)H_2O]$ and haematite (Fe_2O_3). It was also found in a Japanese locality in the company of chrysotile, nesquehonite, brugnatellite $[Mg_6Fe^{3+}(OH)_{13}(CO_3).4H_2O]$ and pyroaurite $[Mg_6Fe_2(OH)_{16}(CO_3).4H_2O]$. The structure of dypingite, its hydrothermal formation (together with nesqehonite) is the first such observation, its structure has not been completely clarified yet.

Hydromagnesite $Mg_5[(CO_3)_2OH]_2.4H_2O$.

It appears together with nesquehonite-dypingite in the form of well defined crystallites *(Plate III, Fig.9)*.

Giorgiosite: $Mg_5(CO_3)_4(OH)_2.5H_2O$

Its presence in the powder-like coatings on the surface of the aragonite-calcite dripstones was identified by X-ray diffraction together with nesquehonite-dypingite-hydromagnesite as well as northupite.

Northupite $[Na_3Mg\{Cl, (CO_3)_2\}]$

It is the most characteristic mineral of the Recsk thermal waters. At least two generations of it can be recognized:

/a/ idiomorphic octahedral crystals that can directly be derived from the thermal water *(Plate III, Figs.10, 11 and 12)*.

/b/ hypidiomorphic-anhedral crystallites which could form with the reorganization of nesquehonite under the influence of saturated NaCl solutions in an epigene way. Its formation may be explained by the following chemical process:

$$2(MgCO_3.3H_2O)+3NaCl=Na_3Mg[Cl, (CO_3)_2]+MgCl_2+6H_2O$$

A portion of the chlorine might be substituted by $(SO_4)^{2-}$ but the occurrence of the chlorine free tychite $Na_6Mg_2[SO_4, (CO_3)_4]$ at Recsk has not been observed yet. The clear transparent crystals of northupite have low refractive index (n=1.51—1.53), are 60—100 μm in size and crystal forms of (100) and (111)—(110) can be recognized on them *(Plate III, Figs. 11 and 12)*. After the morphology it can not be distinguished from tschermigite (n=1.46—1.47) $[NH_4Al(SO_4)_2]$ which usually occures as grains 20—40 μm in size. These phases were identified by X-ray diffraction, and further confirmed by the presence of NH_4 and Al.

The northupite was originally found on the surface of karstic dolomites overflooded by hypersaline solutions of Tchad (Africa). It was observed together with barringtonite and nahcolite; its likely formation process is

$$MgCO_3.2H_2O+2NaHCO_3+NaCl=Na_3Mg[Cl, (CO_3)_2]+H_2O$$

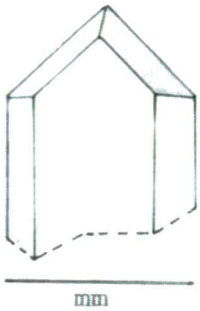

Fig. 9. Hydromagnesite

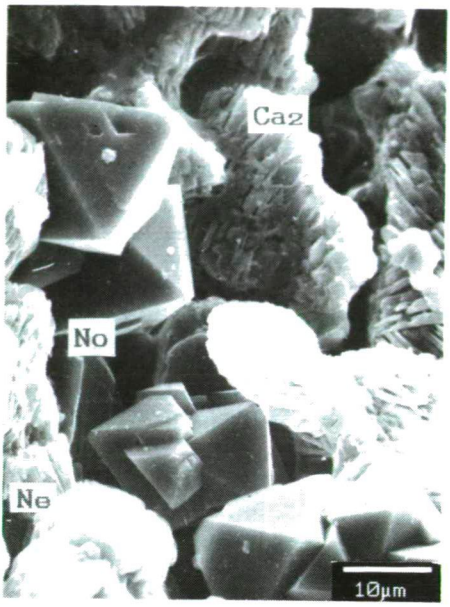

Fig. 10. SEM photograph of northupite clusters in the company of nesquehonite (Ne) and aragonite.

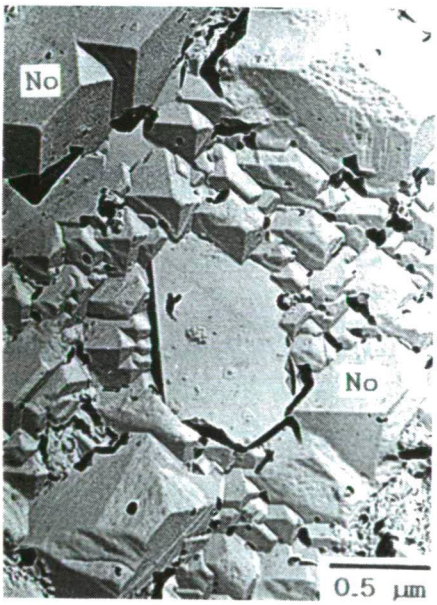

Fig. 11. TEM picture of a cluster of idiomorphic northupite (No) crystals with resorption formations and (111) twinning.

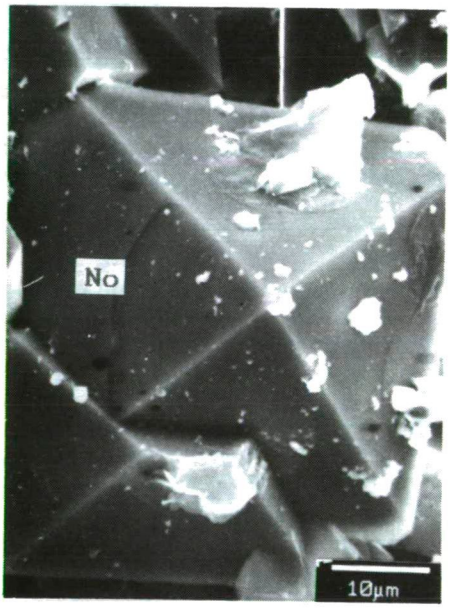

Fig. 12. SEM photograph of a northupite octahedron. The anhedral grains on its surface are hydromagnesite (?) and giorgiosite (?).

This rare mineral was found in clay formations of borax- and salt lakes, in oil shales of California, Wyoming in the company of shortite-trona-bradleyite-pirrsonite and gaylussite.

Astrakhanite (Blödite, Simonyite) = $Na_2Mg(SO_4)_2.4H_2O$

For the time being it is a nearly single phase polycrystalline formation in the deeper (-890 m) drifts. It appears in megascopic nodular formations as well as in film-like coatings. It can be observed in differentiated distribution on the surface of calcite-aragonite dripstones in the company of:

/a/ halite-brochantite-gypsum
/b/ halite-goldichite [$KFe(SO_4)_4.2H_2O$]-brochantite-arcanite
/c/ halite-nesquehonite-northupite
/d/ halite-gaylussite-pirssonite

The single phase astrakanite is a polycrystalline formation of hypidiomorphic-anhedral grains with a "psammitic" texture. Some rare sulphates and carbonates may accompany it. The formation of these rare phases may be explained by a possible recrystallization initiating effect of the epitherms on the astrakhanite:

$$Na_2Mg(SO_4)_2.4H_2O+[Ca^{2+}\text{-}K^{+}\text{-}NH_4^{+}\text{-}CO_3]_{aq}= \text{Pi, Ga-Th-Mi-La-Sy-Va-Gi+X+Y}$$

Pi (Pirssonite)=$Na_2Ca(CO_3)_2.2H_2O$
Ga (Gaylussite)= $Na_2Ca(CO_3)_2.5H_2O$
Th (Thenardite)= Na_2SO_4
Mi (Mirabilite)= $Na_2SO_4.10H_2O$
La (Langbeinite)= $K_2Mg(SO_4)_2$
Sy (Syngenite) = $K_2Ca(SO_4)_2.H_2O$
Va (Vanthoffite) = $Na_6Mg(SO_4)_4$
Gi (Gypsum) = $CaSO_4.2H_2O$
X = $MgSO_{4(ag)}$, $MgCl_{2aq}$
Y = hypothetic phases = $KH(SO_4)$ (Mercallite)
$K_8H_6(SO_4)_7$ [Misenite]
$(NH_4)_3Na(SO_4)_2$ — [NH_4- Glaserite]

See them in *Plate IV—V.*

Vanthoffite [$Na_6Mg(SO_4)_4$ and *Langbeinite* [$K_2Mg(SO_4)_2$]

Nearly isometric water-clear grains, crystallites are on the surface of astrakhanite.

Epsomite ($MgSO_4.7H_2O$)

Its presence was diagnostized by X-ray diffraction in the dripstones of the -690 m and -890 m drifts and it was accompanied by gypsum-glauberite-mirabilite-syngenite or sometimes by burkeite and goldichite.

Palygorskite (sepiolite-parasepiolite-saponite)

It is a characteristic accompanying mineral of the polymetallic ore veins of the Mátra Mts. (Parádsasvár, Mátraszentimre). At Recsk it was identified in the acid insoluble residue of the outer-edge crystalline limestone (exoskarn) as well as of the dripstones in the company of quartz-opal-kaolinite-zeolite(?). Its crystals are fine feather-like formations *(Plate IV, Fig. 14)* or fibrous constituents of

Fig. 13. TEM picture of anhedral astrakhanite (blödite) grains with psammitic texture.

Fig. 14. TEM photograph of some feather-like palygorskite (Pa) crystallites. Acid insoluble residue of a calcite-aragonite dripstone.

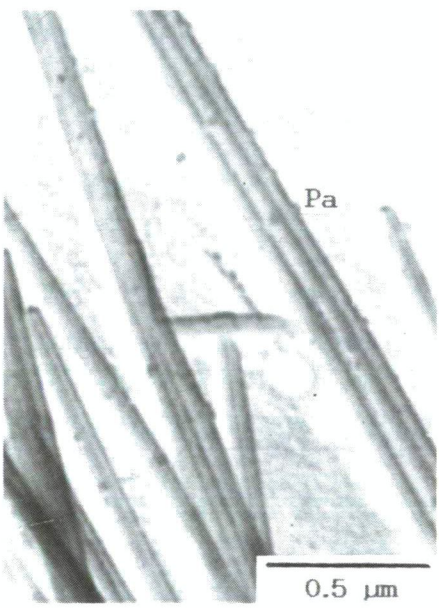

Fig. 15. TEM picture of idiomorphic lathey palygorskite crystals with oriented intergrowths (Parádsasvár).

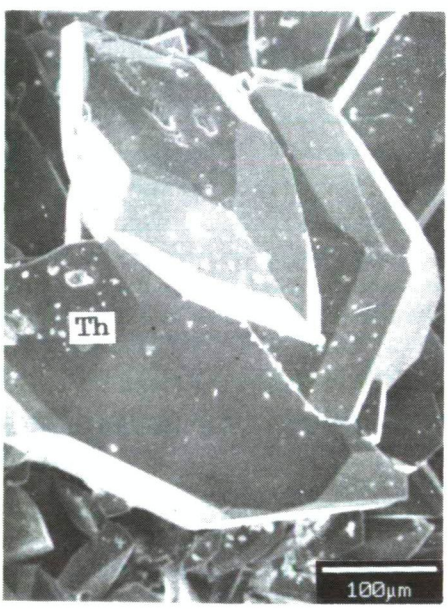

Fig. 16. SEM photograph of a cluster of idiomorphic thenardite (Th) crystals.

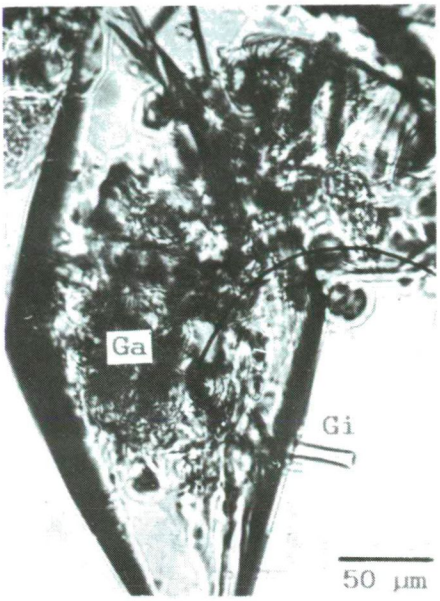

Fig. 17. Microphotograph of gaylussite (Ga) in the company of gypsum (Gi).

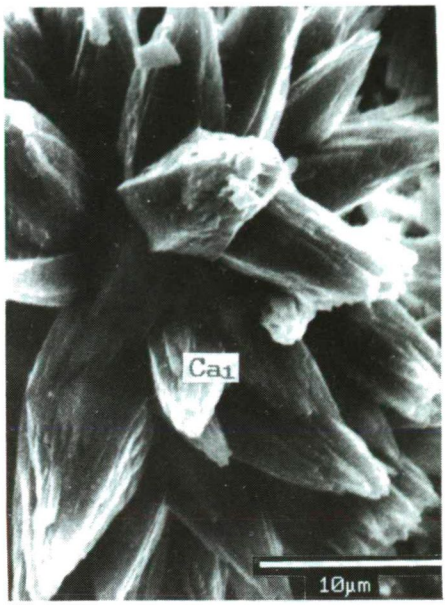

Fig. 18. SEM photograph of calcite showing (4041) and (hkil) forms.

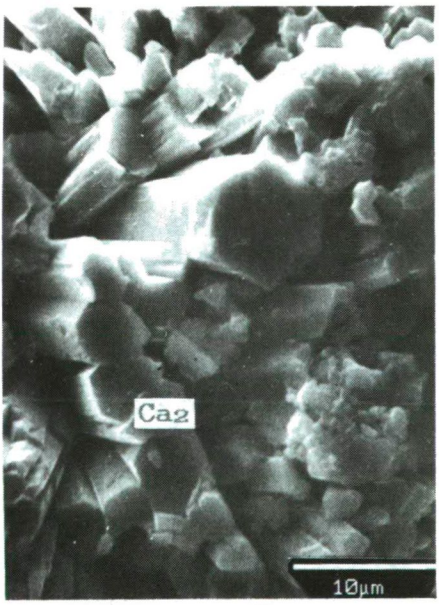

Fig. 19. SEM photograph of upgrown aragonite (Ca_2) crystallites and cyclic twins on the surface of a calcite dripstone.

Fig. 20. Microphotograph of powder-like halite (Ha) and gypsum (Gi) precipitation on the surface of a nesquehonite ooide. The outer edge of the halite crystals showing decrescence is slightly brownish coloured and anisotropic (=H hydrohalite (?)).

cotton-like coatings (Parádsasvár, *Plate IV, Fig. 15*). The chemical composition of the single phase palygorskite is:

SiO_2	=	60.90 %	
TiO_2	=	0.01 %	
Al_2O_3	=	13.33 %	
Fe_2O_3	=	0.13 %	
FeO	=	0.39 %	
MnO	=	0.09 %	
MgO	=	10.03 %	
CaO	=	0.71 %	($CaCO_3$)
Na_2O	=	0.04 %	
K_2O	=	0.04 %	
P_2O5	=	0.006 %	
H_2O	=	14.31 %	
Σ		99.986 %	

Its calculated chemical formula is:

$$[Mg_{0.961}Al_{0.996}]\,[Ti_{0.003}Fe_{0.025}Fe_{0.020}Mn_{0.005}Na_{0.008}K_{0.005}]$$
$$[(OH)_{0.407}Si_{3.995}O_{10}]^{IV}\cdot 2.203H_2O,$$

that is, it can be characterized by a slight cation surplus in the [VI] coordinated site. The occurrence of the palygorskite in recent dripstones may be regarded as a dissolution product of the dolomite that arrived to the dripstones in a migration process as an allothigenous constituent. On the other hand, however, the palygorskite of the limestone and the dolomite (sepiolite, saponite) can recrystallize into diopside, actinolite or tremolite in the high thermal stress affected contactized territories (skarn), accordingly it may be regarded as a forerunner of these minerals.

SUMMARY

The majority of the ionic structure mineral precipitations of the Recsk epihydrothermal waters are similar to the evaporation products of hypersaline (NaCl-soda-borax) lakes (nesquehonite-northupite). The astrakhanite (blödite), epsomite, thenardite are typical covering salt products of evaporite deposits.

The nesquehonite-dypingite-hydromagnesite (giorgiosite) (at Recsk with 4—10 ppm Cr and 7—250 ppm Ni content) are crack-filling minerals of near to surface serpentinized magmatites of oceanic origin, or accompanying minerals magnesite-asbestos deposits. Some of these minerals (e.g. nesquehonite) were also described from antracite and coal deposits.

The Mg-containing mineral precipitations of the ascendent hydrotherms of the Cu-porhyric skarn ore field may be regarded as indications of special genetic-geochemical conditions;

— substantial portion of their constituents may be leached out of the Cretaceous serpentinized, chloritized magmatites of oceanic origin from near the Darno fault (gabbro-wehrlite-diabase).

— they may have been mobilized, along the Darno fault, from the Miocene evaporite deposits of the Inner-Carpathian Mts., following the Eocene Cu-porphyric skarn ore deposition process.
— The Darno is a "rejuvenated rift structure" (?). The hydrothermal appearance of these Mg-minerals may be regarded as a special ("Recsk") local paragenetic phenomenon.

ACKNOWLEDGEMENT

The author wish to express their thanks to ÉVA GASZTONYI and GÉZA SZEBÉNYI, geologists of the RECSK ORE MINE, for kindly letting the authors use their chemical data on the water samples and rocks.

REFERENCES

BAKSA, CS. (1975): A recski mélyszinti szubvulkáni andezittest és telérei (The subvolcanic andesite body of Recsk and its dikes.) Földt. Közl. **105**, 612—624. (In Hungarian with English summary)
BAKSA, CS. (1984): A recski ércesedés genetikai vázlata (Genetic aspects of the Recsk mineralized complex.) Földt. Közl. **114**, 335—348. (In Hungarian with English summary)
CSILLAG, J. (1975): A recski terület magmás hatásra átalakult képződményei (Rocks transformed upon magmatic effect in the Recsk area, Hungary) Földt. Közl. **105**, 646—671. (In Hungarian with English summary)
DÓDONY, I., KISS, J. (1976): Crystal Structures and Genetical Studies on the Palygorskite-Sepiolite-Saponite (Montmorillonite) Group. Acta. Geol. Sci. Hung. **20**, 1—17.
FÜGEDI, P. U., NÁNDOR, A., SÁSDI, L. (1990): A recski ércbánya mélyszintjének hidrotermális vízkőkiválásai (Scale precipitation at the lower level of the Recsk ore mine) Karszt és Barlang, 13—18. (In Hungarian with English summary)
KISVARSÁNYI, G. (1954): Parádfürdő környéki ércesedés (Ore formation near Parádfürdő in Hungary) Föld. Közl. **84**, 191—200. (In Hungarian with Russian and English summary)
KISVARSÁNYI, G. (1988): Vertical and Horizontal Zoning of Ores in the Porphyry Copper System of Recsk, Hungary. Conf. on Tectonic of Ore Deposits and the Vertical and Horizontal Ore Systems. Univ. of Missouri-Rolla. 174—179.
KISS, J., (1964): Allitos és sziallitos ásványok és szerepük a Középső-Mátra ércesedésében (Minéraux allitiques et sialltiques et leur role dans la métallisation de la partie centrale de la Montagne Mátra, Hongrie du Nord) Földt. Közl. **94**, 422—431. (In Hungarian with French summary)
KISS, J. (1980): Mettalogenese du gisement du type porphyry copper a Recsk (Hongrie NE). European Copper Deposit, Belgrade, 77—82.
KISS, J. (1982): Ércteleptan II (Ore Deposits II.) Tankönyvkiadó, Budapest, 205—220. (In Hungarian)
PANTÓ, GY. (1952): Bányaföldtani felvétel Recsk és Parád környékén (Mining geological investigation in the Recsk-Parád area) MÁFI Évi Jel. az 1949. évről, 67—80. (In Hungarian with French and Russian summary)
SZTRÓKAY, K. (1940): A recski ércek ásványos összetétele és genetikai vizsgálata (The mineral composition and genetic investigation of the Recsk ores) Math. Term. Tud. Ért. **70**, 722—748. (In Hungarian with German summary)

Manuscript received, 13 April, 1993

Acta Mineralogica-Petrographica, Szeged, XXXIV, 21—39, 1993

IGNEOUS PETROLOGY OF THE BULFAT AREA (NORTH-EAST IRAQI ZAGROS THRUST ZONE)

GY. BUDA*

Department of Mineralogy of Eötvös L. University

ABSTRACT

Two intrusions can be distinguished in the Bulfat-postcollision igneous complex, an older one with a nearly complete differentiation series; from ultrabasic rocks through to nepheline syenite and younger one composed of olivine gabbro, with olivine diorite at the chilled margin. Peridotite occurs at the lowest part of the older intrusion, probably tectonically emplaced. The original rock was harzburgite but most has been altered to serpentinite. The older intrusion is composed predominantly of gabbro and diorite, both containing many xenoliths. The chemical composition of these rocks differ from the normal calc-alkaline magmatic suite. Calcium enrichment is widespread due to magmatic assimilation of the calcareous rocks. At the latter stage of differentiation silica migrated into the host country rocks where a skarn zone developed, this caused silica deficiency in the magma and locally nepheline crystallized at the expense of alkali feldspars. This complex process of assimilation and silica migration resulted in the original calc-alkaline magma changing to an alkalic-calcic suite. Foliation and mylonitization are widespread due to intensive tectonism during the emplacement and cooling of the magma. The younger olivine gabbro and diorite intruded through the older igneous complex without calcareous rock assimilation. A slight alkali characteristics (e.g. kaersutite) is observed suggesting crustal contamination.

The igneous complex is considered to be a postcollision event with emplacement into the continental crust after the Arabian and Iranian plates collided during late Cretaceous or early Paleogene.

INTRODUCTION

The Bulfat metamorphic-magmatic complex is situated in the Iraqi Zagros thrust zone as a north-east member of igneous complexes at the boundaries between the Arabian and Iranian plates. The southern complexes (Mawat, Penjwin) are Cretaceous ophiolites without thermal contact aureoles represent mantle and oceanic crust (MASEK and ETABI 1973; BUDA and HASHIMI 1977). The Bulfat alkali-calcic igneous complex has a large thermal contact zone. It is believed to be a postcollision intrusion emplaced in the continental crust after the Arabian and Iranian plates collided during late Cretaceous or early Paleogene (BUDA, SAHAGIAN and SALEM 1978, JASSIM, WALDHAUSROVA and SUK 1982a, JASSIM, BUDA, NEUŽILOVA and SUK 1982 b). The present paper deals only with the petrology of the intrusive complex.

* H-1088 Budapest, Múzeum krt. 4/A. Hungary

Fig. 1. Igneous and metamorphic rocks of Bulfat thrust block (Northeast Iraq).

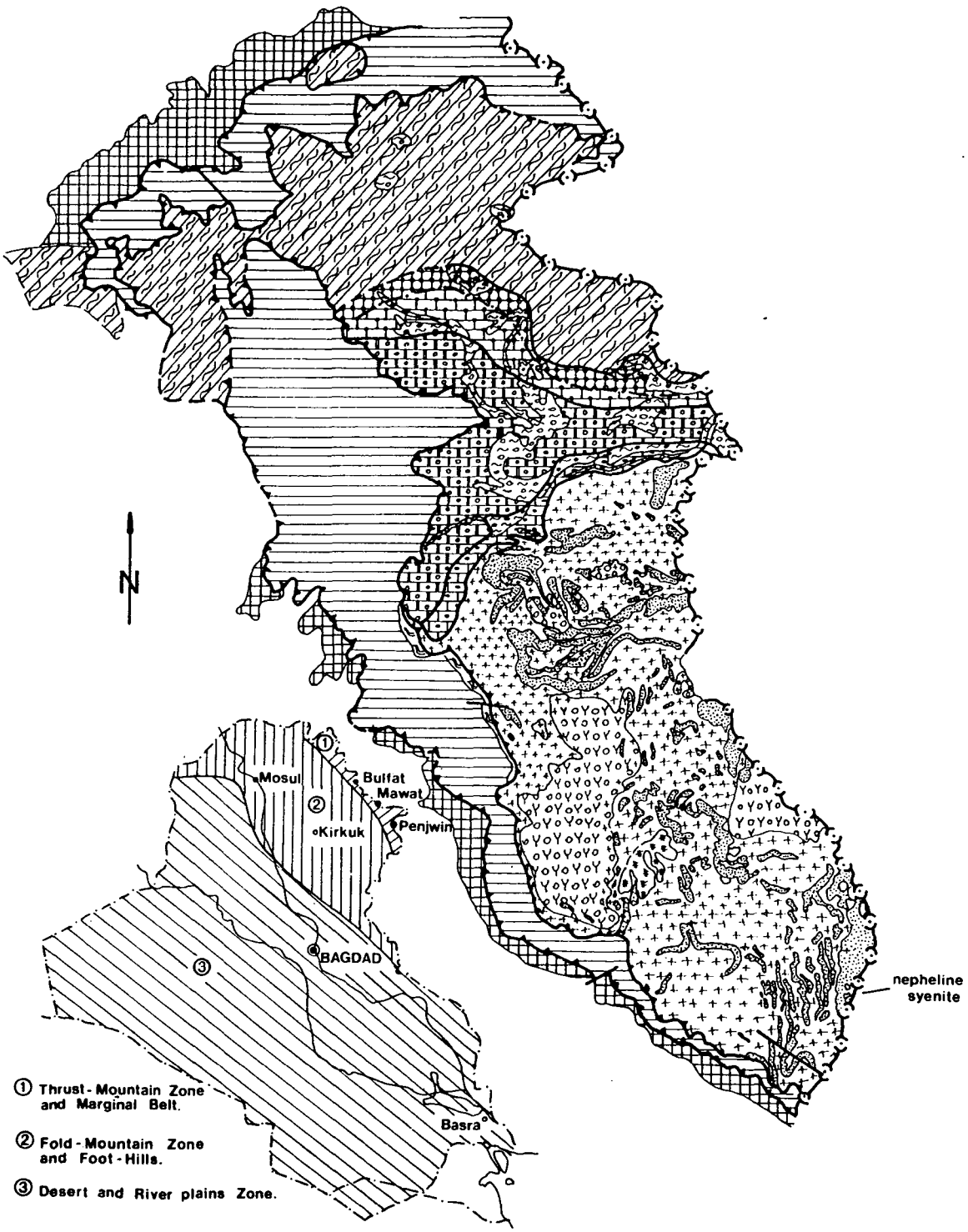

IGNEOUS AND METAMORPHIC ROCKS OF BULFAT THRUST BLOCK (NORTHEAST IRAQ)

0 1 2 3 km

LEGEND

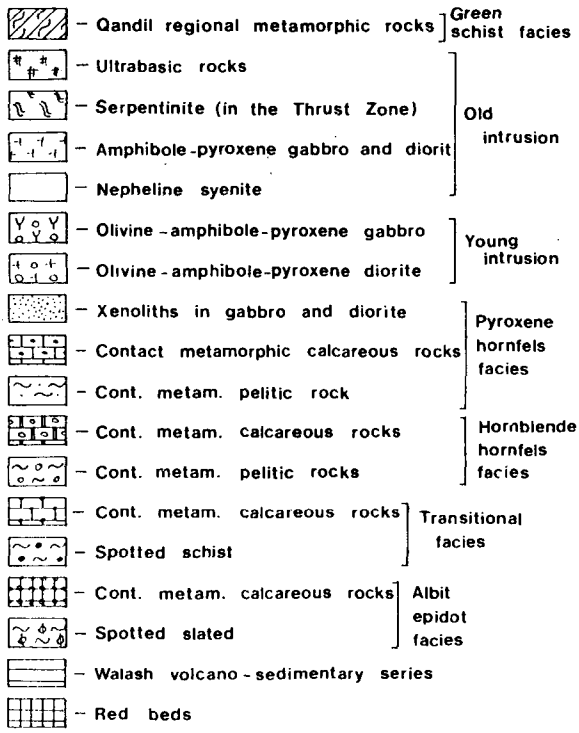

GEOLOGICAL SETTING OF INTRUSIVE COMPLEX

The exact shape and size of the intrusive complex unknown as it stretches into Iran and presently no data is available from this area. The mapped outcrop of the elongated plutonic complex is about 15—19 km in a NNW—SSE direction and up to 5—7 km in width. Contact metamorphosed calcareous rocks occur on the highest summits (about 2340 m) and most probably capped the intrusive body. The complex is tilted towards the east (88°/45°). The exposed thickness through the complex is about 1500 m. In summary the lower part of the complex consist of probable tectonical emplaced peridotite, in the middle gabbro-diorite and in the upper part nepheline syenite occurs just below the contact with the calcareous skarn rock (*Fig. 1*). The main pluton was intruded by a younger, smaller olivine gabbro-diorite.

The principal types of plutonic rocks observed are follows:

A. *Ultrabasic rocks* (subordinate); including harzburgite and serpentinite;

B. *Basic and intermediate rocks (older intrusion)*: including pyroxene gabbro, pyroxene diorite, pyroxene-amphibole diorite, amphibole diorite and contaminated rocks: pyroxene diorite, pyroxenite, nepheline syenite.

C. *Basic and intermediate rocks (younger intrusion)*; including olivine-amphibole-pyroxene gabbro and diorite.

The larger and earlier intrusive has a wide thermal contact aureole. In north it extends up to 2.5 km from the last outcrop of the intrusive body. It is considered probably that the igneous body dips gently beneath the metamorphic (Quandil Formation) rocks giving reason for the apparently anomalously wide contact-metamorphic aureole. The western and southern borders of the complex are structurally controlled. Along these tectonic zones the plutonic-metamorphic complex has been thrusted over the Walash volcano-sedimentary formation. The movement has been facilitated by the serpentinite acting as a lubricant for the thrust-slice. Consequently the current position of the igneous-metamorphic complex is allochthonous having been transported from the ENE to its present position.

PETROGRAPHY OF THE IGNEOUS COMPLEX

OLDER INTRUSION

A. Ultrabasic rocks

Harzburgite: The main constituent is olivine (Fo_{92}, Table 1). Kink-bands, wavy extension and granulation are always present, indicating a strong solid-state deformation, along cracks and cleavages, strongly serpentinized. Many clinopyroxenes have been altered to tremolite and many orthopyroxenes to talc and serpentine (bastite), but some small remnants of pyroxene can be recognized. The orthopyroxene was probably enstatite (Mg_{95} Fe_5, calculated from CIPW norms). The clinopyroxene composition is most probably diopside ($Ca_{53}Mg_{44}Fe_3$, calculated from CIPW norms). Tremolitic hornblende (Table 1) is common, occurring as acicular, slender-prismatic, colourless crystals; it is an alteration product of clinopyroxene. Serpentine is a ubiquitous constituent; sometimes the whole rock serpentinized. Chromite is an accessory mineral (0.5V%—2.5V%), it forms rounded, anhedral or rare subhedral crystals. Usually they are opaque, sometimes the middle of the crystal is reddish-brown and the rim is black (opaque). The rim

is Fe-rich and the core is Cr-, Al-rich and Fe-poor chromite. These grains are surrounded by Cr-bearing Mg-chlorite and sometimes by magnetite. These are altered crystals formed simultaneously with serpentinization (BUDA 1988). During alteration, Al and a small amount of Cr were released and formed chlorite instead of serpentine, with Fe realtively enriched in the rim. Alteration of olivine released iron, which formed magnetite in the middle of serpentine veinlets. Calcite also may occur as a secondary mineral.

TABLE 1

Microprobe analyses of olivine, tremolite and accessory chromites from ultrabasic rocks

	OLIVINE			TREMOLITE		CHROMITE		
wt %	1	2	3	4			5	6
SiO_2	40.01	39.96	41.26	54.04		Cr_2O_3	46.92	48.39
TiO_2	-	0.03	0.07	0.05		Al_2O_3	6.58	10.61
Al_2O_3	-	0.02	-	4.33		FeO	36.25	30.27
FeO	8.21	8.27	7.90	2.56		MgO	5.60	7.37
MnO	0.18	0.15	0.08	0.09		MnO	0.35	0.26
MgO	51.23	51.29	50.51	22.97		ZnO	0.31	0.30
CaO	0.04	0.01	0.02	12.50		SiO_2	0.08	0.32
Na_2O	-	-	-	1.03		TiO_2	0.18	0.12
K_2O	-	-	-	0.06		Σ	96.27	97.64
Σ	99.67	99.73	99.84	97.63				
				Numbers of ions on the basis				
		of 4 (o)			23 (o)		of 4 (o)	
Si	0.979	0.978	1.002	Si	7.346	Cr	1.320	1.299
Al	-	0.001	-	Al^{IV}	0.654	Al	0.276	0.425
Ti	-	0.001	-	Al^{VI}	0.040	Fe^{3+}	0.393	0.248
Mg	1.869	1.870	1.829	Ti	0.005	Ti	0.005	0.005
Fe	0.168	0.169	0.180	Fe^{3+}	0.291	Si	0.003	0.017
Mn	0.004	0.003	0.002	Mg	4.654	Fe^{2+}	0.686	0.612
Ca	0.001	-	0.001	Mn	0.010	Mg	0.297	0.373
				Ca	1.821	Mn	0.011	0.008
Fo	91.8	91.7	92.0	Na	0.179	Zn	0.008	0.008
Fa	8.2	8.3	8.0	Na	0.092			
				K	0.010			

1. Olivine from amphibole peridotite; 2. Olivine from serpentinized peridotite; 3. Olivine from amphibole peridotite; 4. Tremolitic hornblende (γ/c=22°) from serpentinized peridotite; 5. Ferrianchromite from amphibole peridotite; 6. Ferrianchromite from serpentinized peridotite

The composition of the chromite (Table 1) is ferrianchromite according to THAYER's (1964) classification. Its chemical character differs from the chromite composition of ophiolitic complexes of Iraq (BUDA 1988).

The mineralogical composition of the unaltered rocks was harzburgite, was calculated from chemical analyses using CIPW norms (Table 2a).

Serpentinite occurs in the thrust zones, and acted as a lubricant that promoted tectonic movement. Two main thrust zones can be distinguished, the first one in the immediate vicinity of the igneous body and the second about 3—5 km from, and approximately parallel with, the first one.

The rocks are strongly foliated. They frequently form a "mesh" texture. The fibrous variety is chrysotile and the flaky one is most probably antigorite. Bastite is also very common, it may contain remnant of pyroxene. Mg-rich, chlorite is also common. Bastite, chlorite and talc indicate orthopyroxene in the original rock, therefore the rock was probably harzburgite. Few samples contain large amounts of tremolite (as tremolitic schist), which was originally clinopyroxenite, perhaps a dike. The accessory minerals are magnetite and chromite. The common strong foliation indicates dynamometamorphism caused by the thrust movement.

B. Basic and intermediate rocks

a. Pyroxene gabbro occurs in the north-eastern part of the plutonic body near the Iranian border. The rock is coarse-or medium-grained. The plagioclase is tabular, sometimes prismatic. Twin lamellae are deformed, showing wavy extinction. The average An content is An_{66} (An_{52}—An_{77}, measured by U-stage) or An_{69} (An_{67}—An_{72}, measured by microprobe, Table 3). The pyroxene is eu-or subhedral, the large tabular crystals show ophitic texture, with green or pink colour. Composition is salite (Table 3). Amphibole occurs in a very small amount. Two types can be distinguished. The first is green, pleochroic (γ'= green, α'= colourless or yellowish-green), mostly fibrous, and occurs around the green pyroxene as an uralitization product ($\gamma/c=17°$). The second is greenish-brown hornblende (γ' = brownish-green, α' = yellowish-green), also formed by uralitization of the Ti-rich pinkish pyroxene. Some samples contain a very small amount of Mg—Ti biotite (Table 3). Chlorite was formed by alteration of biotite and amphibole. Zoisite and calcite are not very common. Titanite and apatite occur in an accessory amount.

The rock contains about equal amounts of pyroxene and plagioclase and less than 3V% of amphibole (Table 2b). According to STRECKEISEN'S (1967) classification, the rock is mesotype pyroxene gabbro *(Fig. 2)*.

The bulk chemical composition shows slightly udersaturated characters (Ne norms, Table 2a), Ca-content is rather high and Mg- and Fe- contents are low. This Ca enrichment, which is characteristic in the whole igneous intrusion, is most probably due to limestone assimilation.

b. Pyroxene diorite: is coarse- or medium-grained. It occurs in two belts. One is in the eastern part of igneous body, forming a north-south belt, usually far from the calcareous xenoliths. The other is an east-west belt at a lower elevation (average: 1600 m).

The main constituent is plagioclase, which forms large tabular or lath-shaped crystals. The most frequent twins are albite, manebach and albite/ala. Some crystals are zoned. In the sheared belt (central part) the plagioclase is granulated and shows wavy extinction and bent twin lamellae (An_{28}—An_{47}). Pyroxene is common, mostly forming large prismatic, slightly greenish or colourless crystals. It contains more Fe than the pyroxenes in the gabbroic rocks, indicating a later stage of crystallization (Table 4). Some pyroxenes are deformed, showing wavy extinction. The rims of the crystals are uralitized (green hornblende, $\gamma/c = 29°$) or surrounded by kaersutite (Table 4). Kaersutite can form large euhedral crystals, some of which contain small rounded grains of pyroxene. Biotite is very rare, mostly occurring around the opaque grains (Ti-magnetite or ilmenite). The biotites are strongly pleochroic, indicating Ti enrichment (γ'= reddish-brown,

TABLE 2a

Average chemical composition, CIPW norms of plutonic rock of BULFAT

wt %	1	2	3	4	5	6	7	8	9	10
SiO_2	40.39	48.57	53.41	52.23	51.39	42.31	56.55	61.13	49.78	51.30
TiO_2	0.06	1.11	0.88	1.49	1.61	3.40	0.52	0.04	0.46	1.16
Al_2O_3	0.74	15.84	16.69	16.08	19.51	9.00	20.34	18.45	21.08	16.98
Cr_2O_3	0.25	0.03	0.03	0.01	0.01	0.01	0.02	0.04	0.01	0.03
Fe_2O_3	4.29	2.46	1.90	1.87	1.92	4.68	2.53	0.34	1.48	1.96
FeO	3.89	3.59	3.48	6.01	3.79	7.70	2.99	0.48	4.66	5.90
MnO	0.10	0.11	0.10	0.15	0.10	0.19	0.11	0.03	0.11	0.14
MgO	40.54	6.19	4.53	5.51	2.20	6.64	0.60	0.30	6.87	6.30
CaO	1.11	17.27	12.17	7.93	12.15	22.29	2.32	3.64	9.93	9.46
ZnO	0.04	0.14	0.13	0.05	0.10	0.06	0.09	-	0.13	0.46
Na_2O	0.11	2.23	4.03	5.00	4.69	0.96	8.09	7.70	3.54	4.42
K_2O	0.04	0.36	0.57	1.05	0.52	0.20	3.39	4.48	0.13	0.31
P_2O_5	0.08	0.25	0.09	0.29	0.36	0.70	0.13	0.02	0.10	0.22
CO_2	0.14	0.20	0.07	0.10	0.07	0.13	0.08	-	0.06	0.18
H_2O^+	7.31	1.22	1.25	1.89	1.45	1.08	1.52	1.32	0.99	0.91
H_2O^-	0.45	0.14	0.22	0.27	0.20	0.21	0.26	0.30	0.13	0.14
F	-	0.01	0.01	0.04	0.03	0.04	0.03	-	0.02	0.04
Cl	-	0.01	0.01	0.01	0.01	0.01	0.01	-	0.01	0.01
S	-	0.06	0.03	0.04	0.05	0.05	0.04	-	0.07	0.12
Σ	99.5	99.79	99.60	100.02	100.16	99.66	99.63	98.23	99.56	100.04
					CIPW norms					
Q	-	-	1.05	-	-	-	-	-	-	-
Or	0.24	2.13	3.37	6.20	3.07	1.18	20.03	26.47	0.77	1.83
Ab	0.93	16.30	34.08	41.02	36.31	1.01	49.16	52.27	29.94	37.38
An	1.41	32.15	25.77	18.34	30.65	19.66	9.19	2.46	41.25	25.58
Ne	-	1.39	-	0.69	1.82	3.85	10.44	6.96	-	-
Wo	1.15	20.41	14.04	7.79	8.89	23.54	0.44	1.38	2.94	7.89
En	0.96	15.41	9.79	4.79	5.48	16.53	0.16	0.75	1.95	4.99
Fs	0.04	2.93	3.08	2.55	2.90	5.01	0.29	0.59	0.77	2.41
Wt	-	0.79	-	-	2.40	12.36	-	5.08	-	-
Et	22.99	-	1.49	-	-	-	-	-	5.02	2.05
Ft	0.84	-	0.47	-	-	-	-	-	1.99	0.99
Fo	53.95	-	-	6.26	-	-	0.94	-	7.11	6.06
Fa	2.17	-	-	3.67	-	-	1.90	-	3.10	3.22
Mt	6.22	3.57	2.76	2.71	2.78	6.79	3.67	0.49	2.15	2.84
Il	0.11	2.11	1.67	2.83	3.06	6.46	1.00	0.08	0.87	2.20
Ap	0.19	0.59	0.21	0.69	0.85	1.66	0.31	0.05	0.24	0.52
Ca	0.32	0.46	0.16	0.23	0.16	0.30	0.18	-	0.14	0.41

TABLE 2b

Average modal composition of plutonic rocks of Bulfat

	1	2	3	4	5	6	7	8	9	10
Plag.	-	45.35	73.1	54.0	66.4	7.6	88.0	+	74.0	67.2
Oliv.	65.51	-	-	-	-	-	Kf.ne.plag	+	10.3	5.5
Pyrox.	6.10	46.20	24.1	4.2	26.0	84.1	-		9.6	18.2
Amph.	7.73	2.60	2.6	39.3	2.3	0.7	10.8		4.5	7.3
Biot.	-	0.40	-	-	-	-	2.2		+	0.1
Serp.	18.73	-	-	-	-	-	-	-	-	-
Chlor.	0.40	1.95	0.2	1.0	-	-	-		Bow 0.2	-
Talc	0.30	-	-	-	-	-	-	-	-	-
Zoiz.	-	+	-	+	-	-	-	-	-	-
Calc.	+	0.75	-	-	-	1.2	-	-	-	-
Tit.	-	1.15	+	-	1.9	4.2	1.0	-	-	-
Ap.	-	0.70	+	1.0	1.7	1.6	+	+	0.3	0.3
Chrom.	1.13	-	-	-	-	-	-		-	-
Mag.	0.10	0.90	-	0.5	1.7	woll 0.6		+	1.4	1.4

1. Amphibole peridotite (Average of four samples); 2. Pyroxene gabbro (Average of three samples); 3. Pyroxene diorite (Average of two samples); 4. Pyroxene-amphibole diorite (Average of three samples); 5. Contaminated pyroxene diorite (Average of three samples); 6. Contaminated pyroxenite (Average of two samples); 7. Nepheline syenite (Average of four samples); 8. Pegmatite; 9. Olivine gabbro (Average of three samples); 10. Olivine diorite (Average of three samples).

α' = yellowish-brown). Titanite is not very common. It forms large anhedral crystals with polysynthetic twins. The SiO_2 content of the rocks is between 51—55 wt% (Table 2a). The rock is leucocratic pyroxene diorite (*Fig.* 2, Table 2b).

TABLE 3

Microprobe analyses of pyroxene, plagioclase and biotite from pyroxene gabbro

	PYROXENE			PLAGIOCLASE		BIOTITE
wt %	1	2	3	4	5	6
SiO_2	48.10	51.23	47.44	52.66	53.80	36.19
TiO_2	1.69	1.29	1.97	-	-	4.43
Al_2O_3	6.32	3.87	5.70	30.44	29.74	5.73
FeO	10.52	6.00	9.50	0.27	0.10	15.02
MnO	0.25	0.20	0.22	0.05	0.03	0.20
MgO	10.22	13.78	10.26	0.19	0.01	14.63
CaO	22.36	23.01	24.03	13.72	13.10	0.03
Na_2O	0.72	0.67	0.76	2.91	3.44	0.20
K_2O	-	0.02	0.01	0.16	0.13	9.27
Σ	100.18	100.07	99.44	100.40	100.35	95.70
			Numbers of ions on the basis of			
		6 (o)		32 (o)		22 (o)
Si	1.817	1.894	1.808	Si 9.503	9.684	Si 5.397
Al^{IV}	0.183	0.106	0.192	Al 6.476	6.311	AlIV 2.603
Al^{VI}	0.099	0.063	0.064	Ti -	-	AlVI 0.162
Ti	0.048	0.036	0.056	Mg 0.051	0.002	Ti 0.497
Mg	0.575	0.759	0.583	Fe 0.041	0.015	Fe 1.873
Fe	0.332	0.186	0.288	Mn 0.008	0.004	Mn 0.025
Mn	0.008	0.006	0.007	Na 1.017	1.201	Mg 3.251
Ca	0.905	0.912	0.981	Ca 2.653	2.653	Ca 0.004
Na	0.053	0.048	0.056	K 0.037	0.030	Na 0.057
K	-	0.001	0.000			K 1.764
Mg	28.5	37.8	28.6	Ab 27.4	32.0	
Fe	24.1	14.4	20.6	An 71.6	67.2	
Ca	47.4	47.8	50.8	Or 1.0	0.8	

1. Salite (green, γ/c = 48 °, No. 285); 2. Salite (zoned, slightly green γ/c = 42 °, No. 27); 3. Salite (pinkish, γ/c = 39 °, No. 306); 4. Bytownite (No. 285); 5. Labradorite (No. 27); 6. Biotite (γ' = reddish brown, α' = yellowish brown, No. 27).

c. Pyroxene-amphibole gabbro and diorite. This group of rock is variable in many respects. The grain size is medium-to coarse. The majority are strongly sheared, foliated, mylonitized and some are folded. Well-developed ophitic texture and layering (white feldspar-rich layers alternate with dark pyroxene-, amphibole-rich ones) can be observed. They occur in the middle and northern part of the

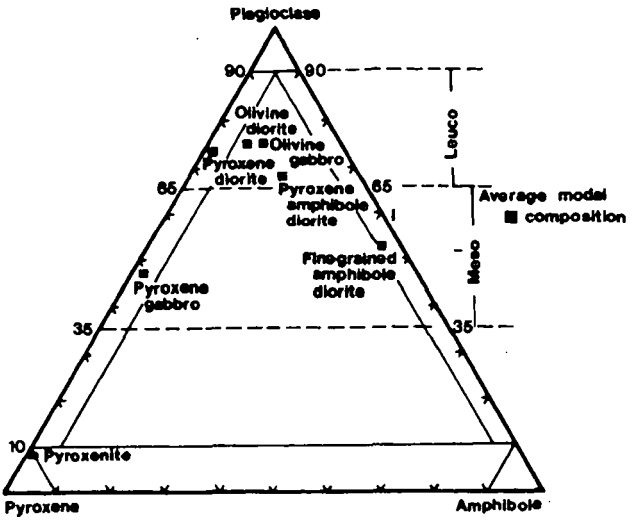

Fig. 2. Modal composition of the basic plutonic rocks of Bulfat.

intrusion. Plagioclase is the prevailing constituent, with average composition about An_{42}, but with a range between An_{28-76}. Sometimes two generations of plagioclase can be distinguished. The large grains with a higher An content are usually altered (saussuritisation). They formed earlier than the small, rounded, fresh grains around them. Granulation can also be observed. The large, strongly deformed, crystals are surrounded by finer grains of angular plagioclase of the same composition. Faint zonation is also common. Pyroxene occurs in nearly every sample, but in variable amounts depending on the degree of uralitization. Usually a very small relict of pyroxene can be observed in the middle of amphibole. The pyroxene is usually colourless or slightly greenish, with fine ilmenite lamellae (Average: $\gamma/c = 43°$).

In the northern part of the intrusion, few samples contain hypersthene in ophitic texture with lath-shaped plagioclase. They most probably formed by contamination of pelitic rocks.

The amount of amphibole is variable (3—29 V%). Three varieties can be distinguished: /1/ uralitization product of pyroxene. It is fibrous actinolite ($\gamma/c = 18°$); /2/ green hornblende ($\gamma/c = 24°—27°$) that is pleochroic (γ' = dark-green, bluish-green α' = pale-yellowish-green); /3/ prismatic or tabular brown hornblende. It commonly has ophitic texture, and is strongly pleochroic (γ'= dark or reddish-brown, α' = yellowish-brown, $\gamma/c = 32°$). Biotite was determined in few samples as an accessory mineral. They are small prismatic crystals with strong pleochroism (γ' = dark-reddish-brown, α' = yellowish-brown). Apatite and titanite occur as accessory minerals. The latter was observed around the opaque minerals as an alteration product indicating Ti enrichment in the opaque (Ti-magnetite and ilmenite).

Chlorite is a common alteration product of amphibole and biotite. It sometimes forms aggregates or secondary vein fillings. Zoisite and calcite are alteration products of plagioclase. Prehnite occurs as a vein filling.

d. Fine-grained pyroxene-amphibole diorite and amphibole diorite. The fine-grained, amphibole-rich variety is foliated, some are folded and laminated.

TABLE 4

Microprobe analyses of pyroxene and amphibole from pyroxene diorite and fine-grained pyroxene amphibole diorite

	PYROXENE	AMPHIBOLE	AMPHIBOLE		PYROXENE
wt %	1	2	3	4	5
SiO_2	50.62	41.46	41.36	42.98	54.26
TiO_2	0.62	4.90	4.25	3.67	0.29
Al_2O_3	1.86	11.21	11.04	10.38	1.58
FeO	12.78	13.40	17.10	14.90	9.50
MnO	0.38	0.25	0.44	0.35	0.40
MgO	9.83	11.74	10.30	11.03	12.67
CaO	23.45	11.74	11.32	10.38	20.41
Na_2O	0.43	2.43	3.05	2.88	0.78
K_2O	0.01	0.89	0.92	0.89	0.03
Σ	99.98	98.02	99.78	97.46	99.98
		Numbers of ions on the basis of			
	6 (o)	23 (o)	23 (o)		6 (o)
Si	1.939	6.171	6.138	6.410	2.014
Al^{IV}	0.061	1.829	1.862	1.590	—
Al^{VI}	0.023	0.137	0.069	0.234	0.069
Ti	0.018	0.548	0.474	0.412	0.008
Mg	0.561	2.605	2.278	2.452	0.701
Fe^{3+}			0.191	0.213	
Fe^{2+}	0.409	1.668	1.932	1.645	0.295
Mn	0.012	0.032	0.055	0.044	0.012
Ca	0.962	1.872	1.800	1.659	0.814
Na	0.032	0.128	0.200	0.341	0.056
Na		0.573	0.678	0.492	—
K	—	0.169	0.174	0.169	0.001
Mg	27.7				Mg 35.8
Fe	23.1				Fe 19.8
Ca	49.2				Ca 44.4

1. Salite from pyroxene diorite, (green, γ/c=47°, No. 56); 2. Kaersutite from pyroxene diorite (γ'=reddish brown, α'= yellowish brown γ/c=17°, No. 251); 3. Magnesian-hastingsite (γ'=greenish-brown, α'=yellowish green, γ/c=28°) from fine grained pyroxene-amphibole diorite (No. 43); 4. Ferroan pargasitic hornblende (γ'=greenish brown, α'=yellowish green) from the same rock (No. 52); 5. Ca-augite (greenish, γ/c=39°) from the same rock (No. 52).

Two main types were distinguished: thin layers of fine-grained diorite alternating with the coarse-grained gabbro and the chilled margin of the intrusion near the xenoliths or at the outer contact.

The main constituent is plagioclase. Some are strongly deformed, with wavy extinction and bent twin lamellae. (An_{35-20}). A faint zonation is rather common, which is characteristic at the margin of the intrusion, together with lower anorthite content. Pyroxene occurs in a minor amount as anhedral grains or as irregular patches in the amphibole. Pyroxene was sometimes found without any trace of uralitization. The composition is Ca-rich augite (Table 4).

Amphibole is very common. Two varieties can be distinguished: green-hornblende, ($\gamma/c = 26°$) formed by uralitization and magnesian-hastingsite or ferroan pargasitic-hornblende with strong pleochroism (Table 4). Nepheline is very rare; it occurs as a tabular, usually altered, grain. Calcite was sometimes observed as an interstitial constituent, indicating contamination from the Ca-rich xenoliths. Biotite was found in a very small amount, sometimes in the amphibole as an alteration product. Apatite and titanite occur as accessory minerals. Opaque minerals are Ti-magnetite and ilmenite.

The rocks is mesotype pyroxene-amphibole diorite, according to the average modal composition (*Fig.* 2, Table 2b). Contamination can be observed in these rocks, for example at the calcareous contact. They are undersaturated, containing nepheline norms (Table 2a), which sometimes also appear in the modal.

e. Contaminated rocks: Two types of contaminated rock can be distinguished: pyroxene diorite and pyroxenite. Both rocks occur at the contact with calcareous rock.

Pyroxene diorite is coarse- or sometimes medium-grained, with tabular plagioclase, large black prismatic pyroxene and yellowish-brown titanite. It occurs in the southern and northern part of the intrusion, always next to the contact marble. The plagioclase composition is An_{43} but some much lower values (An_{28}) were also determined. Pyroxene is always present, but in variable amount (4—43 V%). It appears in large prismatic or anhedral form, some of which show typical ophitic texture. The pleochroism is γ' = purplish or pinkish, α' = greenish, yellowish-pink. Colour zonation is common. Two types can be observed. In the first, the crystal core is slightly pinkish, which goes gradually into pinkish or pinkish-brown pleochroic rim. The composition of the core is salite and the rim is titanoferrosalite (Table 5). In the second the core is pinkish and contains higher Ti. This colour gradually goes into green, due to decreasing Ti and increasing Fe content. The composition of the core is titanoferrosalite and the rim is ferrosalite. The extinction angle of the Ti-rich salite is $\gamma/c = 38°$ and the Fe-rich is $\gamma/c = 43°$. The brown hornblende is an uralitization product of pyroxene. They are strongly pleochroic (γ' = dark-reddish-brown, α' = yellowish-brown) which is caused by the high Ti-content ($\gamma/c = 21°$). This rock usually contains large, slightly yellowish, sub- or euhedral titanite. Nepheline is rare. Apatite is common, mostly as large prismatic crystals. Calcite also occurs, but it is not an alteration product of plagioclase because it forms a well-separated crystal. Most probably it derived from the adjacent calcareous rock. Secondary minerals are chlorite, zoisite and prehnite. Opaque minerals are rather common, most probably titanomagnetite or ilmenite. Titanite rims are common around them. These rocks are slightly udersaturated, containing nepheline norms (Table 2a). Silica most probably escaped and formed Ca-silicate minerals at the immediate contact with limestone and caused silica deficiencies in the magma. According to the modal composition, two types were distinguished, leuco-pyroxene diorite and meso-pyroxene-amphibole diorite.

Pyroxenite contains coarse, medium-grained, black, slightly pinkish pyroxene and white interstitial plagioclase. It occurs at the immediate contact with the coarse-grained forsterite-, diopside- wollastonite- and melilite marble or diopside hornfels or less commonly, in the coarse-grained marble.

TABLE 5

Microprobe analyses of clinopyroxene and nepheline from contaminated pyroxene diorite

	PYROXENE						NEPH.
wt %	1	2	3	4	5	6	7
SiO_2	52.83	48.31	47.54	47.86	48.17	47.43	45.62
TiO_2	1.62	3.22	2.70	2.63	2.23	1.19	-
Al_2O_3	2.82	6.00	4.92	3.83	4.13	3.94	33.84
FeO	9.13	12.14	14.74	15.02	16.26	20.78	0.16
MnO	0.26	0.32	0.35	0.35	0.37	0.40	-
MgO	11.25	7.78	7.48	7.66	6.75	4.02	-
CaO	20.66	20.66	21.70	21.38	21.18	20.58	1.61
Na_2O	0.75	0.89	0.83	0.98	0.89	1.01	12.53
K_2O	0.02	-	-	-	-	-	5.22
Σ	99.34	99.32	100.26	99.71	99.98	99.35	98.98
	Numbers of ions on the basis of 6 oxygen						32 (o)
Si	1.974	1.845	1.836	1.859	1.870	1.893	8.668
Al^{IV}	0.026	0.155	0.164	0.141	0.130	0.107	7.580
Al^{VI}	0.098	0.115	0.060	0.034	0.059	0.078	-
Ti	0.046	0.092	0.078	0.076	0.065	0.036	-
Mg	0.626	0.443	0.430	0.444	0.391	0.239	-
Fe	0.285	0.388	0.476	0.488	0.528	0.693	0.025
Mn	0.008	0.010	0.011	0.011	0.012	0.013	-
Ca	0.827	0.845	0.898	0.890	0.881	0.880	0.328
Na	0.054	0.066	0.062	0.074	0.067	0.078	4.615
K	0.001	-	-	-	-	-	1.265
	Atomic ratios						
Mg	32.1	22.6	21.4	22.1	19.6	11.8	-
Fe	22.7	30.9	30.8	30.2	33.0	40.8	-
Ca	45.2	46.5	47.8	47.7	47.4	47.4	-

1. Salite, core of a large crystal (pinkish, No. 22); 2. Titanoferrosalite, rim of the same crystal (brownish, No. 22); 3. Titanoferrosalite core of a large crystal (pinkish, No. 55); 4. Titanoferrosalite intermediate zone of the same crystal (pinkish, No. 55); 5. Titanoferrosalite, outer zone of the same crystal (greenish, No. 55); 6. Ferrosalite, rim of the same crystal (green, No. 55); 7. Nepheline (No. 55).

The main constituent is pinkish, pleochroic and zoned large prismatic or anhedral titanosalite, titanoferrosalite and Ti-augite (85—90 V%). The colour zonation is similar to the first type of zoned pyroxene in diorite, but in this case the core has a higher Ti content (Table 6). Some pyroxene is altered to strongly pleochroic, Ti-rich amphibole (γ'=dark-green, greenish-brown, α'=yellowish-brown). Plagioclase is subordinate, anhedral and fills the intersticies among the pyroxene. The composition is andesine (An_{42}) or labradorite (An_{52-58}). Titanite

is common as large subhedral or euhedral crystals. They are slightly pleochroic (brownish or pinkish) with polysynthetic twins. Apatite is also common in some samples. It forms large eu- or subhedral prismatic grains and occurs in pyroxene as an inclusion. Calcite fills intersticies between pyroxene grains as plagioclase does. Wollastonite and biotite are very rare. Prehnite is an alteration product of plagioclase. The rock has very high Ca and Ti content (Table 2a) due to the prevailing Ti-augite and titanite. The wollastonite and nepheline norms suggest Si migration towards the calcareous rock (Table 2a).

f. Nepheline syenite is mostly medium-grained. The amphiboles are oriented and occur in a feldspar- and nepheline- bearing groundmass. Some biotite can also be recognized. The nepheline syenite has a very restricted occurrence at the south-eastern part of the igneous complex at a very high elevation *(Fig. 1)*. It is usually surrounded by calcareous metamorphic rocks. The prevailing mineral is oligoclase (An_{28}) but orthoclase is also common with string perthites. Very rarely, cross-hatched anorthoclase can be observed. Nepheline occurs in every sample as an anhedral, prismatic or tabular crystal. Commonly altered to colourless mica. Hastingsitic hornblende (Table 7) is prismatic, oriented, and strongly pleochroic. Biotite is Fe-rich (siderophyllite, Table 7). It occurs together with amphibole or around the opaque minerals. Titanite is usually small, rounded, and mostly yellowish in colour. Opaque minerals are sometimes surrounded by anhedral titanite, indicating that they have formed from it by alteration. SiO_2 content of the rock indicates an intermediate composition but with a high content of alkalis (Table 2a). According to nepheline, orthoclase micropertite, and hastingsitic hornblende, the rock is an undersaturated sodium-type syenite.

Two kinds of genesis can be proposed: /1/ Alkaline rock formation by differentiation and assimilation from calc-alkaline or alkali-calcic magma. /2/ Alkaline rock crystallization from alkali magma.

The very common occurrence of carbonate-rich xenoliths in the intrusion could produce a relative alkali enrichment at the contact, caused by silica migration to country rocks. Silica deficiency would consequently occur in the melt (instead of plagioclase, nepheline would crystallize). Silica-poor magma could even intrude into metasediments. This way of forming of alkali magma is restricted only to a small area like in Bulfat.

According to the agpaitic coefficient, mineralogical composition the Bulfat alkaline rocks belong to the miaskitic nepheline-syenite group. In this type of rocks, zircon, pyrochlore, and in the potassium-rich variety, uranium enrichment can occur. Further detailed studies are recommended in order to prove whether carbonatite occurs in the area, which could be suspected from the miaskitic character, from melilite occurrences etc.

The close association with calcareous metasediments and very restricted occurrences suggests "limestone assimilation" genesis, but if chemical and mineralogical composition are taken into consideration, the second type of genesis also possible.

TABLE 6

Microprobe analyses of pyroxene from contaminated pyroxenite

	PYROXENE				
wt %	1	2	3	4	5
SiO_2	46.34	45.25	44.18	43.99	43.83
TiO_2	2.29	2.75	3.10	3.31	3.35
Al_2O_3	6.55	7.90	8.53	9.66	9.74
FeO	14.65	9.68	15.21	15.46	15.59
MnO	0.26	0.18	0.24	0.21	0.25
MgO	7.10	9.43	5.85	5.54	5.15
CaO	21.36	23.73	21.13	21.21	21.25
Na_2O	0.50	0.69	0.48	0.55	0.65
K_2O	—	0.02	—	—	0.05
Σ	99.05	99.63	98.72	99.93	99.86
	Numbers of ions on the basis of 6 (o)				
Si	1.804	1.729	1.734	1.706	1.705
Al^{IV}	0.196	0.271	0.266	0.294	0.295
Al^{VI}	0.105	0.085	0.129	0.148	0.152
Ti	0.067	0.079	0.092	0.097	0.098
Mg	0.412	0.537	0.342	0.320	0.298
Fe	0.477	0.309	0.499	0.502	0.507
Mn	0.009	0.006	0.008	0.008	0.008
Ca	0.891	0.972	0.889	0.881	0.886
Na	0.038	0.051	0.036	0.041	0.049
K	—	0.001	—	—	0.003
			Atomic ratios		
Mg	20.6	26.3	17.1	16.0	14.9
Fe	32.9	23.6	36.6	37.9	38.3
Ca	46.5	50.1	46.3	46.1	46.8

Titanoferrosalite, core of a crystal (pinkish, No. 71A); 2. Titansalite, rim of the same crystal; 3. Titanoferrosalite, core of a crystal (pinkish, No. 2C); 4. Titanoferrosalite, intermediate zone of the same crystal (No. 2C); 5. Titanoferrosalite, rim of the same crystal (No. 2C).

TABLE 7

Microprobe analyses of amphibole, biotite and orthoclase from nepheline syenite

	AMPHIBOLE	BIOTITE	ORTHOCLASE
wt %	1	2	3
SiO_2	40.05	34.60	67.19
TiO_2	1.70	2.21	-
Al_2O_3	9.40	13.24	17.59
FeO	29.94	34.08	0.05
MnO	0.77	0.90	0.07
MgO	2.13	2.92	0.03
CaO	9.15	0.04	0.34
Na_2O	2.83	0.16	3.28
K_2O	1.89	9.29	11.22
Σ	97.83	97.44	99.76
	Numbers of ions on the basis of		
	23 (O)	22 (O)	32 (O)
Si	6.406	5.611	Si 12.194
Al^{IV}	1.594	2.389	Al^{IV} 3.762
Al^{VI}	0.178	0.142	Al -
Ti	0.204	0.269	Ti -
Fe^{3+}	0.599	-	Mg 0.008
Mg	0.508	0.705	Fe 0.009
Fe^{2+}	3.406	4.622	Mn 0.011
Mn	0.104	0.124	Na 1.154
Ca	1.568	0.007	Ca 0.067
Na	0.432	0.050	K 2.598
Na	0.446		
K	0.386	1.923	
			Ab 30.2
			An 1.8
			Or 68.0

1. Hastingsitic hornblende (γ'=dark green, α'=yellowish green, γ/c=30°, No. 55C); 2. Fe-biotite (γ'=black, α'= yellowish brown, No. 55C); 3. Orthoclase (No. 55C).

These rocks are different from the pyroxene-amphibole gabbro and diorite in many respects. Their fresh colours are grey or brownish-grey and on weathered surfaces they are always brown. The grain sizes are variable but usually coarse- or medium-grained. Oriented, foliated varieties are not as common as in the pyroxene-amphibole gabbro or diorite. They occur in the western part of the plutonic complex. According to the plagioclase composition and SiO_2 content, two varieties were distinguished:

— olivine-amphibole pyroxene gabbro and olivine-amphibole-pyroxene diorite

Olivine-amphibole-pyroxene gabbro: The main constituent is plagioclase (74V%, average: An_{55}). The coarse-grained variety contains large tabular and finer-grained one has lath-shaped plagioclase, some of which are zoned. Strongly deformed (bent twin lamellae, wavy extiction), granulated plagioclases were observed only in the sheared zone. The crystals show ordered structure, indicating a typical plutonic origin. The most frequent twin law is albite, but albite/ala, albite/pericline, acline/pericline laws were also observed. Olivine occurs in every sample (Fo_{60-70}, Table 8). They are subhedral, or less commonly euhedral, transected by cracks and cleavages where very fine-grained "dust-like" magnetite occurs. They are usually surrounded by pyroxene or brown hornblende. Bowlingite (saponite) is the most common alteration product, although serpentinization was also observed. Bowlingite occurs along the rims and cracks (cleavages), or sometimes the whole olivine crystal has been altered to bowlingite. Every sample contains pyroxene in a variable amount (0.32—27V%). They form large tabular or prismatic crystals. The tabular ones commonly show ophitic texture. They are colourless or slightly pinkish and greenish. (100) parting is common, containing ilmenite, which is characteristic of diallage. The composition is salite-augite (Table 8). The rims of the crystals are usually altered to amphibole. Some form aggregates with olivine and brown hornblende. In this case, a sharp boundary occurs between the brown hornblende and pyroxene indicating the later stage of crystallization of amphibole. The amphibole is rather common. Two varieties can be distinguished: magnesio-hastingsite (Table 8) formed from pyroxene (uralitization) and strongly pleochroic or tabular (sometimes with ophitic texture) kaersutite (Table 8). They occur separately and around the pyroxene or ilmenite. This type of amphibole indicates an alkaline enrichment during the later stage of crystallization. Biotite is very rare and mostly occurs around the kaersutitic hornblende. It forms very small, prismatic, strongly pleochroic crystals (γ'= dark-reddish-brown, α'= yellowish-brown).

Two kinds of opaque minerals were distinguished: magnetite, which occurs along the cleavages and cracks of olivine; ilmenite which is anhedral and mostly surrounded by kaersutite and biotite. Apatite occurs in an accessory amount. Average SiO_2 content is less than 50 wt% (Table 2a).

Olivine-amphibole-pyroxene diorite: mineralogical composition of this rock is the same as the olivine amphibole pyroxene gabbro, although some differences can be observed in detail.

The following features are characteristic of this rock: /1/ An content of plagioclase less than 50 mol% (Average: An_{43}); /2/ zoned plagioclases are common; /3/ biotite is more common; /4/ SiO_2 is more than 50 wt% and Al_2O_3 content (Table 2a) is lower than in gabbro. This rock is the marginal facies of the olivine-gabbro intrusion and represents a slightly lower crystallization temperature.

Microprobe analyses of olivine, clinopyroxene, amphibole and plagioclase from olivine gabbro and diorite

	OLIVINE			PLAGIOCLASE		PYROXENE			AMPHIBOLE			
wt %	1	2	3	4	5	6	7	8	9	10	11	12
SiO_2	35.52	36.72	36.11	56.52	57.96	51.59	49.93	51.90	42.34	41.30	42.98	43.32
TiO_2	0.03	-	0.02	0.02	0.07	0.56	1.50	0.73	4.34	5.52	3.36	4.76
Al_2O_3	0.02	0.02	0.03	27.57	26.48	2.49	4.03	1.61	12.07	12.48	10.59	10.15
FeO	34.59	26.85	35.78	0.16	0.12	8.64	6.48	9.20	13.27	10.04	14.83	12.36
MnO	0.75	0.60	0.69	-	0.02	0.41	0.23	0.33	0.25	0.18	0.29	0.23
MgO	29.01	35.58	26.22	0.02	-	14.32	14.02	14.31	12.62	13.16	11.30	12.69
CaO	-	-	0.04	11.38	10.27	21.05	22.70	21.41	11.04	11.84	10.38	11.22
Na_2O	-	-	0.01	4.21	4.84	0.37	0.67	0.33	2.49	2.73	2.85	2.27
K_2O	-	-	0.02	0.17	0.16	-	0.03	0.03	0.58	0.49	0.95	0.96
Σ	99.92	99.77	98.92	100.05	99.92	99.43	99.59	99.85	99.00	97.74	97.53	97.96
						Numbers of ions on the basis of						
		4 (o)		32 (o)			6 (o)				23 (o)	
Si	0.987	0.983	1.018	10.140	10.375	Si 1.931	1.864	1.942	Si 6.119	6.059	6.387	6.377
Al	0.001	0.001	0.001	5.831	5.588	Al^{IV} 0.069	0.136	0.058	Al^{IV} 1.881	1.941	1.613	1.623
Ti	0.001	-	-	0.003	0.010	Al^{VI} 0.041	0.041	0.013	Al^{VI} 0.175	0.217	0.242	0.138
Mg	1.202	1.419	1.101	0.005	-	Ti 0.016	0.042	0.021	Ti 0.472	0.609	0.375	0.527
Fe	0.804	0.601	0.843	0.024	0.018	Mg 0.799	0.780	0.798	Fe^{3+} 0.532	-	0.311	0.063
Mn	0.018	0.014	0.016	-	0.003	Fe 0.271	0.202	0.288	Mg 2.719	2.878	2.503	2.784
Ca	-	-	0.001	2.187	1.969	Mn 0.013	0.007	0.011	Fe^{2+} 1.072	1.232	1.532	1.459
Na				1.464	1.680	Ca 0.844	0.908	0.859	Mn 0.030	0.022	0.037	0.029
K				0.039	0.037	Na 0.027	0.048	0.024	Mn 0.001	-	-	-
						K -	0.001	0.001	Ca 1.710	1.861	1.653	1.770
									Na 0.289	0.139	0.347	0.230
									Na 0.409	0.638	0.474	0.418
									K 0.107	0.092	0.180	0.180
						Atomic ratios						
Mg	59.9	70.2	56.6	Ab 39.7	45.6	Mg 39.8	38.4	39.6				
Fe	40.1	29.8	43.4	An 59.3	53.4	Fe 16.9	14.5	16.6				
				Or 1.0	1.0	Ca 43.3	47.1	43.8				

1. Olivine from gabbro (No. 221); 2. Olivine from gabbro (No. 304); 3. Olivine from diorite (No. 50); 4. Labradorite from gabbro (No. 221); 5. Labradorite from gabbro (No. 304); 6. Augite from gabbro (No. 221); 7. Salite from gabbro (No. 304); 8. Augite from diorite (No. 50); 9. Magnesio-hastingsite from gabbro (No. 221); 10. Kaersutite from gabbro (No. 304); 11. Kaersutite from diorite (No. 50); 12. Magnesian hastingsitic-hornblende from diorite (No. 52).

Pegmatites are white, coarse-grained, feldspar-rich dikes in the plutonic and sometimes in the metamorphic complexes. They have different composition depending on their occurrences. The feldspar of the pegmatite which occurs in pyroxene-amphibole gabbro and diorite is sodium rich (An_{32}). It contains orthoclase microperthite, cross-hatched microcline and biotite. The pegmatites near the nepheline syenite contain nepheline. Dikes, that transect the calcareous metamorphic rocks are very rich in alkalies due most probably to limestone assimilation. The pegmatitic dike rocks in olivine gabbro or diorite are calcium rich. The composition of plagioclase is labradorite (An_{56}), which commonly has been altered to zoisite and prehnite.

SUMMARY

a. Petrochemistry of plutonic rocks. The majority of the plutonic rocks belong to the alkali-calcic suite. The alkali-lime index of the pyroxene-amphibole gabbro-diorite series is 54 and the olivine gabbro-diorite is 55. Beside the two main gabbro-diorite series, a minor amount of alkaline rocks also occur. Nepheline syenite most probably formed by differentiation and assimilation (alkali-lime index: 44). The average bulk chemical composition of the Bulfat plutonic rock shows a different trend from the calc-alkaline suite *(Fig. 3)*.

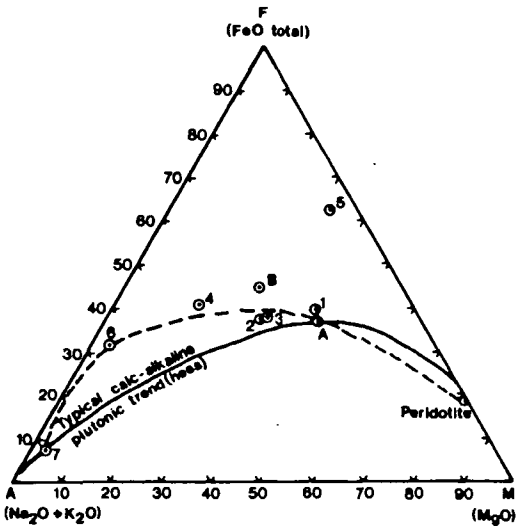

Fig. 3. AFM plot of Bulfat plutonic rocks. 1. Harzburgite; 2. Pyroxene gabbro; 3. Pyroxene diorite; 4. Pyroxene-amphibole diorite; 5. Contaminated pyroxene diorite; 6. Contaminated pyroxenite; 7. Nepheline syenite; 8. Pegmatite A. Olivine gabbro, B. Olivine diorite.

The Bulfat pyroxene gabbro has higher Ca and lower Mg or Fe contents than the average calc-alkaline gabbro. In the diorite, not only the Ca but also the Na content is high, the higher Fe content of pyroxene and larger amount of amphibole correspond with the normal trend of differentiation. Na-rich alkali-nepheline syenite crystallized during the later stage of differentiation.

The higher Ca content, together with alkali enrichment, suggests contamination and assimilation.

The olivine gabbro contains high Al and Na and low Fe, Mg and Ca. This olivine-bearing rock differs from the pyroxene-amphibole gabbro-diorite series with respect to chemical and mineralogical compositions and most probably represents a well-differentiated, feldspar-rich younger intrusion.

b. Composition of rock-forming minerals: The crystal differentiation can be followed by compositional changes of rock-forming minerals. The anorthite content of plagioclases decreases from the gabbro to nepheline syenite (Table 9, *Fig. 4).* Albite-rich plagioclase occurs together with potash feldspars and nepheline at the latter stage of magmatic differentiation.

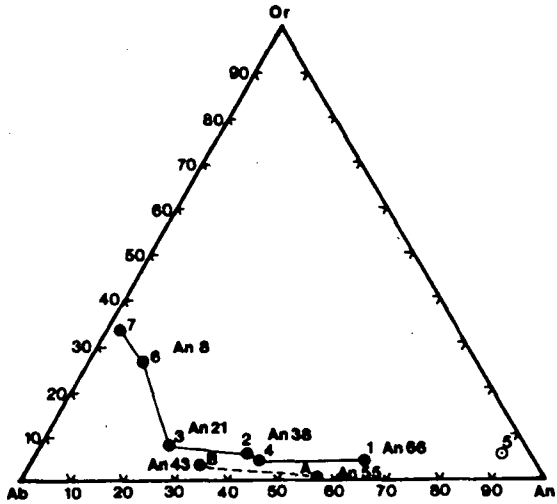

Fig. 4. Ab-An-Or CIPW plot of plutonic rocks of Bulfat. 1. Pyroxene gabbro; 2. Pyroxene diorite; 3. Pyroxene-amphibole diorite; 4. Contaminated pyroxenite; 6. Nepheline syenite; 7. Pegmatite. A. Olivine gabbro. B. Olivine diorite.
Remark: An content of plagioclases measured by optical or microprobe methods

Ca-rich clinopyroxene (salite) occurs in gabbro. Their Ca content decreased toward the latter stage of crystallization and augite crystallized in the pyroxene-amphibole diorite. The iron content of amphibole increases (100 Mg/Mg+Fe=61, 54, 13) towards the more acidic members of sequences.

Similar trends can be observed in the olivine gabbro and diorite; Fe enrichment is characteristic of the latter stage of crystallization (Table 9).

c. Contaminations: the Quandil metasediment (mostly calcareous) was partly assimilated by the basic intrusion. This assimilation contaminated the magma and shifted its (calc-alkaline) composition towards the alkalic-suite. The contamination is inferred from the following observations: /1/ The gabbro is rich in Ca and poor in Mg and Fe. /2/ Nepheline norms and mods are common, especially at the immediate contact with calcareous xenoliths and at the top of the whole magmatic sequence. The very small nepheline syenite occurrences are completely surrounded by calcareous rocks. /3/ Presence of Ti-augite (80 V%) between the igneous and calcareous rocks. Assimilation of calcareous rocks most probably caused Ca enrichment in the magma and dilution of all other elements (Mg, Fe, Si, Al, etc.)

Silica deficiences resulted from this dilution and nepheline appeared in addition to plagioclase. Silica deficiences could have resulted from reaction

between the magmatic plagioclase, ilmenite and calcite, resulting in the crystallization of Ti-augite, nepheline and wollastonite.

calcite + plagioclase + ilmenite = Ti-augite + nepheline + wollastonite

The possibility of depletion of aluminium from the magma is not excluded because of the presence of Al-rich Ti-augite and gehlenite at the immediate contact.

TABLE 9

Composition of rock forming-minerals

Rock name	Plagioclase An %	Olivine Fo	Clinopyroxene Ca	Mg	Fe	Amphibole $Mg/Mg+Fe^{2+}$	Elevation (m)
Pyroxene gabbro	66	-	49	31	20	-	2050
Pyroxene diorite	38	-	49	28	23	0.61	1680
Pyroxene-amph. diorite	21	-	44	36	20	0.57	1420
Nepheline syenite	8 orthoclase+nepheline	-	-	-	-	0.13	2240
Contaminated rocks:							
Pyroxene diorite	36 (nepheline)	-	47	23	30	-	1860
Pyroxenite	-	-	46	18	36	-	2040
Olivine gabbro	55	65	45	39	16	0.71	
Olivine diorite	43	57	44	39	17	0.64	

ACKNOWLEDGEMENTS

Thanks are due to the team of Czech geologists who carried out the geological mapping of the area and collected samples. Grateful acknowledgement is made Dr. Z. KOTROBA, Dr. P. JAKEŠ and Dr. Z. SULČEK for electronmicroprobe and chemical analyses. The writer would like to acknowledge the chemists of Geological Survey and Mineral Investigation of Iraq for rock chemical analyses of some samples. Finally we are grateful to Dr. W. S. AL-HASHIMI the Head of the Petrological and Mineralogical Department for his constant encouragement throughout the various stages of work.

REFERENCES

BUDA G., HASHIMI W. S. AL. (1977): petrology of Mawat ophiolitic complex, Northern Iraq. Journ. Geol. Soc. Iraq. **10**. 60—98.

BUDA G., SAHAGIAN G. and SALEM W. (1978): Igneous and metamorphic petrology of Qalah Dizeh area. D. G. Geol. Surv. Min. In., Baghdad (Manuscript), 117.

BUDA G., (1988): Chromite occurrences in Iraqi Zagros. Act.Min.Pet.Szeged. **XXIX**, 69—79.

JASSIM, S. Z., WALDHAUSROVA, J. and SUK, M. (1982a): Evolution of magmatic activity in Iraqi Zagros complexes. Krystalinikum. **16**, 87—108.

JASSIM, S. Z., BUDA, G., NEUŽILOVA, M. and SUK, M. (1982b): Metamorphic development of the Iraqi Zagros Ophiolitic Zone. Krystalinikum. **16**, 21—60.

MASEK, J., ETABI, W. (1973): Petrology of Mawat igneous metamorphic complex. NIMCO report SOM Library. Baghdad. (Manuscript), 49.

STRECKEISEN, A. (1967): Classification and nomenclature of igneous rocks. Neues Jb. Mineral. Abb. **107**, 144—240.
THAYER, T. P. (1964): Principal features and origin of podiform chromite deposits and some observations on the Guleman Soridag District. Turkey. Econ. Geol. **59**, 1497—1524.

Manuscript received, 10 April, 1993

Acta Mineralogica-Petrographica, Szeged, XXXIV, 41—50, 1993

AGE OF BEITAN GNEISS; IMPLICATION FOR LATE PRECAMBRIAN CRUSTAL EVOLUTION IN SOUTH EASTERN DESERT, EGYPT

M. F. GHONEIM*, S. M. ALY*

Department of Geology, Faculty of Science, Tanta University

and

M. H. EL-BARAGA**

Geological Survey of Egypt.

ABSTRACT

The gneiss-migmatite rocks of Hodein area, which represents the southeastern extension of Beitan Gneisses, cover about 98 km^2 and trend NW-SE. These rocks are overthrusted by supracrustal cover mainly arc-ophiolite assemblage and granitic rocks. Petrologically, the rocks are divided into biotite-gneisses, hornblende-gneisses, biotite-hornblende-gneisses, garnet-biotite-hornblende-gneisses and augen-biotite-gneisses.

The whole rock Sm-Nd isochron age of the Beitan gneisses yield 889±8 Ma (MSWD=8.5) which is consistent with Rb-Sr age (863±15 Ma, MSWD=9). This rock has initial ϵ^{i}_{Nd} and ϵ^{i}_{Sr}-values (-8.6 and +9.5, respectively) which reveals the age of early Pan-African. Moreover, the Nd-model age (T_{DM}) of these rocks range from 1.46 to 2.65 Ga, negative ϵ^{i}_{Nd} and low ϵ^{i}_{Sr}-values reveal the existence of early Pan-African continental crust. The data are tested against mantlecrust mixing model. It is suggested that these rocks were derived throughout assimilation of about 35—50% Nd-enriched, slightly Sr-depleted lower crust component by a mildly depleted subcontinental mantle source.

INTRODUCTION

The Pan-African thermo-tectonic event originally proposed by KENNEDY, (1964) is now widely accepted to cover a longer lapse of time between 450—550 Ma. The gneiss and migmatites have a limited distribution in the Eastern Desert (*Fig. 1*). Earlier investigators considered these gneisses to be fragmenets of much older continental crustal (HUME 1934). STURCHIO et al. (1983) considered the Meatiq gneisses as one of the classical examples of the famous gneisses in the Eastern Desert, to have formed from sheared and recrystallized felsic igneous rocks at 580—625 Ma accompanying the development of metamorphic core complex. On the other hand, DIXON (1979) HASSAN and HASHAD (1990) believe that the Pan-African basement exposed in the Meatiq area, consists of an infracrustal basement overthrusted by a supracrustal cover. The infracrustal rocks

* Tanta, Egypt
**Cairo, Egypt

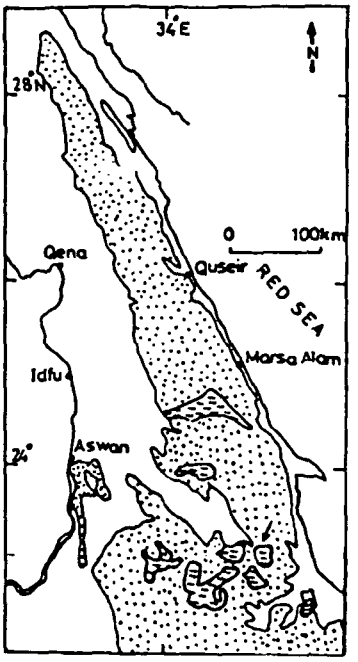

Fig. 1. Distribution of gneisses belts in Egypt, (Arrow denotes the studied area).

developed as a result of Meatiq orogeny, where granitic-gneisses; migmatite-gneisses and migmatized-amphibolites were formed.

EL GABY *et al.* (1988) suggested that the Archaean nucleus located in the southwestern corner of Egypt was fringed by an early Proterozoic continental mass (HARRIS et al. 1984) that extended past Aswan into the Eastern Desert, at least as far as Wadi Sikait on the eastern flank of the Hafafit Swell. The old continent was fringed by an island arc ca.700—800 Ma ago. Around 700 Ma ago, the island arc was swept against the old continent, there by thrusting back-arc ophiolites and the island arc volcanics and volcanoclastics onto the margin of the old continent. Intrusion of subduction-related and mantle-derived magmas induced softening and remobilization of the early Proterozoic continental crust or "infrastructure" around 655 Ma ago.

The radiometric ages obtained from the Feiran gneisses in southern-Sinai yield 682-641 Ma (BENTOR 1985). Gneisses from the Uweinat area in SE-Libya prove a Late-Archaean age as well as a Mid-Proterozoic event (KLERKX and DEUTSCH 1977; HARRIS et al. 1984). The oldest Pan-African rock type in the Nubian Desert Gneisses have their Rb-Sr age of 918±40 Ma (MSWD=34.1, $(^{87}Sr/^{86}Sr)_i$= 0.7167±7), whereas $^{143}Nd/^{144}Nd)_i$= 0.511152 and ϵ^t_{Nd}=-15.8 and T_{CHUR} = 2004 Ma; EL GABY *et al.* 1988). EL GABY et al. (op. cit.) show that negative ϵ^t_{Nd}-value indicates that within the continental plate of NE-Africa during the Pan-African episode involved reworking of pre-existing crust. These isotopic data are suspected to consider that large regions of the south Eastern Desert consist of pre-Pan-African gneisses, and separated by ophiolites. They substantiate the incorporation of

some old continental crust at least in parts of the Eastern Desert (EL GABY *et al.* 1988). KRÖNER *et al.* (1988) suspected that no conclusive evidence exists for the presence of pre-Pan-African crust in the Eastern Desert of Egypt. They emphasised that the evolutionary scenario for the Eastern Desert favour the hypothesis of accretion of new crust along a highly irregular active plate margin.

The present paper is aimed to assign age of emplacement of Hodein gneisses to help in regional correlation and geological interpretation of this rock as well as to examine the nature of pre-existing crust in wadi Beitan area.

GEOLOGIC SETTING

The Hodein area is located in the south Eastern desert of Egypt and composed of an assemblage of Precambrian rocks including gneisses and migmatites, supracrustal mainly arc-ophiolite (metavolcanics and volcanoclastic metasediments and metagabbro complex) and Older Granites. The gneisses-migmatites rocks are recorded in elongated low-lying belt, trending mainly NW—SE which parallel to the old structural trend dominated in south Eastern Desert. The gneisses-migmatite belt covers ca. 98 km^2 (ca.22 km in length and ranging between 1—10 km in width.) Moreover, contact between gneisses-migmatites and metagabbro complex is marked by a thin zone (ca.1—3 m width) of schistose, sheared and mylonitized rocks from both rock units developing along a thrust fault trending NW—SE and dip gently toward NE. The contact against the tonalite and granite is sharp and irregular. The gneiss-migmatite rocks are sometimes banded by foliated granite and containing off-shoots and apophysis from granites inside it.

The gneisses under consideration are highly foliated and composed mainly of fine to medium grained biotite-gneisses, hornblende-gneisses, biotite-hornblende-gneisses, garnet-biotite-hornblende-gneisses, augen-biotite-gneisses, para-amphibolites and mylonites.

SAMPLING AND ANALYTICAL TECHNIQUES

At Hodein area four gneiss samples were selected on the basis of both field and petrographic studies. Whole rock samples were analysed for Rb-Sr and Sm-Nd isotopic compositions at the Mineralogical-Geological Museum in Oslo, Norway. The chemistry and mass spectrometry procedures were described by MEARNS (1986). Laboratory total system blanks are typically ≤1ng for both Nd and Sr and are thus negligible for this study. Blank concentrations were measured by isotope dilution using mixed ^{87}Rb-^{84}Sr and ^{149}Sm-^{148}Nd spikes. Rb-Sr were loaded on Ta-Re single filament while Sm-Nd were loaded on the side filament of a double Re filament assembly. Isotopic ratios were measured on a VG 354 fully automated 5-collector peak hopping and static modes. Nd measurements were normalised to yield a $^{146}Nd/^{144}Nd=0.7219$. The decay constant used for $\lambda Sm=6.54\cdot10^{-12}y^{-1}$ and $\lambda Rb=1.42\cdot10^{-11}y^{-1}$. ϵ^{t}_{Nd} and ϵ^{t}_{Sr} values are calculated relative to CHUR with present day $^{147}Sm/^{144}Nd=0.1967$, $^{143}Nd/^{144}Nd=0.512647$, $^{87}Rb/^{86}Sr=0.0827$, and $^{87}Sr/^{86}Sr=0.7045$ (ALLÉGRE *et al.* 1983), using Rb-Sr ages to correct for in situ radiogenic ^{143}Nd.

Rb-Sr and Sm-Nd Geochronology

The whole rock Rb/Sr and Sm/Nd isotopic data for the samples from Wadi Beitan gneisses are given in Table 1. The slope and intercept were determined using the regression method formulated by YORK (1969). The slope and intercept are given at the 2 sigma (68% confidence level). The four points yield a whole rock Rb-Sr isochron age of 863±15 Ma (MSWD=9, *Fig. 2A*) and initial $^{87}Sr/^{86}Sr$ isotopic ratio of 0.70412±0.00005. The provided age is in agreement with that calculated by Sm-Nd method which assign 889±8 Ma (MSWD=8.5, *Fig. 2B*), with initial $^{143}Nd/^{144}Nd$ ratio 0.51104±0.000002.

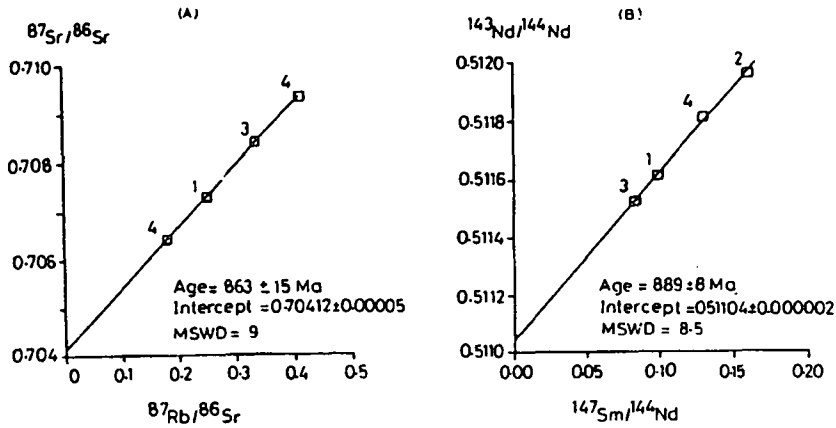

Fig. 2. (A) Rb-Sr and (B) Sm-Nd isochron diagrams for Beitan gneisses.

The assigned age shows that the Wadi Beitan gneisses pertain to the early Pan-African time (near by 863 Ma) similar to other rocks formed during the major magmatic episode affecting the southwestern part of the Eastern Desert between 1000—850 Ma (HASHAD 1980). Neverthless, the calculated initial $^{87}Sr/^{86}Sr$ isotopic ratios of Wadi Beitan gneisses are around 0.7051 (BENTOR 1985). STURCHIO *et al.* (1983) proved that low initial $^{87}Sr/^{86}Sr$ (ca 0.7030) indicate a lack of remelted older continental crust. Therefore, the initial $^{87}Sr/^{86}Sr$ ratios greater than 0.705 are most likely to represent various degrees of contamination by more radiogenic crustal material and/or due to partial melting of the upper mantle or lower crust. A mixing hypothesis of the present rocks is clarified by plotting $^{87}Sr/^{86}Sr$ ratios versus their corresponding 1/Sr values which should bear a linear trend with positive slope among two isotopically and chemically distinct components mixed in various proportions (*Fig. 3*). Although, the Wadi Beitan gneisses have moderately high initial $^{87}Sr/^{86}Sr$-isotopic ratios, they, however lie within the range reported for that of the Eastern Desert of Egypt (HASHAD 1980; BENTOR 1985; STERN 1979). The present initial $^{87}Sr/^{86}Sr$ ratios (0.70412) are too low for rocks to have been derived from old upper sialic crust (0.7369) and higher than the upper mantle (0.70362) range of FAURE and POWELL (1972). Similarly the initial $^{143}Nd/^{144}Nd$ ratios of this gneiss rocks (0.511528—0.511972) are lower than that of CHUR (0.512638; DEPAOLO and WASSERBERG 1976). *Figs. 4* and *5* show the initial $^{143}Nd/^{144}Nd$ ratios relative to the growth line of CHUR which indicate that

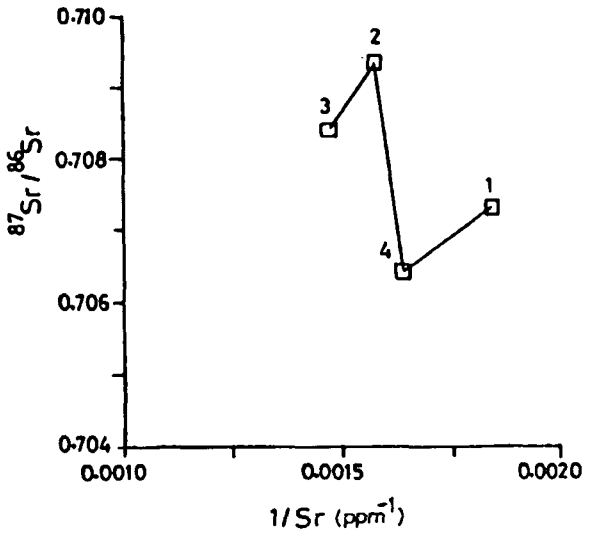

Fig. 3. $^{87}Sr/^{86}Sr$ vs. 1/Sr ratio diagram.

the Beitan gneiss is formed by residual solution derived from the depleted mantle source (FAURE 1986, p.210). They might have mixed source of a depleted upper mantle and lower crustal component.

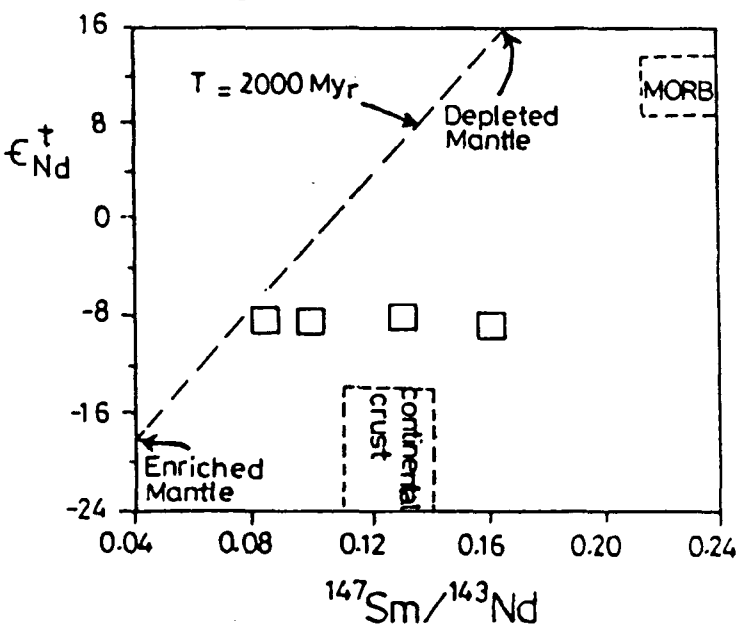

Fig. 4. ϵ^t_{Nd} vs. $^{147}Sm/^{144}Nd$ diagram (MCCULLOCH *et al.* 1983) for the studied gneisses.

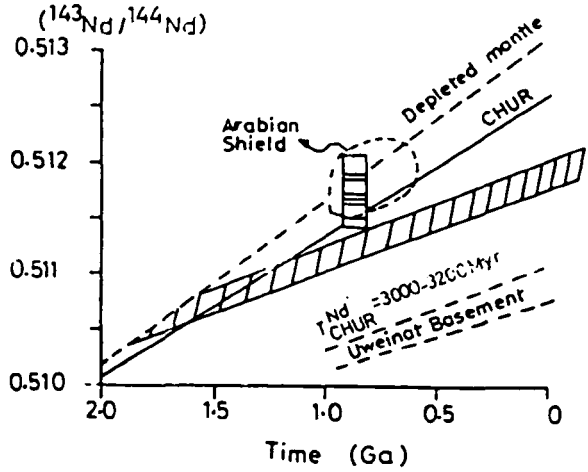

Fig. 5. ($^{143}Nd/^{144}Nd)_i$ vs. time variation diagram for the studied gneisses. The stippled region is taken from HARRIS *et al.* (1984). Field of Arabian data taken from DUYVERMAN *et al.* (1982).

It is worth to mention that the full agreement of the assigned age both Rb-Sr and Sm-Nd methods would suggest isotopic homogenization during the above mentioned mixing either during rejuivenation with early Pan-African magmatic crust or else, during a regional metamorphic event as suggested by EL SHAZLY *et al.* (1973), similar to the Abu Swayel metasediments.

Nd and Sr Isotopic Characteristics

The calculated ϵ^t_{Nd}-values at 863±15 Ma of the Wadi Beitan gneisses are negative and ranging as low as -8.6 (Table 1). DUYVERMAN *et al.* (1982) show similar range of ϵ^t_{Nd}-value for the Darmara granite Saudi Arabia. They considered that these ranges characterise a moderate degree of remobilisation of pre-existing crust. Meanwhile, the narrow range of calculating ϵ^t_{Sr}-values (+9.7 to +9.5) suggest again isotopic homogenity at the time formation due to mixing and/or partial melting. However, Wadi Beitan gneisses have ϵ^t_{Nd} (-8.6) and ϵ^t_{Sr} (+9.5) which favour an enriched mantle source (HARMS *et al.* 1990) and lie near the continental crust on DEPAOLO 1981, Fig.6). It is noted that the low ϵ^t_{Nd}-value from the Pan-African samples primarily reflect the age of Pre-existing crust (HARRIS *et al.* 1984).

The calculated Nd-model ages (T_{DM}) relative to the depleted mantle (DEPAOLO 1981) for the Wadi Beitan gneisses yield range from 1.46 to 2.65 Ga (Table 1). This Nd-model ages is comparable with that of magmatic plutonism in the Eastern Desert as described by HARRIS *et al.* (1984). They considered that such isotopic variations reflect derivation of these rocks from mixed source, including both Archean and Pan-African materials. Accordingly, both the calculated model-Nd ages as well as the low ϵ^t_{Nd} and ϵ^t_{Sr} of the studied gneiss samples reinforces the extraction of the protoliths from mantle material of an early/middle Proterozic crust *(Fig. 6)*.

TABLE 1

Rb/Sr–Sm/Nd isotopic data of Gneiss from Eastern Desert, Egypt.

Rb (ppm)	Sr (ppm)	$\frac{(^{87}Rb}{^{86}Sr)\ at}$	$\frac{(^{87}Sr^{*}}{^{86}Sr)\ + 2\sigma}$	$\frac{(^{87}Sr}{^{86}Sr)\ i^{**}}$	ϵ^{i}_{Sr}	Sm (ppm)	Nd (ppm)	$\frac{(^{147}Sm}{^{144}Nd)\ at}$	$\frac{(^{143}Nd^{*}}{^{144}Nd)\ + 2\sigma}$	$\frac{(^{143}Nd}{^{144}Nd)_{i}^{**}}$	ϵ^{i}_{Nd}	T_{DM} (Ga)
47	542	0.250876	0.707314+10	0.707326	9.5	2.35	15.00	0.098724	0.511613+17	0.511619	-8.5	1.56
90	634	0.410773	0.709361+24	0.709368	9.5	1.70	13.20	0.159219	0.511694+41	0.511972	-8.6	2.65
79	680	0.336145	0.708421+13	0.708415	9.7	3.90	11.42	0.083116	0.511527+29	0.511528	-8.4	1.46
38	610	0.180209	0.706422+20	0.706424	9.6	3.60	18.20	0.129170	0.511812+15	0.511796	-8.1	1.82

ϵ^{i}_{Nd} and T_{DM} are the deviation from the value expected in a chondritic reservoir (CHUR) at time T (863 Ma) and is defined by DEPAOLO (1981).
($\lambda^{87}Rb = 1.42 \cdot 10^{-11}\ yr^{-1}$ $(^{87}Rb/^{86}Sr)^{o}_{UR} = 0.0816$, $(^{87}Sr/^{86}Sr)^{o}_{UR} = 0.7045$, $\lambda^{147}Sm = 6.54 \cdot 10^{-12}\ yr^{-1}$, $(^{147}Sm/^{144}Nd)^{o}_{CHUR} = 0.1967$,
$(^{143}Nd/^{144}Nd)^{o}_{CHUR} = 0.512638$

* Errors refer to least significant digits and are 2σ mean.
** i = initial ratio

From the combined ϵ^t_{Nd}-ϵ^t_{Sr} diagram (*Fig. 6*) it is clear that the Beitan gneiss occupies an area bounded by ϵ^t_{Nd}-values of -8.6 to -8.1 and ϵ^t_{Sr}-values +9.5 to +9.7, and fall in range of ϵ^t_{Nd}-values (+7.5 to -10.3). It characterises Pan-African rocks of NE-Africa (HARRIS *et al.* 1984) and to that reported by HARMS *et al.* (1990) (-8.8 to -5.3). Meanwhile, the negative ϵ^t_{Nd} and positive ϵ^t_{Sr}-values offered by the present gneisses simply the presence of old basement beneath the southern Eastern Desert, which strongly supports the role of assimilation of enriched, continental crust by basaltic magma derived from a depleted subcontinental mantle source (*Fig. 6,* HARMS *et al.* op. cit.).

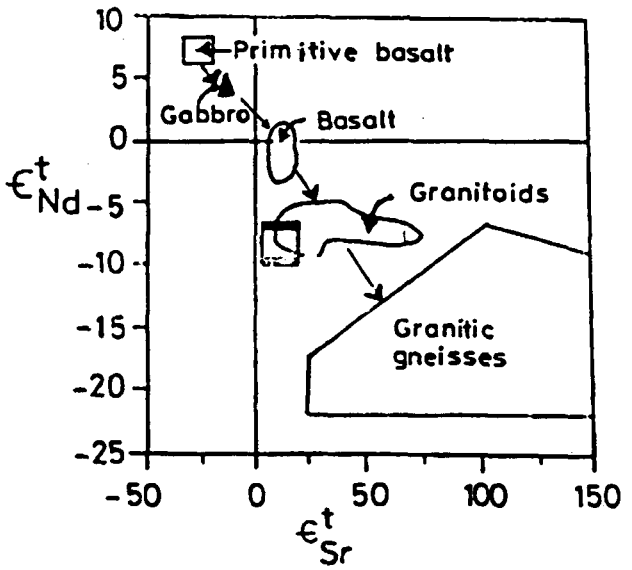

Fig. 6. ϵ^t_{Nd} vs. ϵ^t_{Sr} variation diagram shows Nd isotope characteristics of gneisses and granitoids, from southern Egypt and northern Sudan. Curve are indicating probable paths of mixing of mantle and crustal rocks. Fields are taken from HARMS *et al.* (1990).

ORIGIN AND SOURCE OF MAGMA

The narrow range of the initial ϵ^t_{Nd} and moderate initial ϵ^t_{Sr} values of the studied gneiss samples emphasis some constraints on the possible source region and the processes which may have been involved in the formation of this rock. The data simply preclude a single mantle or crustal source.

The source of the gneiss and granitoid rocks in the Arabian-Nubian Shield are still a matter of debate (HARRIS *et al.* 1984; HARMS *et al.* 1990, SULTAN *et al.* 1990). Some workers consider the Arabian Shield had been originated from juvenile mantle-derived oceanic and intra-oceanic island arc (DUYVERMAN *et al.* 1982; STERN and HEDGE 1985; HARRIS *et al.* op. cit.). The available combined isotopic data on the studied gneisses, show strong negative initial ϵ^t_{Nd} (-8.1 to -8.6) and low ϵ^t_{Sr} (+9.5 to +9.7) narrow ranges. These obviously reflect the role

of crustal contamination during their petrogenesis. This also was confirmed by the $^{87}Sr/^{86}Sr$-1/Sr binary plot which enhanced the role of crustal contamination during the evolution of the studied gneisses (*Fig. 3*). However, the well-defined isochrons shown by most of the studied gneiss rocks *(Fig. 2)* imply that the magmas were isotopically homogenous after interaction with the crustal material. In this approach a mixing model (DEPAOLO 1981) by assimilation of upper and lower crustal rocks (UC and LC, respectively; FAURE 1986) in basaltic magma derived from mildly depleted mantle source (M. FAURE op. cit.) are included in *Fig. 7* with hypothetical mixing trends (M-UC and M-LC). Also, the gneisses (A; sample no. Nd-G6) from SW-Egypt (HARMS et al. 1990) are used as Pan-African crustal end member to construct the mixing trends (M-A, *Fig. 7*). The values of weight percent of the crustal contamination in mafic melt are indicated on the curves shown in *Fig. 7.*

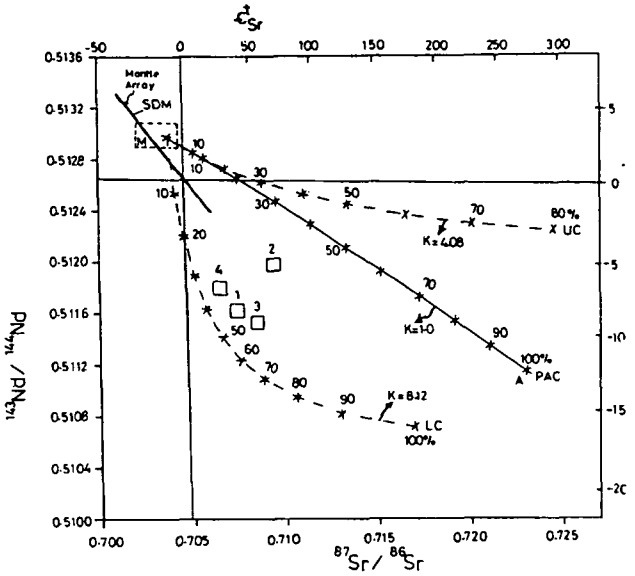

Fig. 7. Isotopic composition of initial Nd and Sr ratios among the analyzed gneisses. Solid line "Mantle Array" (ALLÉGRE *et al.* 1983, O'NIOS *et al.* 1977). The degree of crustal contamination is marked with intervals of 10%. SDM: The strongly depleted source of MORB ($^{87}Sr/^{86}Sr$=0.7025, $^{143}Nd/^{144}Nd$=0.5132) (DEPAOLO 1981); M: a mildly depleted mantle average Colombia River Basalt ($^{87}Sr/^{86}Sr$=0.70362, $^{143}Nd/^{144}Nd$=0.5130)(CARLSON *et al.* 1981); UC: upper crust, average of Paleozoic granitic rocks from Berridale, southereastern Australia ($^{87}Sr/^{86}Sr$=0.7369, $^{143}Nd/^{144}Nd$=0.51212) (MCCULLOCH and CHAPPELL 1982); LC: Lower crust, average of early Precambrian granulites from the Fyfe Hills, East Antarctica ($^{87}Sr/^{86}Sr$=0.7107, $^{143}Nd/^{144}Nd$=0.51071) (DEPAOLO *et al.* 1982); A: average of granitic gneisses, southeastern Egypt, sample no.ND-G6 ($^{87}Sr/^{86}Sr$=0.72304, $^{143}Nd/^{144}Nd$=0.511152) (HARMS *et al.* 1990); PAC: Pan-African Crust and K: Degree of curvature.

The plots of Wadi Beitan gneisses lie within a limited area bounded by $^{143}Nd/^{144}Nd$ (0.511528—0.511972) and 87Sr/86Sr (0.706424—0.709368). The sample plots also lie close to the M-LC trend which correspond to contamination of mantle derived magma by crustal rocks of low ϵ^t_{Sr} in the Late-Proterozoic time. Hypothetical mixing model M-LC trend suggests that the Wadi Beitan gneisses have experinsed about 35—50% crustal contamination.

The calculated amount of crustal component involved during the formation of the present gneisses proofs a limited Sr-contribution from the crust and assumes assimilation of Sr-poor crustal rocks or mixing with Sr-poor anatectic melt. The high plagioclase stability as a residual phase and extensive fractionation of potash feldspar may explain the low content of Sr in crust derived melt. Nd concentration on the other hand, are unaffected during the fractionating phases. The $^{147}Sm/^{144}Nd$ of the studied samples (Table 1) retain typical gneiss values of 0.083 to 0.159. Accordingly the negative ϵ^{t}_{Nd} of the studied gneisses confirm their dependence on the degree of contamination. Contrasting inference from different isotopic systems (Sr, Nd and Pb) was also described by SULTAN *et al.* (1990) for some granitic rocks in the Nubian Shield. They reported low initial $^{87}Sr/^{86}Sr$ ratio (0.7029) for approximately 20% crustally contaminated Aswan granites. This feature is explained by overshadowing of the Nd and Sr isotopic composition of the older crustal component by more primative material.

CONCLUSIONS

1. The studied part of Beitan gneisses (98 km^2) forms NW-SE trending belt and consist of gneisses-migmatites. The rocks are overthrusted by arc-ophiolite assemblage as well as granitic rocks.
2. Both Rb-Sr and Sm-Nd dating are compatible indicating early Pan-African age; whole rock isochron assign Sm-Nd 889±8 Ma (MSWD=8.5) and Rb-Sr 863±15 Ma (MSWD=9).
3. The calculated initial ratios for both $^{87}Sr/^{86}Sr$ (0.70412± 0.00005) and ($^{143}Nd/^{144}Nd$ (0.51104·0.000002) are generally higher than rocks which have been derived from mantle and lower than that of older upper sialic crust. Meanwhile, the negative ϵ^{t}_{Nd} (-8.1 to -8.6) as well as narrow range o fϵ^{t}_{Sr} (+9.5 to +9.7), suggest a mixed source of a depleted upper mantle and lower crust components. The well defined isochrons of the studied gneiss imply that they were isotopically homogeneous after the above mentioned mixing.
4. The relatively high values of initial $^{87}Sr/^{86}Sr$ ratio and low $^{143}Nd/^{144}Nd$ as well as negative value of ϵ^{t}_{Nd} as compared with CHUR, all together favour essential para-origin of Beitan gneiss (Para-gneisses).
5. The Beitan gneiss plots lie close to the mantle-lower crust trend (M-LC) which correspond to contamination of mantle derived magma by crustal rocks. Hypothetical mixing model (DEPAOLO 1981) suggests that Beitan gneisses have experinsed ca. 35—50% crustal contamination.
6. The assigned age of Beitan gneisses would represents the data of homogenization which had took place during rejuvenation of early-Pan-African crust.

REFERENCES

ALLÉGRE C. J., HART S. R. and MINSTER J. F. (1983): Chemical structure and evolution of the mantle and continents determined by inversion of Nd and Sr isotopic data. II Numerical experiments and discussion. Earth Planet. Sci. Lett. **37**, 191—213.

BENTOR Y. K. 1985: The crustal evolution of the Arabo-Nubian massif with special reference to the Sinai Peninsula. Precamb. Res. **28**, 1—74.

CARLSON R.W., LUGMAIR G.W. and MACDOUGALL J. D. (1981): Columbia River volcanism: The question of mantle heterogeneity or crustal contamination. Geochim. Cosmochim. Acta. **45**, 2483—2499.

DEPAOLO D. J. (1981): A neodymium and stronium isotopic study of the Mesozoic calc-alkaline granitic batholiths of the Sierra Nevada and Peninsular Ranges, California. Jour. Geophys. Res. Bull. **86**, 10470—10488.

DEPAOLO D. J. and WASSERBERG G. J. (1976): Nd-isotopic variations and petrogenic models. Jour. Geophys. Res. Lett. **3**, 249—252.

DEPAOLO D. J., MANTON W. I., GREW E. S. and HALPERN M. (1982): Sm-Nd, Rb-Sr and U-Th-Pb systematics of granulite facies rocks from Fyfe Hills, Enderby Land, Antarctica. Nature. **298**, 614—618.

DIXON T. H. (1979): The evolution of continental crust in the Late-Precambrian Egyptian shield. Ph.D. thesis Univ. California, San Diego.

DUYVERMAN H. J., HARRIS N. B.W. and HAWKESWORTH C.T. (1982): Crustal accretion in the Pan-African: Nd and Sr isotope evidence from the Arabian Shield. Earth Planet. Sci. Lett. **59**, 315—326.

EL GABY S., LIST F. K. and TEHRANI R. (1988): Geology, evolution and metallogenessis of the Pan-African belt in Egypt. In: The Pan-African belt of NE-Africa and adjacent areas (eds. S. El Gaby and R.O. Greiling) Friedr, Vieweg Sonn, Braunschweig-Wiesbaden. 17—68.

EL SHAZLY E. M., HASHAD A. H., SAYYAH T. A. and BASSYUNI F. A. (1973): Geochronology of the Abu Swayel area, South Eastern Desert. Egyptian Jour. Geol. **17**, 1—18.

FAURE G. (1986): Pinciples of isotope geology. *2edn*, John Wiley and Sons, 589 p.

FAURE G. and POWELL J. L. (1972): Strontium isotope geology. Springer Berlin.

HABIB M. E., AHMED A. A. and EL-NADY O. M. (1985): Two orogenies in the Meatiq area of the Central Eastern Desert, Egypt. Precambrian Res. **30**, 83—111.

HARMS U., SCHANDELMEIER H. and DARBYSHIRE D. P. F. (1990): Pan-African reworked Early/Middle Proterozoic crust in NE-Africa west of the Nile: Sr and Nd isotope evidence. Jour. Geol. Soc. Lond. **147**, 859—872.

HARRIS N. B. W., HAWKESWORTH C. J. and RIES A. C. (1984): Crustal evolution in north-east and east Africa from model Nd ages. Nature. **309**, 773—776.

HASHAD A. H. (1980): Present status of geochronological data on the Egyptian basement complex. Bull. Inst. Appl. Geol. (Jeddah). **3**, 31—46.

HASSAN M. A. and HASHAD A. H. (1990): Precambrian of Egypt. In: Geology of Egypt (ed. R. Said).

HUME W. (1934): Geology of Egypt. Vol.2, part I. the Metamorphic Rocks. Geol.Surv. Egypt 424p.

KENNEDY G. C. (1964): The structural differentiation of Africa in the Pan-African (+/-500 m.y.) tectonic episode. Res. Inst. Geol. Univ. Leeds, *8th* Annu. Rep. 1962—1963: 48—49.

KLERKX J. and DEUTSCH S. (1977): Resultats Preliminaires obtenus par la methode Rb/Sr sur l age des formations Precambriennes de la region d'Uweinat (Libye). Musee Royal de l'Afrique Centrale, Annual Report. 1976, 83—94.

KRÖNER A., REISCHMANN T., WUST H. J. and RASHWAN A. A. (1988): Is there any Pre-Pan in Pan-African belt of north African (950 Ma) basement in Eastern Desert of Egypt. In: The Pan-African belt of NE-Africa and adjacent areas (eds. S. EL GABY and R. O. GREILING) Friedr, Vieweg Sohn. Braunschweig/ Wiesbaden, 95—119.

MEARNS E.W. (1986): Sm-Nd ages for Norwegian garnet peridotite. Lithos **19**, 269—279.

MUCULLOCH M.T. and CHAPPELL B.W. (1982): Nd-isotopic characteristics of S- and I-type granites. Earth Planet. Sci. Lett. **58**, 51—64.

MUCULLOCH M.T., JAQUES A. L., NELSON D. R. and LEWIS J. D. (1983): Nd and Sr isotopes in Kimberlites and lamproites from Western Australia: an enriched mantle origin. Nature. **302**, 400—403.

O'NIONS R. K., HAMILTON P. J. and EVENSEN N. M. (1977): Variations in $^{143}Nd/^{144}Nd$ and $^{87}SR/^{86}Sr$ ratios in oceanic basalts. Earth Planet. Sci. Lett. **34**, 13—22.

STERN R. J. (1979): Late Precambrian Ensimatic in the Central Eastern Desert of Egypt. Ph.D thesis, Univ. of California, 210p.

STERN R. J. and HEDGE C. E. (1985): Geochronological and isotopic constraints on Late Precambrian crustal evolution in the Eastern Desert of Egypt. Amer. Jour. Sci. **285**, 97—127.

STURCHIO N. C., SULTAN M. and BATIZA R. (1983): Geology and origin of Meatiq dome, Egypt: A Precambrian metamorphic core complex? Geology. 72—76.

SULTAN M., CHAMBERLAIN K. R., BOWRING S. A., ARVIDSON R. E., ABUZIED H. and EL KALIOUBY B. (1990): Geochronologic and isotopic evidence for involvement of pre-Pan-African crust in the Nubian shield, Egypt. Geol. **18**, 761—764.

YORK D. (1969): Least squares fitting of a straight line with correlated errors. Earth Planet. Sci. Lett. **5**, 320—324.

Manuscript received, 3 March, 1993

Acta Mineralogica-Petrographica, Szeged, XXXIV, 51—59, 1993

MIOCENE PYROCLASTICS IN THE PAZSAG-VALLEY, BÜKK-MOUNTAINS, HUNGARY

E. SERES HARTAI*

Department of Geology of Miskolc University

ABSTRACT

The Miocene acidic pyroclastics of the Bükk-Mountains are first of all limited to the marginal parts of the mountains. Only a few small-size disaggregated occurrneces can be found in its central mass. New outcrops were found near the Pazsag- and Hosszú-valleys, beside the foresty road, overlying middle-upper Triassic grey, cherty limestone and argillaceous slate. The pyroclastic material deposited on terrestrial area contains spherical concretions formed around grains of pumice. It has dactitc composition dated about 16 Ma. by K-Ar method.

INTRODUCTION

The rhyolitic tuffs of the Bükk-Mountains have been described first of all from the marginal parts of the mountains. In the central mass of the mountains only a few, decomposed small-size outcrops have been mentioned. BALOGH (1964) found some remains of decomposed tuffs lying south of Nagy-Ökrös. In the karstic holes of the mountains there are some eroded tuffites near Csipkéskút (BALOGH 1957) and Mélysárbérc (JÁMBOR 1961). Based on foraminifers the latters are marine sediments and were deposited in the Middle Miocene.

GEOLOGICAL SETTING

The new outcrops discussed in this study can be found west of Répáshuta, beside the foresty road in Pazsag-valley (*Fig. 1.*). The tuff can be traced in four, morfologically separated plain area of 100—200 m in diameter. At (1) and (3) (*Fig. 1*) there are only fragments of tuffs, while at (2) and (4) real outcrops can be seen. In the case of (1), (2) and (3) the tuff has been preserved in the tectonically preformed karstic dolines of triassic cherty limestone. At the outcrop (4) the tuff is deposited on dark-grey, cross-lamination aleuritic shale. The contact is covered in every case. The tuff is unstratified, but at (2) it has a banked form (*Fig. 2*).

PETROLOGICAL EXAMINATIONS

The studied pyroclastic is a greyish-white, non-decomposed, hard rock. Its main mass consists of fine-grained slightly molten fragments of volcanic glass.

* H—3515 Miskolc-Egyetemváros, Hungary

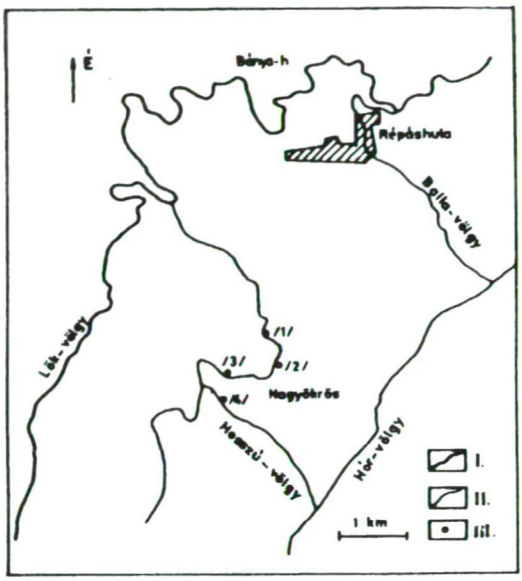

Fig. 1. A sketch about the rhyolite tuff outcrops. Explanation: I. Outcrop locality, II. Road Eger-Miskolc, III. Forestry roads

Fig. 2. Banked dacite tuff in the outcrop

The sizes of the quartz, slightly decomposed felspars and fresh biotite crystals are up to 2 mm. Besides the fragments of crystals it contains dark-grey shale xenoliths of 2—4 mm and flattened pumices of 1—8 cm.

The microscopic texture is vitroclastic, in some places vitro-crystalloclastic. The matrix consists of partially molten fragments of volcanic glass, and it is slightly recrystallized. The sizes of volcanic glass fragments change between 20—150 μ, concave forms are abundant. There are some spheroid-like forms among them. The contours of the glassy fragments are dim, and zeolite, crystobalite and a small amount of clay minerals were formed by the transformation of the matrix. Among the crystal fragments of 0,5—2 mm, the dominant one is the plagioclase (8%), frequently twin-laminated, in some cases it has a zonal structure and its composition is oligoclase — andesine. The fragments of quartz (3%) have a resorption rim in many cases, gas inclusions are frequent. The biotites (4%) are fresh and have pleochroism, in some places — mainly in pumices-underwent a chloritic decay. The amount of the potassium felspars in negligible. Accessory minerals are apatite (80 μ), amphibole (200 μ), zircon (50 μ). The pumice stones are flattened, their piped structure can be noticed as fine fibres. In some cases they have a plastic deformation, the marginal parts are molten, there is no sharp contour to the matrix. Their size extends from 300 μ to a few cm. As xenoliths some fragments of argillaceous shales can be seen (*Fig. 3—6.*).

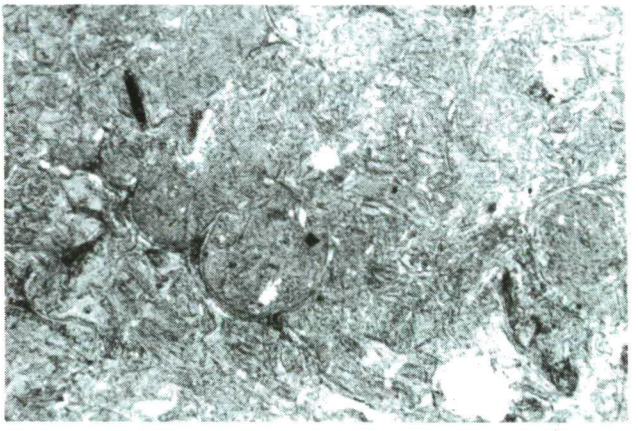

Fig. 3. Slightly baked glassy matrix with spheroid initiatives, plastically deformed glass fragments (N+, 20x)

The data of X-ray diffraction confirm the above mineralogical composition. The microscopically observed zeolite proved to be clinoptilolite (Table 1.). The results of the differential thermal analysis are in conformity with the above ones (*Fig. 7.*). The spectroscopic analysis shows that the distributions of trace elements in the dacitic tuffs from the Pazsag-valley and Hosszú-valley are the same (Table 3.); the amount of Ba, Sr, Zr is higher than their clarke. The Ba and Sr may be hidden in the felspars and volcanic glass, the Zr can be connected to the accessorial zircon.

Based on the chemical analysis (Table 2.) and the results of the other examinations the pyroclastics can be named as dacitic tuff. The well-preserved rock, the low grade of decay, the lack of terrigenous fragments and fossils suggest that the pyroclastics were accumulated on land.

In the area of the outcrops (1) and (2) a special feature of the rock is the tuff envelopment around the pumice-cores (*Fig. 8.*). There is no mention of similar phenomena in the Hungarian references. The so-called tuff-pellets, which are tuff

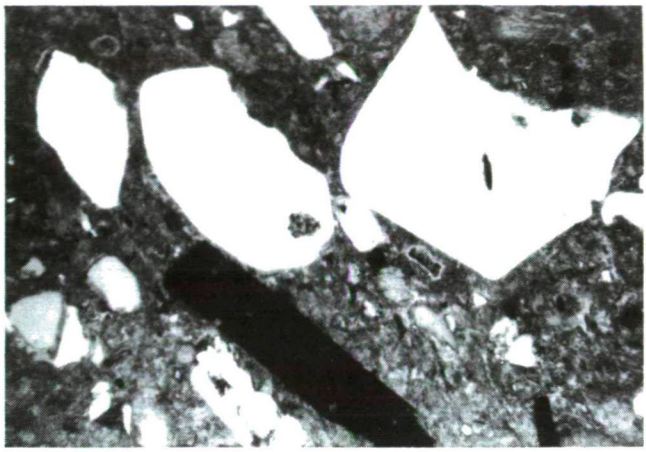

Fig. 4. Oriented plagioclase, biotite and quartz in glassy matrix indicating an ignimbrite character (N+ , 20x)

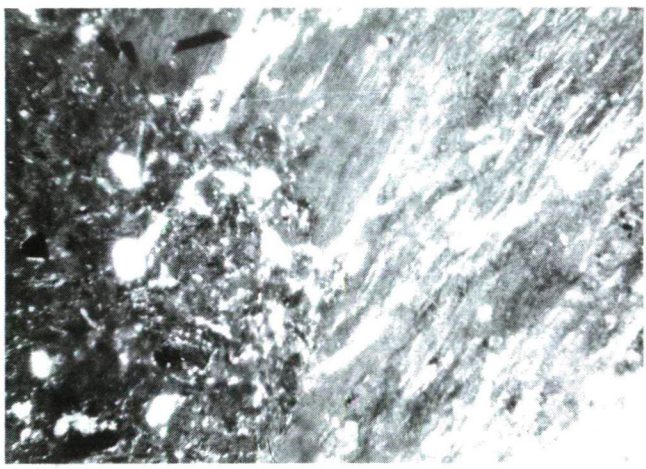

Fig. 5. Pumicite-matrix contact (N+, 20x)

concretions with a decreasing grainsize outwards and a diameter of 3–15 mm are frequent in the Hungarian rhyolitic tuff levels. Their origin is explained as a result of post volcanic activity (KORIM 1951), as rolling of small cores in volcanic dust-cloud (PANTÓ 1962), or accretion of fine volcanic dust and water vapour condensed on bigger grains (RADÓCZ 1976). The above "pellets" are different from the tuff-balls in the examined area. The main differences are the presence of pumice-cores, the bigger size (2—12 cm) and the similar texture of the balls and their surroundings (conversely, the tuff-pellets are fine-grained dust-globules in coarser-grained tuff). The balls are not fixed to definite levels, they are frequent in the outcrops and can be noticed as separated pieces among rock fragments. They are harder and more resistant than the tuff itself (in the wall of the outcrop they stand outer than their surroundings). The piped structure of the pumice-cores was

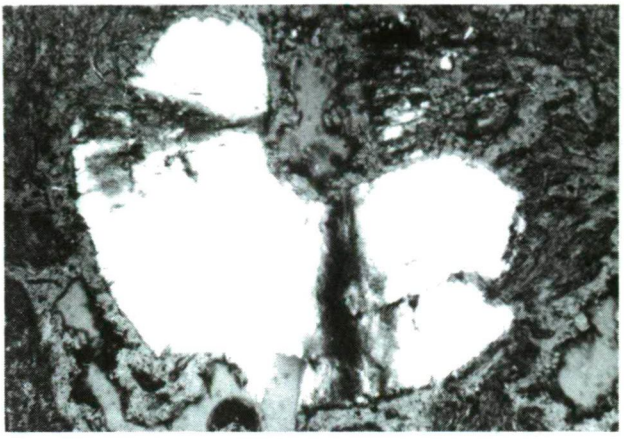

Fig. 6. Radial chalcedony in a matrix with glassy fragments (N+, 30x)

reduced because of the high temperature. The smaller pumices (few mm) have no tuff envelopes. These facts corroborate that the tuff-balls are spheroids formed by the slower cooling around the pumice-cores which have a higher heat-reserve than the fine graind crystal- and glassy fragments.

Similar tuff-balls can be observed NE of Felsőtárkány, in the area of the "Burdigalien" (BALOGH 1964) rhyolite tuff.

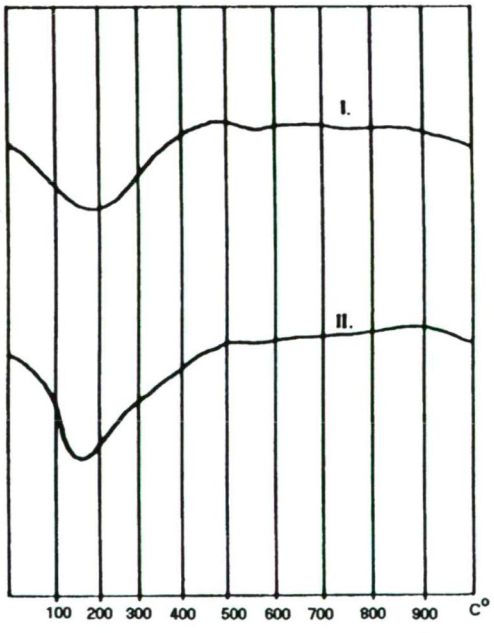

Fig. 7. DTA curves of the samples from the Pazsag-valley (2), (T) and Hosszú-valley (4) (II.)

TABLE 1

Data of X-ray diffraction

dA	I/10		dA	I/10	
9.983	85	B	10.155	15	B
8.936	60	Cl	9.092	51	Cl
7.907	9	Cl	7.950	10	Cl
6.753	6	Pl, Cl	6.753	8	Pl, Cl
5.136	7	Cl	5.901	4	
5.041	8	B	5.267	10	Cl
4.667	8	Pl, B, Cl	5.136	10	B, Cl
4.271	35	Q	4.667	14	Pl, B, Cl
4.068	20	Kr	4.227	40	Q
3.948	58	Pl, B, Cl	4.064	85	Kr
3.737	3	Pl, Cl	3.969	100	B,C
3.633	1	Pl, B	3.790	16	Pl, Cl
3.559	5	Cl	3.635	4	Pl, B
3.413	15	Pl, B	3.445	23	Pl, B
3.343	100	Q, B, Cl	3.338	42	Q, B, Cl
3.194	22	Pl	3.210	45	Pl
3.131	5	Kr, Pl, B, Cl	3.124	8	Kr, Q, B, Cl
2.976	25	Pl, Cl	2.996	40	Pl, Cl
2.803	10	Kr, Cl	2.847	2	Kr
2.731	5	B, Cl	2.803	10	Cl
2.513	12	Pl, B	2.748	2	B
2.445	5	Q, B, Cl	2.583	8	B
2.136	3	Q, B	2.523	4	Pl
2.013	3	Q, B	2.490	8	Kr
1.932	2	B	2.174	4	B
1.826	1	Q	2.018	3	B
1.658	2	Q, B	1.961	3	Q, B
1.541	30	Q, B	1.801	8	Q
1.451	2	Q	1.542	1	Q, B

(1) Dacite tuff, Pazsag-valley. (2) Dacite tuff, Hosszú-valley. Examinations were made at the Department of Mineralogy, ELTE. Explanation: Q=quartz ASTM 5—490; B=biorite ASTM 3T, ASTM 10—492; Pl=plagioclase ASTM 10—360; Kr=Chrystobalite ASTM 11—695; Cl=clinoptiolite ASTM 22—1236

TABLE 2

Data of chemical analysis

	1.	2.
SiO_2	66.17 %	66.87 %
TiO_2	0.30 %	0.08 %
Al_2O_3	11.22 %	12.88 %
Fe_2O_3	1.03 %	1.31 %
FeO	0.88 %	0.44 %
MnO	—	—
MgO	1.81 %	1.41 %
CaO	3.08 %	2.04 %
Na_2O	1.03 %	0.85 %
K_2O	2.15 %	3.90 %
H_2O^+	6.16 %	6.00 %
H_2O^-	4.49 %	4.04 %
P_2O_5	—	—
SO_3	—	—
CO_2	0.21 %	0.17 %
Sum.	98.53 %	99.99 %

(1) Dacite tuff, Pazsag-valley; (2) Dacite tuff, Hosszú-valley. Analyser: BOBÁLY J. ans SÜTŐ Z., OFKFV, Central Laboratory.

TABLE 3

Trace element's data

	1.	2.
Ag	—	—
As	—	—
B	100	100
Ba	1200	1200
Be	—	—
Bi	—	—
Cd	—	—
Cr	100	100
Co	—	—
Cu	40	40
Ga	10	10
Ge	—	—
In	—	—
La	—	—
Mn	800	800
Mo	—	—
Nb	—	—
Ni	—	—

TABLE 3
(continuation)

	1.	2.
Pb	—	—
Sb	—	—
Sc	—	—
Sn	—	—
Sr	1200	1200
Tl	—	—
V	50	50
W	—	—
Zn	—	—
Zr	1200	1200
Y	—	—

(1) Dacite tuff, Pazsag-Valley. (2) Dacite tuff, Hosszú-valley. Analyser: KÁDAS M. OFKFV, Komló, Central Laboratory. PGS-2. Q-spectograph.

Fig. 8. Tuff balls with pumice-cores. Pazsag-valley.

DATING EXAMINATIONS

In order to clearing up the genetical connection between the discussed tuffs and the other acidic pyroclastics in the Bükk Mountains, BALOGH, KADOSA did radioactive measurements to determine the age of the tuffs.

The results are as follows:

Place of occurrence	Examined K cont. fraction (%)	$\frac{^{40}Ar_{rad}}{^{40}Ar_{tot}}$	$\frac{^{40}Ar_{rad}}{(cm^3/g)}$	K-Ar age (Ma.)
Pazsag-valley (2)	biotite 6.29 felspar 0.56	0.39 0.058	$3.979 \cdot 10^{-6}$ $2.205 \cdot 10^{-7}$	16.2±0.8 10.2±2.5
Hosszú-valley (4)	chloritic 5.76 biotite	0.13	$3.638 \cdot 10^{-6}$	16.2±1.8

Based on these data the examined dacitic tuff can be correlated to the so-called "mid-rhyolite tuff".

The dacite tuff of ignimbrite character accumulated on land, proves that the Bükk Mountains were in an emerged position in the middle of the Miocen.

REFERENCES

BALOGH K. 1964: A Bükk hegység földtani képződményei (Geology of the Bükk Mountains): MÁFI Évkönyv. **48**, 2.

HAJÓS M. 1965: Riolittufa gömbkonkréciók vékonycsiszolati vizsgálata (Microscopic examination of spheroid concretions of rhyolite-tuffs): Földt. Közl. 95. **4**, 455.

HÁMOR G., RAVASZ-BARANYAI L., ÁRVA-SÓS E.: A magyarországi riolittufa szintek radiometrikus kora (Radiometric age of the Hungarian rhyolite-tuff levels): MÁFI Évi Jel. 1978-ról, 65—75.

HEVESI A. 1978.: A Bükk szerkezet- és felszínfejlődésnek vázlata (Outline of the structural and morphological development of the Bükk Mountains): Földt. Ért. **27, 2**. 169—205.

JÁMBOR Á. 1959: A bükkhegységi Kisfennsík földtani újravizsgálata (Geological re-ambulation of the Kisfennsík in the Bükk Mountains): MÁFI Évi Jel. 1955—56-ról, 103—122.

JÁMBOR Á. 1961: A Szilvásváradtól K-re fekvő terület felépítése (Geological setting of the area SE of Szilvásvárad): MÁFI Évi Jel. 1957—58-ról, 82—102.

KORIM K. 1951: Konkrécióképződés riolittufában (Concretions in rhyolite-tuff): Földt. Közl. **81**, 332—333.

PANTÓ G. 1961: Az ignimbrit-kérdés (The problem of ignimbrite): MTA Műszaki Oszt. Közl. **29**, 299—332.

RADÓCZ GY. 1976: Akkréciós tufagömbök és települési formáik a Borsodi medence riolittufáiban (Accretional tuff-balls and their depositional forms in the rhyolite-tuffs of the Borsod-basin): Földt. Közl. **92, 2**. 69—77.

VARGA GY. 1981: Újabb adatok az összesült tufatelepek és ignimbritek ismeretéhez (New data to the interpretation of ignimbrites and baked tuffs): MÁFI Évi Jel. 1979-ről, 499—509.

Manuscript received, 23 April, 1993

Acta Mineralogica-Petrographica, Szeged, XXXIV, 61—69, 1993

PETROLOGY AND GEOCHEMISTRY OF LATE PRECAMBRIAN MAFIC DYKE SWARMS IN SOUTHWESTERN SINAI, EGYPT

A. A. M. ABDEL-KARIM*

Dept. of Geology, Faculty of Science, Zagazig University, Egypt

ABSTRACT

The dyke swarms in southwestern Sinai consist of mafic (old) and felsic (young) suites. The mafic one is studied in terms of field, petrography and geochemistry. The mafic suite ranges in composition from basalt to quartz latite with 49—69 % SiO_2 and 1—4.5 % K_2O. They consist of dominant porphyritic basalt, pyroxene and hornblende andesite and hornblende quartz latite and minor plagiophyre and lamprophyre. Porphyritic varieties contain phenocrysts of plagioclase and amphibole and/or clinopyroxene. The eruption of these dyke swarms have been invaded directly before or contemporaneously with the emplacement of a late Precambrian pink granites.

Chemically, these volcanics are K-rich calc-alkaline series, largely peraluminous to metaaluminous nature. They are almost derived from continental crust slightly contaminated by upper mantle materials in orogenic belt. The tectonic setting reveals a mineralogic and chemical similarity with the island arc rather than the continental margin.

INTRODUCTION

The present study deals with the mafic dyke swarms (e.g. pre younger granite volcanics) of the Wadi Baba area in the southwestern part of Sinai (*Fig. 1*). The area is dominantly covered by Precambrian basement rocks including migmatite and gneiss, metagabbro-diorite association, older granite, old (mafic) dykes, younger granite (phase II), young (felsic) dykes and younger granite (phase III) which are partly or totally covered by Paleozoic sediments. Basalt dykes are invaded both the basement and sedimentary cover.

EL-AREF *et al.* (1988) studied the basement rocks east of Abu Zenima and concluded that these dykes represent the limit of Pan-African compression event. They include lamprophyre, andesite, plagiophyre and dolerite cutting the basement rocks except the pink granites. The mafic dyke swarms have age dating range from 586—536 Ma ago (ABDEL-KARIM and AZZAZ, in prep.)

More than 45 samples were collected, of which 21 thin sections, 12 modal and 11 chemical analyses were carried out to complete this work.

GEOLOGICAL SETTING

The geological setting based on field observations and cutting relationships suggest two suites of the dyke swarms. The old suite is mostly rich in the mafics and ranges from basalt to quartz latite including basalt, andesite and quartz latite

* Zagazig, Egypt.

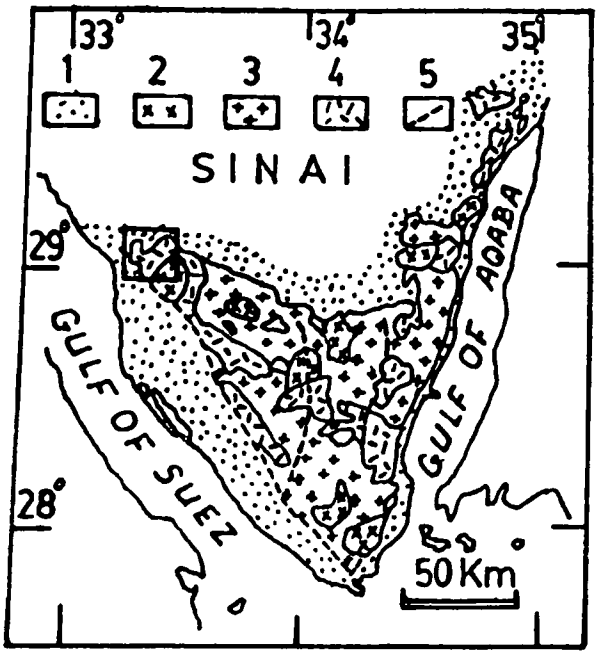

Fig. 1. Generalized geological map of the Precambrian of the Sinai Peninsula (after SHIMRON 1980), used as a location map of the studied dykes. 1: Phanerozoic sediments, 2: Young (alkaline) granitic rocks, 3: Calc alkaline granitic to dioritic rocks, 4: Other Precambrian formations, 5: Major fault lines.

with minor lamprophyre and plagiophyre dykes belonging to the late Precambrian event. The mafic dykes are dominantly strike N—S to NNE—SSW trends. They are invaded the basement rock-units (e.g. migmatites, gneisses, metagabbro-diorite association and older granites) in the examined area except the younger granites, indicating their eruption were directly before or contemporaneously with these granites. The mafic dyke swarms are frequently distributed in the northeastern part of the mapped area (Wadi Nasib, Wadi Lahian, Wadi el-Seih, Wadi Bala and north Wadi Baba). In the middle of Wadi Baba Lamprophyres are cut by basalts, consequently both these dykes cut by younger granites phase-II.

The studied dyke swarms generally vary in width from 0.5 to >10 m and length from few metres to several hundred metres. They are slightly overprinted by a rather low greenschist facies. These swarms are injected in fractures and faults which may be resulted from the effect of variable tectonic deformations in age and style, affected on the northern Arabian Shield.

PETROGRAPHY AND MODAL ANALYSIS

The present mafic dykes have a wide variety of lithologies including porphyritic basalt, pyroxene and hornblende andesite, hornblende quartz latite, plagiophyre and lamprophyre.

The basalt exhibits porphyritic and trachytic textures. Porphyritic varieties are common and usually contain phenocrysts (3—12.8%) of calcic plagioclase

(An_{40-50}) and/or clinopyroxene (augite) embedded in a fine grained groundmass (72—79%) consists of the same minerals (*Fig. 2*) with minor amounts of hornblende, biotite, quartz, chlorite and iron oxides. Andesites have the same textures,

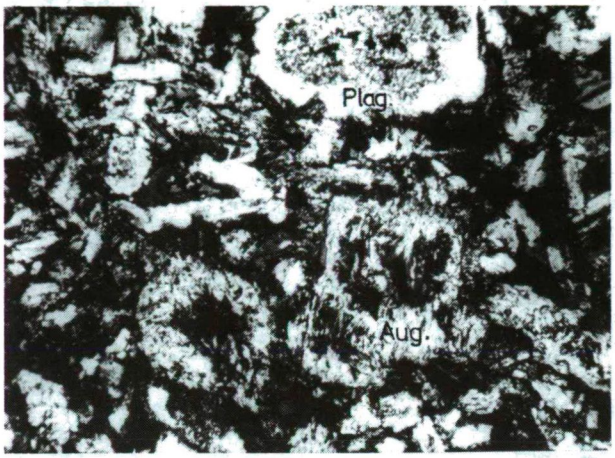

Fig. 2. Photomicrograph of basalt dyke showing phenocrysts of altered plagioclase and augite embedded in a fine grained groundmass of plagioclase, pyroxene, hornblende, biotite and iron oxides. +N., 30x.

porphyritic varieties compose of phenocrysts (14—32%) of pyroxene and hornblende and/or plagioclase (An_{35-45}) embedded in a fine grained groundmass of the same composition and subordinate quartz, biotite, chlorite and iron oxides. The hornblende quartz latite consists of phenocrysts (18.5—31%) of plagioclase (An_{35-40}), hornblende and biotite enclosed in a microcrystalline trachytoid groundmass of the same minerals together with quartz and K-feldspar and minor amounts of chlorite, epidote and titanite (*Fig. 3*). Plagiophyre consist of plagioclase phenocrysts (25—29%) embedded in a fine grained granophyric groundmass of

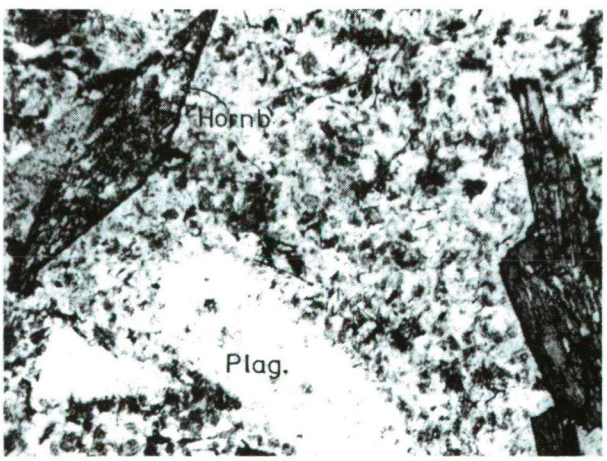

Fig. 3. Photomicrograph of hornblende quartz latite showing phenocrysts of hornblende and plagioclase enclosed in a microcrystalline trachytoid groundmass of the same minerals together with quartz, K-feldspar, biotite, chlorite and iron oxides. 1N., 30x.

plagioclase, K-feldspar, quartz, biotite and hornblende (*Fig. 4*). Lamprophyre consists mainly of fine grained plagioclase and amphibole or their phenocrysts together with subordinate tremolite and chlorite. The partial alteration of the plagioclase to epidote and calcite: the clinopyroxene and amphibole to chlorite and iron oxides (*Fig. 3*) and the amphibole to biotite may suggest a low greenschist facies for these volcanics.

The modal composition of selected twelve mafic dyke samples are plotted on STRECKEISEN's diagram (1979). These dyke swarms range from basalt to andesite and quartz latite (*Fig. 5*).

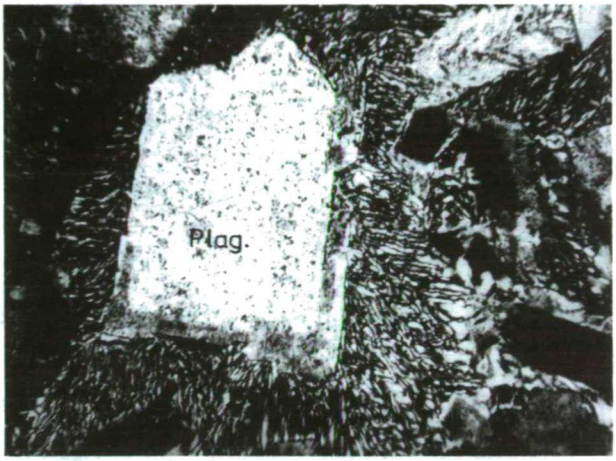

Fig. 4. Photomicrograph of plagiophyre showing phenocrysts of plagioclase embedded in a granophyric groundmass of quartz, plagioclase and K-feldspar. +N., 30x.

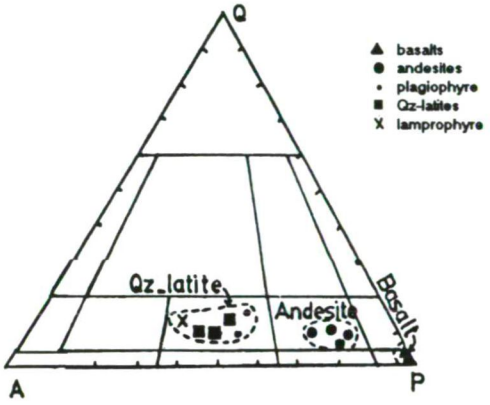

Fig. 5. Plot of the mafic dyke on the Streckeisen's diagram (1979).

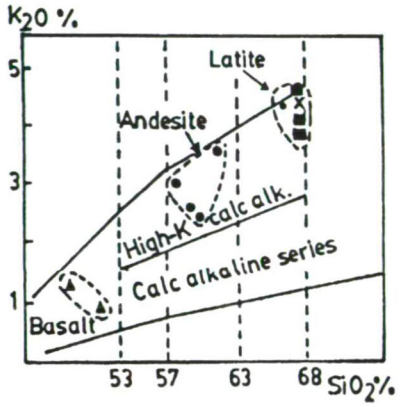

Fig. 6. Plot of the mafic dyke swarms on the K_2O—SiO_2 classification diagram after TAYLOR *et al.* (1981).

GEOCHEMICAL CHARACTERISTICS

Selected eleven samples from the investigated mafic dykes were analyzed for their major element contents by standard wet chemical techniques. The analyses were carried out in the Department of Petrology and Geochemistry of Eötvös University, Hungary. The results appear in Table 1. These data have been utilized to predict the classification, magma type and tectonomagmatic setting of the investigated dyke swarms.

TABLE 1

Major elements composition of the mafic dyke swarms, southwestern Sinai.

	Basalt		High-K Andesite				Quartz Latite				
	Porph.	Bas.	Px and Hb Andesite				Plag.	Hb Quartz Latite			Lamp.
	161	100	271	152	269	284	273	286	140	260	92
SiO_2	49.01	51.50	58.34	59.36	60.90	61.62	66.90	68.55	68.68	69.32	68.99
TiO_2	2.50	1.06	1.07	0.29	0.79	0.50	0.30	0.14	0.24	0.18	<0.10
Al_2O_3	12.50	17.02	14.10	16.25	14.90	14.20	13.90	13.15	14.45	12.72	14.02
Fe_2O_3	3.90	2.37	0.56	1.94	1.13	0.41	1.05	0.89	0.85	0.19	1.15
FeO	5.71	5.88	5.59	4.61	5.08	4.41	1.81	2.40	2.16	3.39	1.84
MnO	0.33	0.10	0.07	0.08	0.06	0.18	0.03	0.05	0.03	0.05	0.04
CaO	10.93	8.53	4.67	5.60	4.30	4.05	1.31	1.78	1.72	2.23	1.23
MgO	6.70	5.69	2.99	2.28	2.17	2.92	1.01	0.76	0.48	1.27	0.51
Na_2O	3.32	4.45	4.87	4.09	4.60	4.21	4.99	4.45	4.97	4.53	4.73
K_2O	1.31	0.90	2.93	2.48	2.36	3.50	4.40	4.61	3.85	4.12	4.48
$+H_2O$	1.90	0.99	2.72	1.73	2.16	2.95	1.74	1.50	1.36	1.08	1.56
$-H_2O$	0.92	0.19	0.27	0.22	0.22	0.37	0.54	0.98	0.68	0.68	0.67
P2O5	0.81	0.29	0.42	0.24	0.22	0.18	0.09	0.05	0.05	0.60	0.05
Sum	99.84	98.97	98.51	99.17	98.89	98.38	98.06	99.31	99.52	99.84	99.37
$\frac{FeO^t}{MgO}$	1.30	1.41	2.03	2.79	2.81	1.64	2.73	4.21	6.09	2.80	5.63

Chemical Classification

The present mafic dykes are classified according to the potash-silica diagram (*Fig. 6*) after TAYLOR *et al.* (1981). On this diagram, the data points spread over the fields of basalt, andesite and quartz latite.

Magma type

The present dyke swarms are high-K calc-alkaline series (*Fig. 6*). The K-enrichment of these volcanics probably suggests their generation in extensional regime at a continental margin. Their calc-alkaline character is also emphasized on the conventional AFM diagram (*Fig. 7*) after IRVINE and BARGAR (1971). On this diagram the data points show a typical calc-alkaline trend. This trend is emphasized again by increase of both TiO_2 and FeO_t contents with the increase of FeO_t/MgO ratios (MIYASHIRO 1974, 1975) (Table 1). However, the calc-alkaline trend of the dyke swarms (*Fig. 7*) probably suggest their compressional regime

environment (PETRO *et al.* 1979). Furthermore, on the NaO_2+K_2O - Al_2O_3 - CaO diagram (*Fig. 8*) after SHAND (1972) the dyke suite is peraluminous to slightly metaaluminous, probably suggest their origin from an attenuated crust near the continental margin.

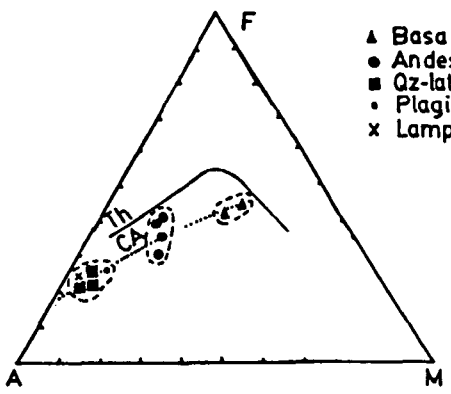

▲ Basalts
● Andesites
■ Qz-latites
• Plagiophyre
x Lamprophyres

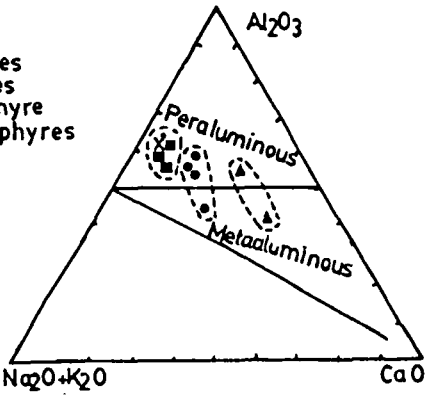

Fig. 7. Plot of the mafic dyke swarms on the AFM diagram after IRVINE and BARAGAR (1971). Dotted line represents the trend of compressional regime after PETRO *et al.* (1979).

Fig. 8. Plot of the mafic dyke swarms on the Na_2O+K_2O-Al_2O_3-CaCO diagram after SHAND (1972).

TECTONIC SETTING

Using the discriminant diagram of GOTTINI and RITTMANN (*Fig. 9*) after RITTMANN (1973), the examined samples plot in the field of an orogenic belt and island arc volcanics indicate their lower crustal materials probably contaminated by a batch of upper mantle. The orogenic environment of an extensional regime of the present dykes is evident again on the MgO - FeOt - Al_2O_3 diagram (*Fig. 10*) after PEARCE *et al.* (1977). Furthermore, the continental origin of the examined suite is emphasized again on the K_2O - TiO_2 - P_2O_5 diagram (*Fig. 11*) after PEARCE *et al.* (1975). The dykes are, moreover, analogous to the mature island arc volcanics from the Western Americas. That is appear on the calc-alkali ratio — silica diagram (*Fig. 12*) after BROWN (1982).

Finally, the present suite of dykes is considered as a cogentic magmatic series, probably derived from continental crust slightly contaminated by an uper mantle material. This magmatic series is subsequently fractionated to variable pulses given rise to three dyke rock groups including basalt, andesite and quartz latite variants. Each group of dykes distinguishes by a definite mineralogic and chemical characteristics. These features can be noticed on the diagrams of *Figs. 5 to 11.* Moreover based on these mineralogic and chemical features (Table 2), the dyke swarms can be comparable with the calc-alkaline island arc volcanics (GREENWOOD *et al.* 1980, BAKER 1982).

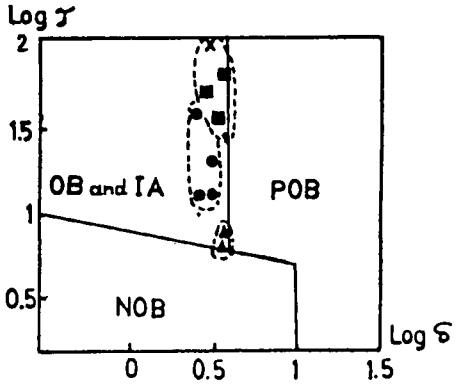

Fig. 9. Plot of the mafic dyke swarms on the log~ — log diagram after RITTMANN (1973). OB: Orogenic belt, IA: Island arc, NOB: Non-orogenic belt, POB: Post-orogenic belt.

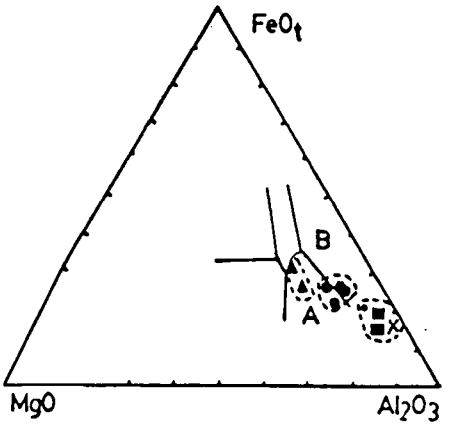

Fig. 10. Plot of the mafic dyke swarms on the $MgO—FeO_t—Al_2O_3$ diagram after PEARCE *et al.* (1977). A and B: Orogenic domain.

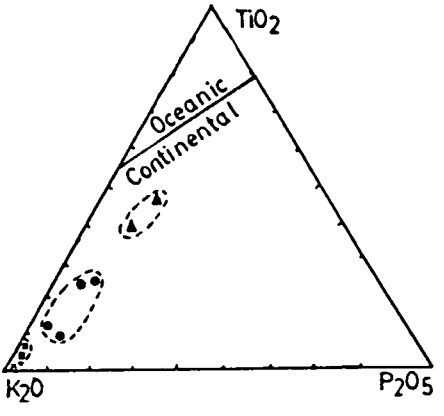

Fig. 11. Plot of the mafic dyke swarms on the $K_2O—TiO_2—P_2O_5$ digram after PEARCE et al. (1975).

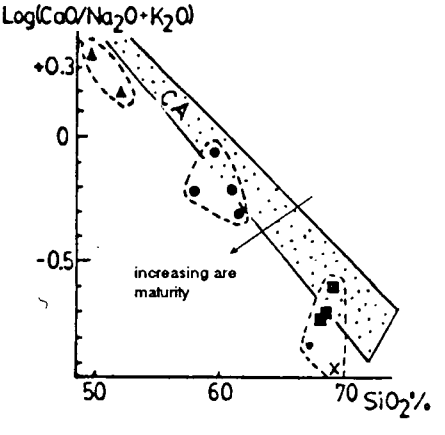

Fig. 12. Plot of the mafic dyke swarms on the log (CaO/Na_2O+K_2O)-SiO_2 digram after BROWEN (1982). CA: Calc-alkaline andesites filed of the mature island arc.

TABLE 2

Comparison of the typical calc-alkaline island arc volcanics (GREENWOOD et al. 1980; BAKER 1982) with the studied dyke swarms.

	Calc-alkaline island arc	The studied dyke swarms
Mafic min.	abundantly	abundantly
Phenocrysts	pyroxene	pyroxene and hornblende
Grain size	mostly porphyritic with calcic plagioclase	porphyritic with calcic plagioclase
Andesite	dominantly	dominantly
SiO_2	50—66 %	49—69 %
Na_2O+K_2O	4—7.7 %	4.3—9 %
Na_2O/K_2O	1.8—2.9	1—2.5 %

CONCLUSION

The conclusion of the foregoing field, petrographic and geochemical study reveals the following.

The late Precambrian mafic dyke swarms of southwestern Sinai consist of a wide variety of lithologies including porphyritic basalt, pyroxene and hornblende andesites, plagiophyre, hornblende quartz latite and lamprophyre. The eruption of these mafic dykes have been invaded directly before or contemporaneously with the emplacement of the late Precambrian younger granites. Based on mineralogic and chemical characteristics, the dyke swarms can be distinguished to three distinctive groups (trimodal ?).

Geochemically, the dyke swarms have high-K calc-alkaline affinity, largely peraluminous to metaaluminous. They represent a cogenetic magmatic series, probably derived from continental crust slightly contaminated by a batch of the upper mantle. This magma is subsequently fractionated to variable pulses range from basalt to quartz latite.

Tectonomagmatic setting reveals that these volcanics are similar to the late Precambrian island arc rather than the continental margin magmatism.

REFERENCES

ABDEL-KARIM A. M. and S. A. AZZAZ: On the age dating of the dyke swarms of southwestern Sinai, Egypt. (in prep.).

BAKER P. E. (1982): Evolution and classification of orogenic volcanic rocks. *In* R. S. THORPE (ed.) : Andesites. John Wiley and Sons. New York. p. 11—23.

BROWN G. C. (1982): Calc-alkaline intrusive rocks: their diversity, evolution and relation to volcanic arcs. *In* R. S. THORPE (ed.): Andesites. John Wiley and Sons. New York, pp. 437—465.

EL-AREF M. M., ABD EL WAHID M. and M. KABESH (1988): On the geology of the basement rocks, East of Abu Zenima, West Central Sinai, Egypt. Egypt. J. Geol. **32** (1—2), pp. 1—25.

IRVINE T. N. and W. R. A. BARGAR (1971): A guide to the chemical classification of the common volcanic rocks. Can. J. Earth Sci. **8**, pp. 523—548.

GREENWOOD W. R., ANDERSONE R. E., FLECT R. J. and R. J. ROBERTS (1980): Precambrian geological history and plate tectonic evolution of the Arabian Shield. Saudi Arabia Gen. Miner. Bull. **24**, 23 p.

MIYASHIRO A. (1974): Volcanic rocks series in island arc and active continental margins. Am. Jour. Sci. **274**, pp. 321—355.

MIYASHIRO A. (1975): Volcanic rock series and tectonic setting. Ann. Rev. Earth Planet. Sci. Lett. **3**, pp. 351—369.

PEARCE T. H., GORMAN P. F. and T. C. BRIKET (1975): The TiO_2—K_2O—P_2O_5 diagram: a method of discriminating between oceanic and non oceanic basalts. Earth Planet. Sci. Lett. **24**, pp. 419-426.

PEARCE T. H., GORMAN B. F. and T. C. BIRKETT (1977): The relationship between major element chemistry and tectonic environment of basic and intermediate volcanic rocks. Earth Planet. Sci. Lett. **36**, pp. 121—131.

PETRO W. L., VOGEL T. A. and J. T. WILBAD (1979): Major elemnet geochemistry of plutonic rock suites from compressional and extensional plate boundaries. Chem. Geol. **26**, pp. 217—235.

RITTMANN A. (1973): Stable mineral assemblages of igneous rocks. Speringer-Verlag. Berlin. 262 p.

SHAND S. J. (1972): The eruptive rocks. John Wiley and Sons, New York.

SHIMRON A. E. (1980): Proterozoic island arc volcanism and sedimentation in Sinai. Precamb. Res. **12**, pp. 437—458.

STRECKEISEN A. (1979): Classification and nomenclature of volcanic rocks. Geology. **7**, pp. 331—335.

TAYLOR R. P., STRONG D. F. and B. J. FRYER (1981): Volatile control of contrasting trace element distributions in peralkaline granitic and volcanic rocks. C. M. P. **77**, pp. 267—271.

Manuscript received, 5 April, 1993

Acta Mineralogica-Petrographica, Szeged, XXXIV, 71—78, 1993

PETROGRAPHY, GEOCHEMISTRY AND K-AR DATING OF SOME METAGABBROS FROM THE CENTRAL EASTERN DESERT OF EGYPT

M. M. EL-MAHALLAWI*

El-Minya University Egypt

E. ÁRVA-SÓS**

Institute of Nuclear Research, Debrecen, Hungary

ABSTRACT

Radiometric ages of some metagabbros using amphiboles were determined with the conventional K-Ar method. The ages of pargasitic hornblende from the Meatiq metagabbro gave 599±32 Ma, 544±21 Ma and 539±21 Ma. The latter two ages reflect some K incorporation after crystallization. The age of 599±32 is the time of total resetting and metamorphism of this rock. This age is slightly below the age of the Abu Ziran Orogeny (613±2 Ma) which cause the obduction of ophiolitic mélange onto the infracrustal basement (HABIB *et al.* 1985); culmination of metamorphism and deformation (STRUCHIO *et al.* 1982) or emplacement of Abu Ziran pluton and timing of major crustal movement (STERN and HEDGE 1985).

The age of tremolitic hornblende from El-Sid pluton gave 421±76 Ma, 440±18 Ma and 543±75 Ma. These ages are too young and their scatter is great due to the very low K content. Moreover, the tremolitic hornblende is strongly strained and sometimes occurred as aggregates of fibrous crystals, raising the possibility of continuous Ar loss. So, the given ages suggest either the termination of Ar diffusion at that time or partial loss during later events subsequent to the pluton's emplacement. A relationship to local tectonic movement might be suggested but is not well documented.

INTRODUCTION

The gabbroic rocks were collectively regarded as one group in the old classifications of the Egyptian Shield. SCHURMANN (1953) differentiated two types of gabbros; older metamorphosed and younger fresh gabbros. The former type was named "epidiorite" (AMIN *et al.* 1953), "epidiorite-diorite association" (EL-RAMLY and AKAAD 1960), "metagabbro-diorite complex" (AKAAD and ESSAWY 1964, EL-RAMLY 1972). A discrimination scheme for the distinction between the metagabbros and fresh gabbros was proposed by TAKLA *et al.* (1981).

The metagabbros are considered as having been intruded during the climax of the orogenic folding and regional metamorphism after the emplacement of the ultramafic rocks (AKAAD and NOWEIR 1980) and have been closely followed by the intrusion of "grey granites" (AKAAD and EL-RAMLY 1960). They have been considered to originate from gabbroic magma by deuteric uralitization (EL-RAMLY

* El-Minya, Egypt
**H—4026 Debrecen, Bem tér 18/c. Hungary

and AKAAD 1960) or by autometamorphism (SABET 1972). NOWEIR and TAKLA (1974) concluded that the metagabbros have suffered medium grade regional metamorphism. Recently, ABU EL-ELA (1985) and ASHMAWY (1987) recognized ophiolitic gabbros and calc-alkaline gabbros related to island arc environment.

K-Ar age dating of metagabbros from Umm Rus area was given by KAMEL *et al.* (1983) which fall within the range 580—606 Ma. This relatively younger age was considered to be related to some thermal effect in the history of the gabbroic mass. COLEMAN *et al.* (1972) reported K-Ar ages for some layered gabbros in the Arabian Shield ranging from 415 to 702 Ma. Most of these ages were obtained on a wholerock and can not be evaluated. FLECK *et al.* (1976) introduced ages of unmetamorphosed gabbros which cluster about 625 Ma.

EXPERIMENTAL METHODS

Radiometric dating was carried out in the Institute of Nuclear Research of the Hungarian Academy of Science (ATOMKI), Debrecen. Flame photometry has been used for potassium determination. Pulverized minerals were digested in HF and $HClO_4$ acids and dissolved in 0.25 N LiCl has been added as internal standard and the solutions were buffered with sodium.

Samples were degassed by high frequency induction heating, the liberated argon has been spiked with ^{38}Ar. A 90° deflection magmatic mass spectrometer of 150 mm radius has been used in static regime for the argon determination. The argon extraction line and the mass spectrometer were developed in the ATOMKI, details of instruments and applied methods have been described elsewhere (BALOGH 1985).

Potassium and argon determinations have been controlled regularly using the Asia 1/65 (Soviet) and GL-O (French) interlaboratory standards.

Four samples of the dated amphiboles were also identified using X-ray diffraction analysis in the Minerology Department, Eötvös Loránd University (ELTE), Budapest.

GEOLOGIC SETTING

El-Sid metagabbro forms and elongated oval massif laying along the Qift-Quseir road. Its larger axis is about 7.2 km and trends N—S in parrallelism with the regional trend of the country rock. A brief field description of the massif have been given by NOWEIR (1986), NOWEIR and TAKLA (1974) and LEBDA (1988). They showed that the metagabbro body is bounded from the east by metavolcanics and from the west by serpentinites. The rock was invaded by the Fawakhir granodiorite particularly at the south-western sector (*Fig. 1*). The pluton was considered as part of ophiolite sequence by RIES *et al.* (1983).

The Meating metagabbro is named by the present authors after the Meating Dome which directly bounded the studied massif from the east. This dome is consisted of a core of granite-gneiss (Umm Baanib pluton) with a mylonitic carapace. The mylonite graded upward into nonmylonitic cover of low-grade ophiolitic rocks comprising the metagabbro which forms scattered elongated bodies of oval shape trending nearly NW—SE (*Fig. 1*). The field study proved that the metagabbro intruded subsequently to the serpentinites, immediately prior to the syntectonic tonalite and granodiorite. The contact between the rock and country is sharp and irregular and abundant isolated apophyses around the main mass are

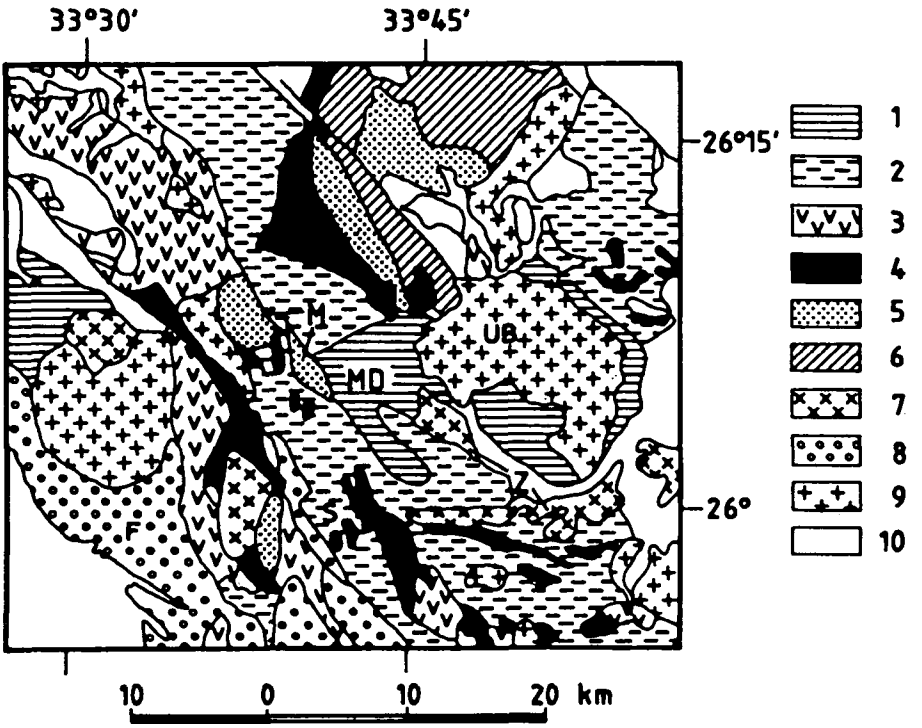

Fig. 1. Geological map of the basement complex of part from the Central Eastern Desert of Egypt (after EL-RAMLY 1972). M=Meatiq metagabbro; S=El-Sid metagabbro; MD=Meatiq Dome; Z=Abu Ziran Pluton; UM=Umm Baanib Pluton; F=Fawakhir Pluton. 1.) Gneiss Group. 2.) Metasediments. 3.) Metavolcanics. 4.) Serpentinite. 5.) Metagabbros. 6.) Diorites. 7.) Older granitoids. 8.) Unmetamorphosed sediments. 9.) Younger granitoids. 10.) Undifferentiated.

common. More details about the geology of this area were given by STRUCHIO *et al.* (1983), RIES *et al.* (1988), EL-GABY *et al.* (1984) and HABIB *et al.* (1985).

PETROGRAPHY

El-Sid metagabbros are of highly heterogeneous nature and vary from amphibolite to metagabbro in composition. They are composed of variable ratios of highly altered andesine and tremolitic hornblende with subordinate amounts of chlorite and epidote. The tremolitic hornblende is commonly found as crystal aggregates which pseudomorph after pyroxene and occasionally are highly deformed. Andesine is usually highly turbid by kaolinite and replaced by sericite and epidote. Few crystals of orthopyroxene (enstatite) and less commonly augite are still preserved.

El-Meatiq metagabbro is dark green massive foliated rock. It is composed essentially of dark-green hornblende and highly altered andesine with subordinate amounts of chlorite, titanomagnetite and apatite. Hornblende pseudomorphs after orthopyroxene with the preservation of the schiller structure. The mineral usually

grades to the bluish green pargasite which forms reaction rims surrounding the peripheries of the hornblende crystals. Andesine is partially or completely altered to sericite, epidote and kaolinite; and corroded and replaced by chlorite and hornblende.

GEOCHEMICAL CHARACTERISTICS

Six samples of the studied metagabbros were analysed for major elements in the Department of Petrology and Geochemistry, ELTE, Budapest. Table 1 shows the chemical composition and the calculated CIPW norm.

TABLE 1

K–Ar ages of the dated amphiboles.

No.	Sample		Mineral	K %	$^{40}Ar_{rad}$ cc STP / Gg	$^{40}Ar_{rad}$ %	K/Ar Age Ma
1807.	El-Sid;	S-50	Tremolitic hornblende	0.229	$3.9794 \cdot 10^{-6}$	40.0	440±18
1808.		S-60	"	0.074	$1.8201 \cdot 10^{-6}$	14.0	543±75
1809.		S-70	"	0.060	$1.1038 \cdot 10^{-6}$	9.0	421±76
1810.	El-Meatiq;	M-20	Pargasitic hornblende	0.889	$2.1922 \cdot 10^{-5}$	77.4	544±21
1811.		M-30	"	0.859	$2.0969 \cdot 10^{-5}$	70.6	539±21
1812.		M-40	"	0.530	$1.4637 \cdot 10^{-5}$	77.2	599±32

The AFM diagram (*Fig. 2*) confirms the distinction of the studied rocks into different types. The Meatiq metagabbro shows a pronounced tendency towards the enrichment of total iron with similar behaviour of the ferrogabbros (MONVISO 1979). On the other hand, El-Sid metagabbro displays slight tendency towards the M end which indicates that its parent melt was relatively magnesium rich. Generally, the studied metagabbros show diversity in magma type range from CA to TH series.

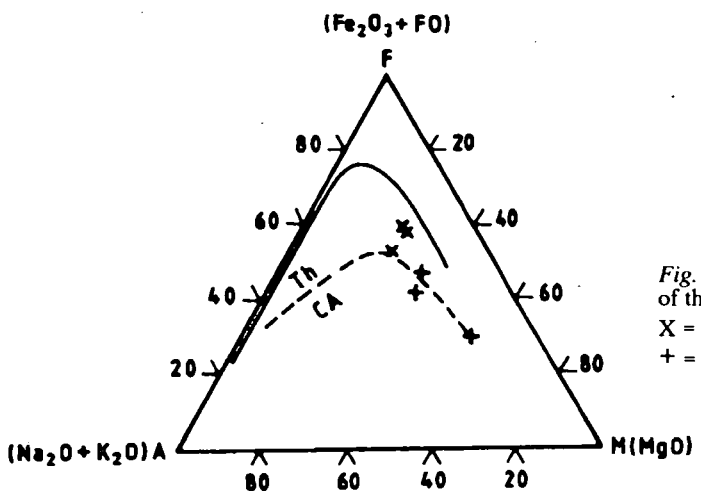

Fig. 2. AFM triangular diagram of the studied metagabbro.
X = Meatiq metagabbro;
+ = El-Sid metagabbro.

The variation diagram (*Fig. 3*) of total alkali versus SiO_2 (MACDONALD and KATSURA 1964) shows that there are pronounced alkali additions during alteration and metamorphism of the studied rocks especially the Meatiq metagabbros. An erratic variation of total alkali with SiO_2 can be recognized within El-Sid pluton.

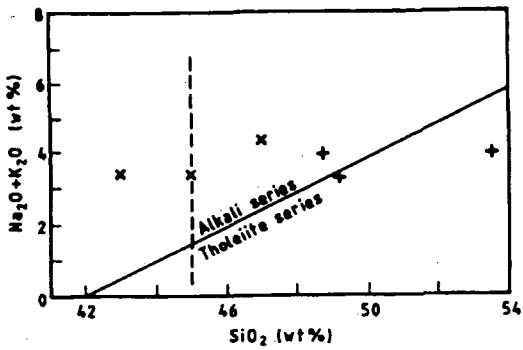

Fig. 3. Variation diagram of total alkalies versus SiO_2 of the studied metagabbros. Symbols as in *Fig. 2.*

GEOCHRONOLOGY

Gechronologic investigations of the Egyptian shield have progressed to the point where some generalization and interpretation of igneous and metamorphic history can be made (e.g. HASHAD 1980; GILLESPIE and DIXON 1983; STERN and HEDGE 1985 and others). Some ages for rocks from the Meatiq dome and the surrounded area were given by STRUCHIO *et al.* (1982) and STERN and HEDGE (op. cit.). The former authors demonstrated concordant Rb-Sr (wholerock and feldspar) and U-Pb (Zircon) isotopic ages. They concluded that the culmination of metamorphism, deformation, and tonalite intrusion occurred at 613±2 Ma. The quartz-monzonite (Umm Baanib pluton) intruded the dome at 579±5 Ma, synchronous with the regional Pan-African plutonism. A Rb- Sr whole-rock of granitic gneiss and mylonitic rocks indicated that the protolith of these rocks had an age of 626±2 Ma. STERN and HEDGE (1985) demonstrated similar age of the emplacement of the tonalite and granodiorite of Abu-Ziran pluton (614±8 Ma, combined Rb- Sr and U-Pb Zircon techniques). They consider it to represent the timing of major crustal movement in this part of the Eastern Desert. These ages were later discussed by EL-GABY *et al.* (1984) and HABIB *et al.* (1985). The older age of 626±2 Ma was referred to the Meatiqian orogeny where granite - gneiss, migmatitic- gneiss and migmatized amphibolite were formed. The next age denotes the Abu-Ziran orogeny which culminated at 613±2 Ma, where the supracrustal cover represents a part of an extensive ophiolitic mélange obducted into the infracrustal basement. Later, both the infracrustal basement and the overlying supracrustal cover were isostatically uplifted, subjected to complex shallow folding giving rise to the major Meatiq domal structure, and were intruded by postkinematic adamellite (Umm Baanib pluton) at 579±6 Ma.

The measured K-Ar ages of the pargasitic hornblende separated from the Meatiq metagabbros gave 599±32 Ma, 544±21 Ma and 539±21 Ma (Table 2). The latter two ages must be excluded as they show greater K content which reflect some K incorporation after the crystallization of hornblende. This phenomenon was also

reflected on the total alkalies vs. SiO_2 variation diagram and from the petrographic investigation. The age of 599±32 Ma is either the true time of formation of the Meatiq metagabbro or the time of total resetting and metamorphism of the age of this rock. The pronounced recrystallization and obliteration of its igneous texture support the latter interpretation. This age is in accordance with the age of Abu Ziran orogeny (613±2 Ma) which causes the obduction of ophiolitic mélange into the infracrustal basement (HABIB *et al.* 1985), culmination of metamorphism and deformation (STRUCHIO *et al.* 1982) or emplacement of Abu- Ziran pluton and timing of major crustal movement (STERN and HEDGE 1985).

TABLE 2

Chemical analyses and CIPW Norm for El-Sid and El-Meatiq metagabbros.

Locality	El-Sid Metagabbro			El-Meatiq Metagabbro		
Samp. No.	S-50	S-60	S-70	M-20	M-30	M-40
SiO_2	53.55	49.22	48.75	45.02	47.04	43.02
TiO_2	1.35	0.15	1.08	2.95	2.65	2.61
Al_2O_3	15.52	15.66	16.82	20.39	15.93	19.60
Fe_2O_3	2.18	0.92	1.58	2.48	1.33	1.98
FeO	5.50	5.42	8.73	9.93	10.26	10.55
MnO	0.13	0.12	0.16	0.13	0.13	0.12
MgO	6.40	11.38	7.82	5.65	5.75	5.00
CaO	8.93	11.23	9.95	8.34	9.25	10.16
Na_2O	3.25	3.12	3.39	1.92	2.86	1.97
K_2O	0.83	0.28	0.60	1.47	1.61	1.48
P_2O_5	0.28	0.25	0.16	0.38	0.32	1.96
Ig. Los.	1.68	2.27	1.82	2.26	2.88	1.90
Total	99.60	100.02	100.86	100.92	100.01	100.35
			CIPW NORM			
qz	4.23	—	—	—	—	—
Or	5.00	1.65	3.55	8.95	9.90	9.05
ab	29.75	27.80	30.45	17.75	26.70	18.30
an	25.80	27.70	28.98	40.00	26.90	38.95
c	—	—	—	1.59	—	1.12
Wo	7.00	10.40	7.74	—	7.46	—
Fs	5.40	2.90	4.02	6.79	2.95	5.01
en	17.98	11.74	7.76	16.85	4.07	6.01
fo	—	3.19	4.78	3.96	9.31	6.21
fa	—	12.93	9.22	2.48	6.74	5.19
mt	2.33	0.96	1.65	2.67	1.44	2.15
il	1.02	0.20	1.50	4.20	3.38	3.76
ap	0.59	0.53	0.35	0.83	0.69	4.25

Radiometric ages of El-Sid metagabbros (Table 2) gave 421±76 Ma, 440 Ma, 440±18 Ma and 543±75 Ma. These ages appear to be too young and the scatter of them is great. Samples S-60 and S-70 could be dated only with great error due to

the very low potassium content. Elf-Sid pluton is intruded by the Fawakhir granodiorite of 574±9 Ma (FULLAGER and GREENBERG 1978). The age of this metagabbro must be older. El-Sid metagabbros has a tremolitic hornblende which is strongly strained and sometimes occurred as aggregates of fibrous crystals, raising the possibility of continuous argon loss. So, the given ages suggest either the termination of Ar diffusion at that times or partial argon loss during later events. This provided evidence of some thermal and/or tectonic activity subsequent to the emplacement. Moreover, these ages are younger than the Pan-African - age and suggest that deformation may have controlled argon loss because regional cooling could not produce an apparent age pattern as complex as observed (FLECK 1976). A relationship to local tectonic movement might be suggested but is not well documented.

Similar young ages were also recorded from the Arabian Shield. FLECK *et al.* (1976) demonstrated K-Ar measurements and concluded that the Shield was affected by two major thermal events between 610—560 Ma and 540—510 Ma. These events rejuvenated the apparent ages of most older rocks, frequently by 15—45 Ma (FLECK *et al.* 1979). The amount of rejuvenation is, however, so irregular in detail that K-Ar ages can at best be interpreted as minimum ages. BENTOR (1985) also concluded that the term Pan-African introduced by KENNEDY (1964) must be considered as a thermotectonic episode which caused widespread resetting of K-Ar ages in Africa to ~ 500 Ma.

REFERENCES

ABU-EL-ELA A. M. (1985). Geology of Wadi Mubarak district, Eastern Desert. Ph. D. Thesis, Tanta Univ.

AKAAD M. K. and EL-RAMLY M. F. (1960). Geological history and classification of the basement rocks of the Central Eastern Desert of Egypt. Geol. Surv. Egypt, pap. **9**, 24 pp. Cairo.

AKAAD M. K. and ESSAWY M. A. (1964). The metagabbro-diorite complex NE Gabal Atud, Eastern Desert and the term "epidiorite". Bull. Sci. Tech., **7**, 83—108. Assiut.

AKAAD M. K. and NOWEIR A. M. (1980). Geology and lithostratigraphy of the Arabian Desert orogenic belt of Egypt between latitude 25° 35' and 25° 30' N. Inst. appl. Geol. Bull., King Abdel Aziz Univ. Jeddah. **3** (4), 127—135.

AMIN M. S., MANSOUR M. S., KABESH M. L. and EL-FAR D. M. (1953). Geology of the Naba district. Geol. Surv. Egypt, 41 pp. Cairo.

ASHMAWY M. H. (1987). The ophiolitic mélange of the south Eastern Desert of Egypt: Remote sensing, field work and petrographic investigations. Berliner geowiss. Abh. **A, 84, 1345**, 1—131.

BALOGH K. (1985): K/Ar dating of Neogene volcanic activity in Hungary: Experimental technique, experiences and methods of chronologic studies. Atomki Rep. D/1 277—288.

BENTOR Y. K. (1985). The crustal evolution of the Arabo-Nubian massif with special reference to Sinai Peninsula. Precambrian Res. **28**, 1—74.

COLEMAN R., BROWN G. and KOLTH T. (1972). Layered gabbro in southwest Saudi Arabia. U. S. Geol. Surv. Prof. paper 800—D, p. D143—D150.

EL-GABY S., EL-NADY O. and KHUDEIR A. (1984). Tectonic evolution of the basement complex in the Central Eastern Desert, of Egypt. Geol. Rundschau **73**, 10109—36.

EL-RAMLY M. F. (1972). A new geological map for the basement rocks in the Eastern and Southwestern Desert of Egypt. Ann. Geol. Surv. Egypt. **2**, 1—18.

EL-RAMLY M. F. and AKAAD M. K. (1960). The basement complex in the Central Eastern Desert of Egypt between latitudes 24°30' and 25°40', N. Geol. Surv. Egypt paper. **8**, 35 pp, Cairo.

FLECK R., COLEMAN R. G., CORNWALL H. R., GREENWOOD W. R., HADLEY D. G., SCHMIDT D. L., PRINZ W. C. and RATTE J. C. (1986). Geochronology of the Arabian Shield, western Saudi Arabia: K-Ar results. Geol. Soc. Amer. Bull. **87**, 9—21.

FLECK R. J., GREENWOOD W. R., HADLEY D. G., ANDERSON R. E. and SCHMIDT D. L. (1979). Rubidium-Strontium geochronology and plate-tectonic evolution of the southern part of the Arabian Shield. U. S. Geol. Surv. Saudi Arabian Project Rep. **245**, 105 pp.

FULLAGAR P. D. and GREENBERG J. K. (1978). Egyptian Younger granites: a single period of plutonism? Precambrian Res. **6**, A 22.

GILLESPIE J. G. and DIXON T. H. (1983). Lead isotope systematics of some igneous rocks from the Egyptian Shield. Precambrian Res. **20**, 63—77.
HABIB M. E., AHMED A. A. and EL-NADY O. M. (1985). Tow orogenies in the Meatiq area of the Central Eastern Desert, Egypt. Precambrian Res. **30**, 83—111.
HASHAD A. H. (1980). Present status of geochronological data on the Egyptian basement complex. I.A.G. Bull. Jeddah. **3**, 31—46.
KAMEL A., EL-BAKRI A., EL-MAHALLAWI M., BALOGH K. and ÁRVA-SÓS E. (1983). K/Ar dating of gabbro and granodiorite, Umm Rus area, Eastern Desert, Egypt. Inter. Basement tectonics. Publ. **5**, 61—67.
KENNEDY W. C. (1964). The structural differentiation of Africa in the Pan-African (±500 million years) tectonic episode. Res. Inst. Afr. Geol. Univ. Leeds, 8th Ann. Rep., 48—49.
LEBDA E. M. A. (1988). Minerology and mineral chemistry of some gabbroid rocks of Egypt. M. Sc. Thesis. Tanta Univ.
MACDONALD C. A. and KATSURA T. (1964). Chemical composition of some Hawian lavas. J. Petrol. **5**, 82—133.
MONVISO "collective name for geologists from Torino" (1979). The Monviso ophiolite complex. Inter. Ophiolite Symp. Cyrus, 332—340.
NOWIR A. M. (1968). Geology of El-Hammamat-Wadi Um Seleimat area, Eastern Desert. Ph. D. Thesis. Assuit Univ.
NOWEIR A. M. and TAKLA M. A. (1974). Studies on the synorogenic basic plutonites of the Central Eastern Desert between Qena-Safaga and Idfu-Mersa Alam Roads. Desert Inst. Bull. ARE. **24**, 77—99.
RIES, A. C., SHACKLETON R. M., GRAHAM R. H., FITCHES W. R. (1983). Pan-African structures, ophiolites and mélange in the Eastern Desert of Egypt: a traverse at 26° N. J. geol. Soc. London. **140**, 75—95.
SABET A. H. (1972). On the stratigraphy of the basement rocks of Egypt. Ann. Geol. Surv. Egypt. **2**, 79—102.
SCHURMAN H. M. E. (1953). The Precambrian of the Gulf of Suez area. Inter. Geol. Congr. 19th Algeria, C.R., sec., 1, Rasc. 115—135.
STERN R. J. and HEDGE C. E. (1985). Geochronologic and isotopic constraints on late Precambrian crustal evolution in the Eastern Desert of Egypt. Amer. J. Sci. **285**, 97—127.
STRUCHIO N. C., SULTAN M., SYLVESTER P. J. and BATIZA R. (1982). Age and origin of Meatiq dome: Implications for stratigraphy and tectonic history of the Central Eastern Desert of Egypt. Precambrian Res. **16**, A 57.
STRUCHIO N. C., SULTAN M. and BATIZA R. (1983). Geology and origin of Meatiq dome, Egypt: A Precambrian metamorphic core complex?. Geology. **2**, 72—76.
TAKLA M. A., BASTA E. Z. and FAWZI E. (1981). Characterization of the older and younger gabbros of Egypt. Delta J. Sci. **5**, 279—314.

Manuscript received, 27 March, 1993

Acta Mineralogica-Petrographica, Szeged, XXXIV, 79—98, 1993

PALAEOMAGNETISM OF SOME SYRIAN ARCS IN NORTH SINAI AND EASTERN DESERT EGYPT; TECTONIC IMPLICATIONS

A. M. KAFAFY* and A. L. ABDELDAYEM*

Department of Geology, Faculty of Science, University of Tanta

ABSTRACT

The palaeomagnetic characteristics of rocks from three Syrian arcs in Sinai and north Eastern Desert have been investigated. Rocks of Triassic, Jurassic and Lower Cretaceous ages were collected from Arif El-Naqa (NE Sinai), Maghara (N Sinai) and Shabrawet (north Eastern Desert) anticlines, respectively.

The studied rocks were subjected to AF and/or thermal demagnetization and found carrying a stable secondary magnetization. This magnetization may have been acquired during the late stage of folding in the Upper Cretaceous-Lower Tertiary time. A chemical origin is proposed for the isolated remanent magnetization as a result of recrystallization of the magnetic carriers that might have taken place due to folding forces.

When the isolated characteristic remanent directions were compared to the expected ones for each area they suggest magnetotectonic models for the studied areas. According to these models, both Arif El-Naqa and Maghara anticlines seem to have been dragged to the SE as a result of thrusting. On the other hand, the Shabrawet anticline seem to have a different tectonic attitude where block rotations around vertical axis might be responsible for the resultant deviated palaeomagnetic directions. The proposed models were geologically tested and found feasible and provide a simple explanation for the obtained palaeomagnetic data.

INTRODUCTION

Rocks assigned ages of Triassic, Jurassic and Lower Cretaceous were collected from three major anticlinal structures (Syrian Arcs, KRENKEL 1925) in Sinai and northern Eastern Desert (*Fig. 1*) in an attempt to study their palaeomagnetic characteristics and to understand their palaeomagnetic evolutional history. These arcs are Arif El-Naqa (NE Sinai), Maghara (N Sinai) and Shabrawet (North Eastern Desert). A section of 180 m thickness of sandstones and carbonates of middle Triassic age was collected from the core of Gebel Arif El Naga anticline. A Jurassic section of more than 1900 m thickness was collected from the core of Gebel Maghara anticline, where alternating carbonates and sandstones outcrop. Lower Cretaceous sandstones and carbonates (130 m thick) were sampled from Gebel Shabrawet.

The studied structural elements seem to have played an important role in the development and evolution of the Mesozoic sedimentary basins in Egypt. Furthermore, it is evident that various movements of the microplates in the Tethyan realm have affected the palaeogeographic evolution of the Mediterranean region during the Mesozoic (DIXON and ROBERTSON 1984). Several models have been proposed for the tectonic evolution of these and other Syrian folds (JENKINS 1990), with the

* Tanta, Egypt.

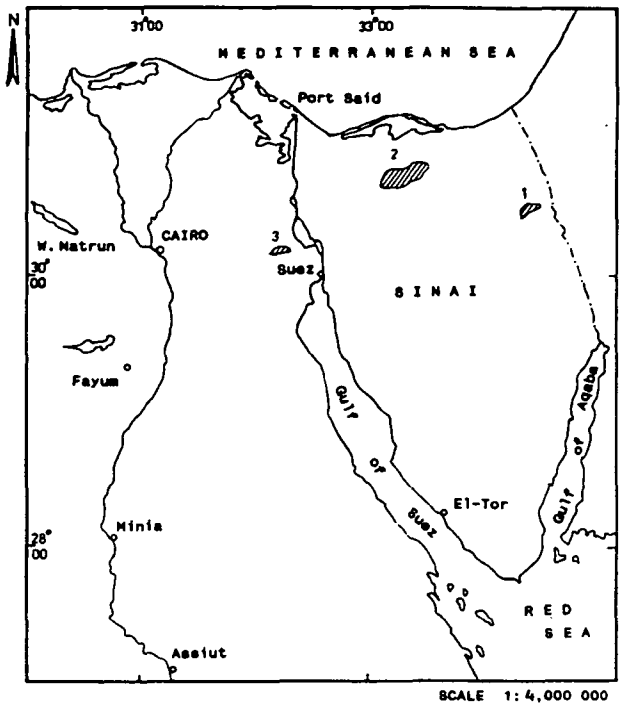

Fig. 1. Location map for the areas under study.
1—G. Arif El Naqa; 2—G. Maghara; 3—G. Shabrawet

main distinction between them is the timing of the initiation and development of the belt:

/1/ The folding was initiated in the Late Paleozoic when the embryonic Gulf of Suez rift was first initiated. Folding was then reactivated throughout the Mesozoic and the deformation climaxed in the Oligocene (for example AGAH 1981).

/2/ The fold system was mainly formed since Cretaceous and was closely related to the compressional stresses created when the Tethys Sea, between the Afro-Arabian and Eurasian land masses, began to close as a result of northerly subduction during the Late Cretaceous (Senonian) period. BARTOV *et al.* (1980), in a detailed study of the stratigraphy and structural history of Gebel Arif El Naga (NE Sinai), postulated that folding started to develop during the Coniacian, continued developing in the Santonian and persisted up to the Late Campanian. MOUSTAFA and KHALIL (1989) attributed the formation of these arcs to a right-lateral convergent wrenching during the Late Cretaceous- Early Tertiary (Laramide orogeny) due to a reactivation of pre-existing deep-seated faults which could have been formed by the late Triassic-Liassic rifting of north Africa-Arabia to form the south margin of the Tethys. On the other hand, RIVA (1986) traced the major tectonic features in Sinai using satellite images and stated that the creation of the Aqaba line due the movement of the Arabian and the African plates, originated stresses that were strongly affected by the oldest

structures, so that it rejuvenated old folds and faults. Continued movements along this line is the cause of the dragging of the pre-existing fold axes which show a change from a N 70° to a N 50° trend.

SAMPLING

Sampling was undertaken during several long field trips. Samples were all obtained by drilling to allow precise sampling. No hand samples were taken to avoid introduction of errors due to transference of orientation marks. A total of 388 oriented core samples were collected at 54 sites (averaging 7 cores from each site), where 16 sites were taken from the Triassic rocks at the core of Gebel Arif El Naga, 26 sites from the Jurassic of Gebel Maghara and 12 sites were finally collected from the Lower Cretaceous of Gebel Shabrawet. The majority of samples were oriented in situ using sun compass, while magnetic compass was only used when the Sun was not available. One site (site 6) was taken from the upper weathered basalt sill intruded in the Triassic section. Bedding orientations were measured at each site to enable structural corrections.

Attention was paid to locate sites on both limbs of these folds so that a fold test (GRAHAM 1949) could be applied. This was only possible in the Arif El Naga area where samples could be collected from both sides. In the other two areas the southern parts were inaccessible and quite disturbed and deformed by thrusting which makes them steep and nearly vertical. Consequently, sampling was mainly concentrated in the northern and central parts of the Maghara and Shabrawet folds where beds were not tectonically disturbed and had shallow dips, rarely exceed 20°.

INITIAL NRM

The initial intensities of the majority of the Triassic samples were generally at least 10 times above the spinner noise level (0.02 mAm/m) with low to fairly moderate values. Only those from the basalt sill from the Triassic outcrop were high, averaging a value of 132.2 mA/m.

The initial intensities of the Jurassic samples showed that 5 of the 26 sites (15, 22, 23, 25, 26) had too low magnetization to be measured using spinner magnetometer and these sites were measured using a cryogenic magnetometer. Three of these sites (22, 23 and 25) were extremely weakly magnetized even for a cryogenic magnetometer with a sensitivity around 0.001 mA/m. Measurements of these three sites were excluded from further analysis. The remaining 21 sites showed inhomogeneous low to fairly moderate intensities with values generally more than ten times that of the spinner sensitivity level, averaging a value of 5.9 mA/m.

The Lower Cretaceous rocks showed inhomogeneous intensities where moderate values were from the lower clastic unit (sites 1 and 2), low values were found in samples from the lower carbonate and upper clastic units, while very low values were from the samples of the upper carbonate unit (sites 11 and 12).

Stability tests

The stability of magnetization was first tested by subjecting a group of selected pilot samples, representing all lithological facies from different outcrops, to demagnetization. Stepwise AF demagnetization was first carried out at steps of 3, 5, 7.5, 10, 15, 20, 25, 30, 40, 50, 60, 70, 80, 90, and 100 mT.

Most, if not all, of the Triassic samples showed a very high stability. Except for some fluctuations of the intensities due to instrumental effects, no significant changes in either directions or intensities were recorded throughout the treatment.

The majority of the Jurassic samples showed a relatively high stability against AF. However, some samples (e.g. *Fig. 2*) showed a steady decrease of intensity, but the directions remained generally unchanged (within ±10° from the original directions).

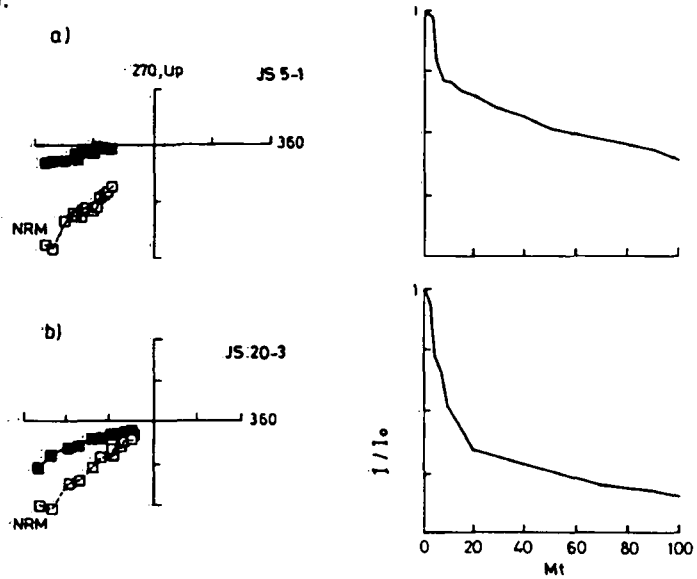

Fig. 2. Directional and intensity changes during progressive A. F. demagnetization of pilot samples from the Jurassic rocks.

Pilot samples from all of the Lower Cretaceous lithologies showed high stability against AF treatment.

As the magnetization of the majority of samples remained virtually constant during AF treatment, another collection of representative samples was selected for thermal treatment using progressive stepwise heating at 12 demagnetization steps incremented up to 680 °C. The bulk susceptibility values were measured at each step in order to monitor any mineralogical changes due to heating.

Unlike the AF method, heating had a clear effect on the magnetization of samples from different lithologies where they showed different behaviours. The magnetization of most of the Triassic samples remained fairly stable up to certain temperatures, with the intensity gradually decreasing as the heating inreased. The sandstone samples (base of the section) all behaved similarly, showing a persistent stability with mostly one component throughout the whole range of treatment (e.g.

Fig. 3). Susceptibility values began to change and showed some increase at ≥550 °C (sample 1.5 in *Fig. 4a*), but there were no significant effects on either the intensity or the direction of the remanence associated with these susceptibility changes. The sample from the basalt sill (*Fig. 3b*) showed one stable direction with

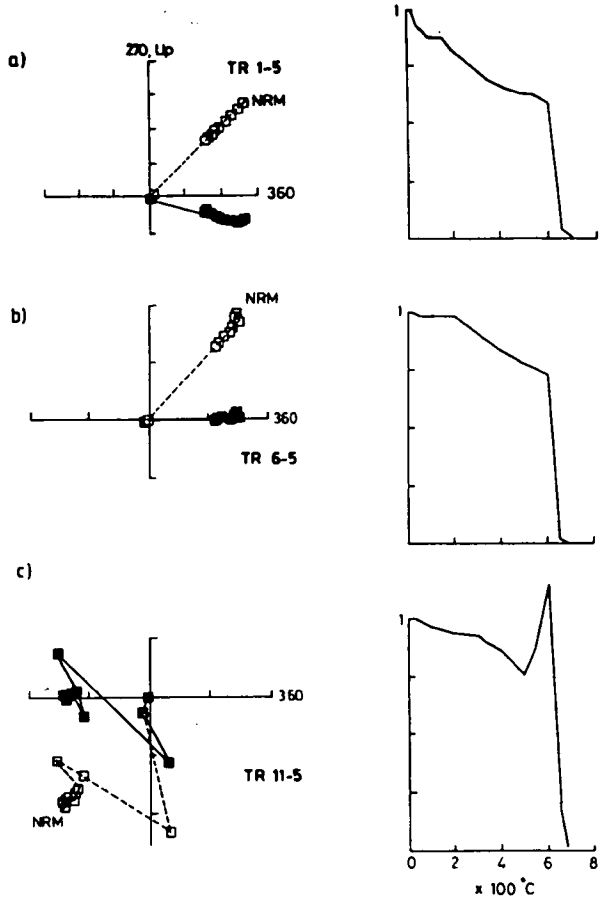

Fig. 3. Directional and intensity changes during stepwise thermal demagnetization of pilot samples from the Triassic rocks.

an intensity gradually decreasing until 600 °C above which the direction began to change, probably due to mineralogical changes associated with the susceptibility increase at ≥500 °C onwards (sample 6.5 in *Fig. 4a*). The remaining samples, mostly carbonates, showed different results, where three samples (representing sites 12, 15 and 16,) lost more than 90% of their magnetization only at 100–150 °C where the intensity dropped to the instrument noise level. Another group of samples from these sites gave similar results. Samples from these three sites were excluded from further analysis in view of their soft and probably viscous magnetization. The remaining Triassic pilot samples showed stable and mostly single magnetic components after the first or second step of heating and up to 400 °C when both the directions and the intensities began to change (e.g. *Fig. 3c*). These

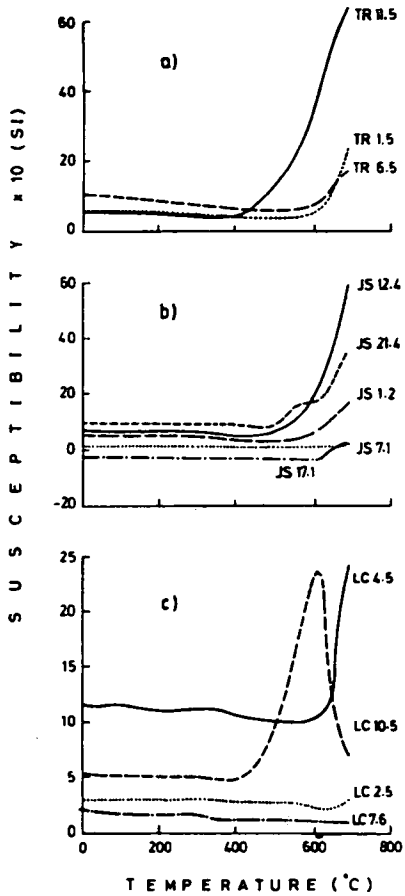

Fig. 4. Bulk susceptibility changes during thermal demagnetization of pilot samples from different localities.
a) Triassic b) Jurassic and c) Lower Cretaceous.

changes could also be attributed to mineralogical changes as indicated by the susceptibility increase at ≥400 °C (e.g. sample 11.5 in *Fig. 4a*).

Stepwise thermal demagnetization applied on a group of Jurassic samples of different lithologies reflected different behaviour. Samples from sites 2, 10 and 24 lost more than 90% of their magnetization by <150 °C and intensities became within the instrument noise. Another group of samples gave similar results, therefore the remaining samples from these sites were excluded from further analysis. Samples from the base of the section (e.g. *Fig. 5a*), after the first heating step, showed a smoothly decaying linear vector up to 500 °C when the intensity began to increase. With continued heating, the intensity decreased again until it dropped rapidly at 680 °C and became unmeasurable. Bulk susceptibility values also began to increase at 500 °C (see sample 1.2 in *Fig. 4b*). The changes in intensity and susceptibility were not accompanied by directional changes of the magnetization. The remaining pilot Jurassic samples gave similar results (*Fig. 5b-e*), except that the intensity and susceptibility values began to increase at higher

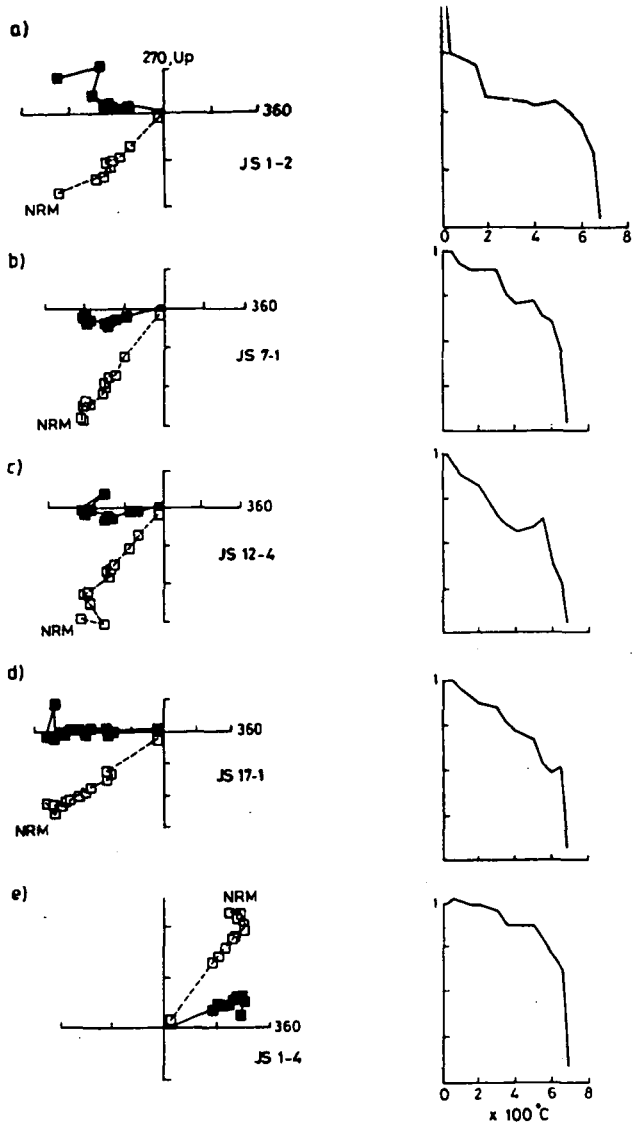

Fig. 5. Directional and intensity changes during stepwise thermal demagnetization of pilot samples from the Jurassic rocks.

temperatures (*Fig. 4a*); these changes led to some directional changes. One sample from the middle of the section (sample 17.1 in *Fig. 4b*) showed a susceptibility change from diamagnetism to paramagnetism at 600 °C.

Stepwise thermal demagnetization on pilot samples from the Lower Cretaceous rocks indicated different behaviour. The intensity of magnetization of a sandstone sample from the base (*Fig. 6a*) remained unchanged up to 200 °C, then began to decrease slowly to 60% at 650 °C and then dropped to 10% of its initial value at 680 °C but without loosing all of its magnetization even when subjected

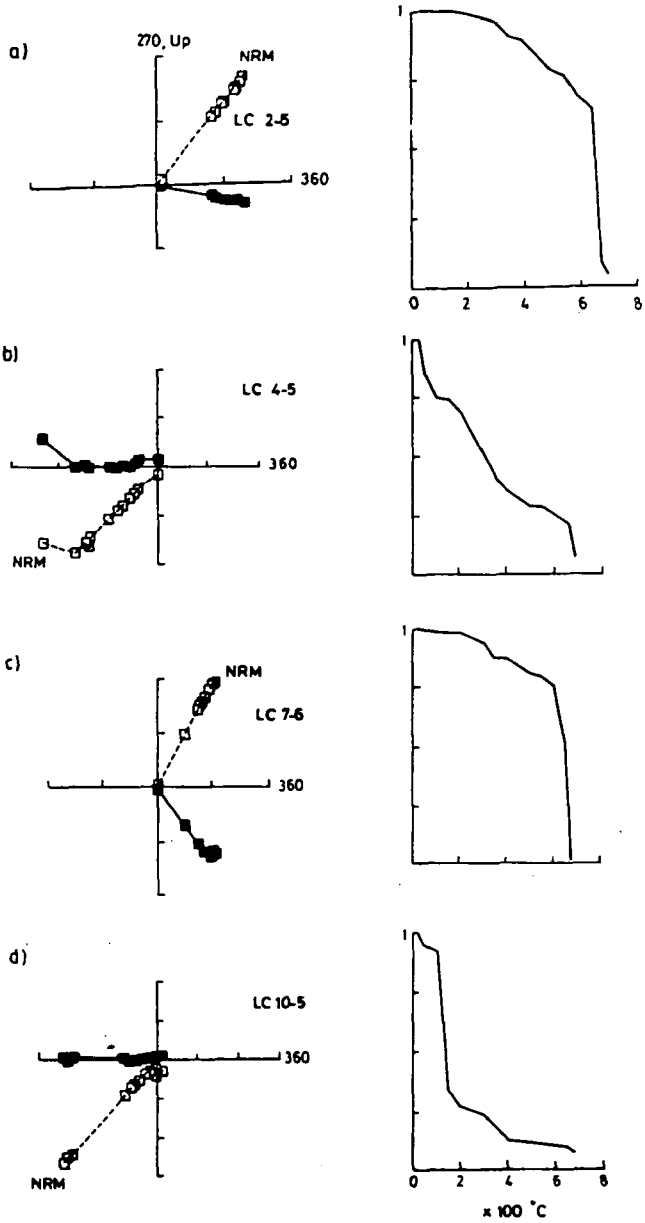

Fig. 6. Directional and intensity changes during stepwise thermal demagnetization of pilot samples from the Lower Cretaceous rocks.

to 700 °C! Directions remained unchanged throughout the whole treatment, reflecting a very high stability. Susceptibility values increased slightly after heating at 600 °C (sample 2.5 in *Fig. 4c*). Samples from the lower carbonate unit of the section (e.g. *Fig. 6b*) showed an initial 15% drop of intensity, which was followed

by a continual decrease until 680 °C when it became too weak to measure. Directions remained unchanged after the first two heating steps and up to 600 °C, then they began to change. This was accompanied by an increase of the susceptibility (sample 4.5 in *Fig. 4c*) up to a value twice that of the initial value indicating that physico-chemical changes at higher temperatures should have occurred. Sample 7.6 representing the upper clastic unit (*Fig. 6c*) showed a continuous slow decrease of intensity until 600 °C, then it dropped quickly and reached instrumental noise at 680 °C. Directions did not change significantly throughout the treatment. Susceptibility continued to decrease very slowly and reached its lowest value at 680 °C (sample 7.6 in *Fig. 4c*). Finally, the carbonate samples from the top of the section (e.g. *Fig. 6d*) showed a remarkable drop of the intensity, down to 30% of the initial value, then gradually decreased continually up to 550 °C when it began to increase to 650 °C and finally dropped to the instrumental noise at 680 °C. Directions remained unchanged after heating to 100 °C and up to 500 °C when they began to change. This was accompanied by susceptibility changes which began to increase (sample 10.5 in *Fig. 4c*) at 400 °C and reached more than three times that of the initial value at 600 °C when it began to decrease.

Bulk demagnetization

Based on the visual and statistical analysis of the stability characteristics (TARLING and SYMONS 1967; KIRSCHVINK 1980), it was decided to use thermal method to demagnetize the Triassic sandstones (base of the section) as well as the samples from the basalt sill. Steps of 300, 350 and 400 °C were found to be the optimum sequential steps to define linear components in most of the pilot samples. On the other hand, due to previously recorded thermally induced mineralogical changes as well as their low intensities, the carbonate samples (top of the section) were treated using AF. Steps of 30, 40 and 50 mT were used as they were found representing the best AF stability range.

In view of the linear analysis of the demagnetization spectra of the Jurassic pilot samples, it was decided to use thermal method to demagnetize the rest of samples from sites which showed no clear response to the AF (mostly from the middle part of the section). The best linear segments defined from the analysis of the pilot behaviour were found at steps of 250, 300, 350 °C at which temperatures most of the viscous magnetization will be removed and thermal induced changes were unlikely to occur.

The visual and statistical analysis of the stability characteristics of most of the Lower Cretaceous pilot samples revealed that the stable linear components of magnetization were much better defined using thermal demagnetization than AF. Steps of 250, 300 and 350 °C were found, in most of the pilot samples, to be sufficient to remove the soft magnetic components and leave a measurable intensity of magnetization in which the most characteristics and linear segments of magnetizations could be isolated but below the level of any recorded mineralogical changes due to heating. Therefore all the remaining samples were subjected to bulk thermal demagnetization at these three steps. Clastic samples showed better stability than the carbonate ones. The latter showed poorly defined, but comparable, within-sample directions. Samples from site 12 were all excluded as they gave unstable scattered directions due to their very low magnetization.

Directions within each sample were compared where deviant directions were discarded from different calculations. The best estimated site-mean directions (FISHER 1953) were then computed using the most reliable sample-mean direction (Table 1). In most sites the mean directions obtained from bulk demagnetization

TABLE 1

Site means cleaned NRM data before and after structural correction

Site	N	In situ Dec. °	In situ Inc. °	Unfolded Dec. °	Unfolded Inc. °	K	α_{95}°
1. Triassic							
1	6	9.6	-47.7	24.0	-66.0	304.2	3.9
2	8	179.5	42.0	174.0	58.0	93.3	5.8
3	7	176.6	29.3	164.0	43.0	18.8	14.3
4	7	25.0	-56.9	21.0	-78.0	78.2	6.9
5	7	190.5	10.3	188.0	29.0	100.6	6.1
6	8	1.7	-42.5	358.0	-58.0	276.2	3.3
7	6	198.2	28.9	190.0	58.0	16.6	16.9
8	8	188.3	36.8	171.0	51.0	96.1	5.7
9	8	177.9	36.5	160.0	48.0	21.5	12.2
10	8	193.2	46.5	169.0	62.0	56.7	7.4
11	8	186.9	46.8	162.0	70.0	208.6	3.9
12	7	Unstable and/or viscous magnetization					
13	7	187.9	31.2	178.0	56.0	14.1	16.7
14	7	185.6	35.2	175.0	62.0	126.9	5.4
15	6	Unstable and/or viscous magnetization					
16	7	Unstable and/or viscous magnetization					
Mean	13	187.3	38.0	176.6	57.5		
		α_{95} = 6.8°		α_{95} = 7.3°			
2. Jurassic							
1	5	199.7	43.0	218.0	16.0	18.5	18.3
2		NRM close to the present magnetic field					
3	7	187.3	54.7	221.0	30.0	109.6	5.8
4	7	188.1	34.1	207.0	27.0	11.6	18.5
5	6	192.3	37.7	213.0	27.0	26.4	13.3
6	8	187.8	39.5	211.0	31.0	236.9	3.6
7	9	185.1	50.3	220.0	39.0	172.8	3.9
8	7	186.9	41.5	212.0	32.0	1392.2	1.9
9	6	186.7	23.7	199.0	14.0	82.9	7.4
10		Soft magnetization					
11	6	187.0	35.7	207.0	24.0	26.8	13.2
12	6	180.4	27.3	195.0	18.0	35.2	11.5
13	6	190.6	48.0	218.0	25.0	226.4	4.5
14	7	180.3	41.5	208.0	28.0	824.6	2.1
15	7	1.6	-50.4	36.0	-33.0	106.4	5.9
16	7	190.2	40.9	211.0	24.0	34.7	10.4
17	7	201.1	38.9	217.0	17.0	32.3	10.8
18	8	3.5	-52.1	36.0	-35.0	192.8	4.0

TABLE 1
(continuation)

Site	N	In situ Dec. °	In situ Inc. °	Unfolded Dec. °	Unfolded Inc. °	K	α_{95}°
19	7	19.1	-45.2	39.0	-23.0	139.3	5.1
20	6	164.9	31.3	191.0	33.0	31.8	12.1
21	8	359.2	-56.1	43.0	-38.0	75.8	6.4
22		Very-low magnetization					
23		Very-low magnetization					
24		Soft magnetization					
25		Very-low magnetization					
26	7	191.0	43.6	217.0	21.0	37.5	10.0
Mean	20	187.1	42.1	212.0	27.0		
		α_{95} =4.40 °		α_{95} =4.27°			
3. Lower Cretaceous							
1	9	8.1	-48.3	23.0	35.0	173.1	3.9
2	8	10.1	-46.8	23.0	36.0	586.1	2.3
3	8	180.0	48.6	201.0	-37.0	76.9	6.4
4	8	182.3	46.9	200.0	-39.0	208.5	3.9
5	7	180.4	44.3	196.0	-39.0	123.5	5.5
6	8	4.4	-42.5	16.0	50.0	328.2	3.1
7	9	343.7	-55.4	22.0	31.0	70.4	6.2
8	7	175.2	42.7	195.0	-33.0	194.7	4.3
9	8	181.4	43.9	198.0	-37.0	57.3	7.4
10	8	178.6	55.1	208.0	-29.0	182.6	4.1
11	7	187.2	51.3	209.0	-36.0	40.3	9.6
12	8	Very-low magnetization					
Mean	11	181.3	48.0	201.0	-37.0		
		α_{95} = 3.6°		α_{95} = 3.7°			

N = Number of samples in each site,
Dec. and Inc. = Magnetic declination (E) and inclination in degrees,
K = Precision parameter (FISHER 1953),
α_{95} = Semi-angle cone of confidence in degrees (FISCHER 1953)

were close to those determined for the pilot samples. The bulk demagnetization successfully increased the within-site grouping in the majority of sites. This also led to improvements in the between-site grouping. Site means were mostly deviant from the present Earth's magnetic field in the studied areas (*Fig. 7*). The improvements of the within- and between-site grouping indicate successful removal of the soft magnetization and the isolation of the stable components(s) of magnetization.

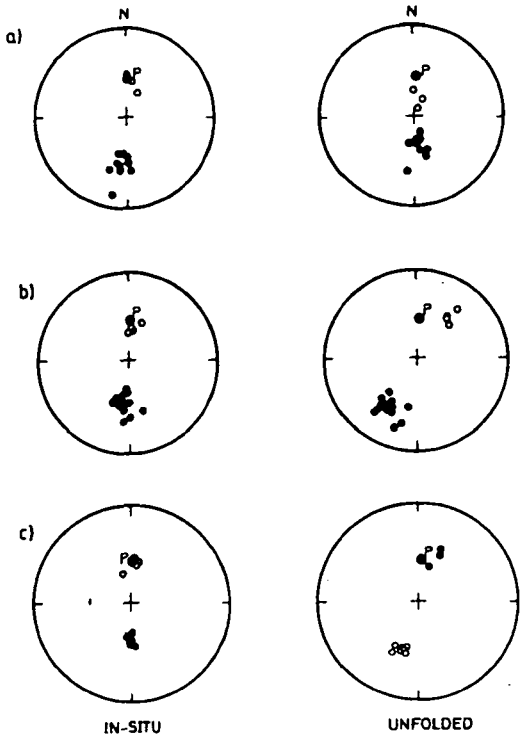

Fig. 7. Equal area stereographic projection of the site mean characteristic NRM of a) Triassic, b) Jurassic and c) Lower Cretaceous rocks before and after structural correction.

FOLD TESTS

In an attempt to date the time of acquisition of magnetization, the Fold Test (GRAHAM 1949, MCFADDEN and JONES 1981, MCFADDEN 1990) was applied on results from each of the studied three folds.

Results of a complete unfolding, i.e. a 100% unplunging and bedding correction on directions from the Triassic of Arif El Naga (Table 2) showed a negative fold test as the correction increased the dispersion of the directions around their mean (*Fig. 7a*, see also values of k and α_{95} in Table 1). Although the results from this test were not statistically reliable, they suggest that magnetization could have been acquired during or after folding.

A proper fold test could not be applied on measurements from Jurassic rocks as sampling was only restricted to the northern limb of the fold (discussed earlier). However plunge and bedding corrections were applied at each site. Using combined geological (JENKINS *et al.* 1982) and mesostructural analysis (EYAL and RECHES 1983), the plunge attitude was considered to be of 250°/20°. Results of a complete correction showed little, and statistically insignificant, improvements in the between-site grouping (Table 1, *Fig. 7b*), but the result had a significant change of directions from N-S to NE-SW. Shallow dipping could be behind the statistical unreliability of the correction. This small improvement of the grouping of directions suggests that magnetization could have been acquired prefolding.

TABLE 2

Stepwise unfolding of the studied folds.

Site	In situ		20 %		40 %		60 %		80 %		100 %	
	Dec°	Inc°	Dec°	Inc°	Dec°	Inc°	Dec°	Inc°	Dec°	Inc°	Dec°	Inc°
1. Triassic												
1	190	48	186	54	189	58	193	61	198	64	204	66
2	180	42	173	48	173	50	173	53	174	55	174	58
3	177	29	172	34	170	36	168	39	167	41	164	43
4	205	57	197	65	198	69	198	72	199	75	201	78
5	191	10	189	16	189	20	189	23	188	26	188	29
6	182	43	176	48	177	50	177	53	177	55	178	58
7	198	29	194	39	194	44	193	49	192	54	190	58
8	188	37	181	42	179	45	177	47	174	49	171	51
9	178	37	171	41	169	43	166	45	163	46	160	48
10	193	47	184	54	181	56	178	58	174	60	169	62
11	186	47	177	54	175	58	172	62	168	66	162	70
13	188	31	183	39	182	44	181	48	180	52	178	56
14	186	35	180	44	179	48	178	53	177	57	175	62
Mean	187	38	182	45	181	48	180	51	178	54	177	58
α_{95} °	6.80°		6.73°		6.78°		6.90°		7.09°		7.35°	+
2. Jurassic												
1	200	43	212	27	214	24	216	22	217	19	218	16
3	187	55	210	41	213	38	216	36	218	33	221	30
4	188	34	199	24	201	25	203	26	205	26	207	27
5	192	38	204	26	206	26	208	27	211	27	213	27
6	188	40	201	29	204	30	206	30	209	31	211	31
7	185	50	206	40	209	40	213	40	217	40	220	39
8	187	42	202	31	204	32	207	32	210	32	212	32
9	187	24	194	14	195	14	196	14	198	14	199	14
11	187	36	199	25	201	25	203	25	205	24	207	24
12	180	27	189	19	191	19	192	19	194	18	195	18
13	191	48	208	34	211	32	214	30	216	28	218	25
14	180	42	197	32	200	31	203	30	205	29	208	28
15	181	50	203	39	207	38	210	37	213	35	216	33
16	190	41	204	28	206	27	208	26	209	25	211	24
17	201	39	212	24	213	22	214	21	216	19	217	17
18	184	52	205	40	208	39	211	38	214	36	216	35
19	199	45	212	30	214	28	216	27	217	25	219	23
20	165	31	179	29	181	31	184	32	187	32	191	33
21	179	56	206	45	211	44	215	42	219	40	223	38
26	191	44	206	30	209	28	212	26	214	23	217	21

TABLE 2
(continuation)

Site	In situ		20 %		40 %		60 %		80 %		100 %	
	Dec°	Inc°	Dec°	Inc°	Dec°	Inc°	Dec°	Inc°	Dec°	Inc°	Dec°	Inc°
Mean	187	42	202	31	205	30	207	29	210	28	212	27
α_{95} °	4.40°		4.27°		4.23°		4.22°		4.25°		4.27° +	
3. Lower Creaceous												
1	188	48	211	12	211	0	211	-12	208	-24	203	-35
2	190	47	211	11	212	-1	211	-13	208	-25	203	-36
3	180	49	206	15	207	2	206	-11	205	-24	201	-37
4	182	47	206	13	206	0	206	-13	204	-26	200	-39
5	180	44	203	11	203	-2	203	-14	200	-27	196	-39
6	184	43	203	7	203	-8	202	-22	200	-36	196	-50
7	164	55	202	26	203	12	204	-3	203	-17	202	-31
8	175	43	199	13	200	2	199	-10	198	-22	195	-33
10	179	55	209	21	209	8	210	-4	209	-17	208	-29
11	187	51	211	14	211	2	211	-11	210	-23	209	-36
Mean	181	48	206	14	206	1	206	-12	204	-24	201	-37
α°	3.65°		3.73°		3.73°		3.69°		3.65°		3.71° +	

As no Lower Cretaceous samples were taken from the southern limb of the Shabrwet anticline, a complete fold test could not also be applied. However plunge and bedding corrections were applied as different sites had different attitudes. Using the plunge of 247°/35° (AL-AHWANI 1982, OMRAN 1989), a complete correction was carried out. Results indicated that the correction changed the directions significantly and even led to a change of polarity in some sites, but with little or statistically insignificant improvements of the between-site grouping (*Fig. 7c*, Table 1). The apparent improvement of the between-site grouping after the correction suggests that magnetization might have been acquired pre-folding.

In order to define whether the magnetization was acquired during or after folding a proportional stepwise unfolding (PERROUD 1983; MCCLELLAND BROWN 1983) was applied. Results at 20% increment intervals (Table 2) showed little changes in α_{95} values suggesting that the populations from the fold limbs attain their tightest grouping when the fold is restored to 20% only. This stepwise unfolding suggests a syn-deformational remanent magnetization acquired probably during the very late stages of the main phase of folding and yields a mean direction of D = 182°, I = 45°, k = 38.9, α_{95}= 6.7° for the magnetization acquired by these Triassic rocks (Table 3). The equivalent overall mean palaeomagnetic pole was then calculated and found to be of Lat. = 32.3 °S, Long = 32.9 °E, and A_{95}= 6.1°.

The tightest grouping of the Jurassic site mean directions was found between 40% and 60% correction (Table 2), which suggests that the magnetization could have been acquired during folding, i.e, syn-deformational magnetization. In consequence, magnetization acquired by these rocks could be of the same age as the folding, i.e Upper Cretaceous-Lower Tertiary (MOUSTAFA and KHALIL 1989). The obtained directions at 60% correction are considered to be the characteristic magnetization acquired by these rocks. Site mean directions (Table 3) yielded an

TABLE 3

Site mean characteristic NRM and the equivalent VGPs for different outcrops.

Site	N	Dec. °	Inc. °	Int.	VGPs	
					Lat. °	Long. °
1. Triassic						
1	6	6.0	-54.0	7.980	24.9	209.0
2	8	173.0	48.0	1.415	-30.2	41.6
3	7	172.0	34.0	1.503	-40.4	44.5
4	7	17.0	-65.0	11.133	11.2	202.7
5	7	189.0	16.0	4.709	-50.5	20.4
6	8	356.0	-48.0	127.512	30.5	218.5
7	6	194.0	39.0	0.450	-35.9	18.4
8	8	181.0	42.0	5.107	-35.4	33.4
9	8	171.0	41.0	7.649	-35.5	44.6
10	8	184.0	54.0	6.732	-25.0	30.8
11	8	177.0	54.0	25.928	-25.1	37.2
13	7	183.0	39.0	15.797	-37.5	31.0
14	7	180.0	44.0	3.486	-33.9	34.5
Mean	13	182.0	45.0		-32.3	32.9
		α_{95} = 6.7 °			A_{95} = 6.1 °	
2. Jurassic						
1	5	216.0	22.0	0.219	-35.5	348.3
3	7	216.0	36.0	3.135	-28.7	354.3
4	7	203.0	26.0	0.559	-40.4	003.4
5	6	208.0	27.0	0.714	-37.6	358.3
6	8	206.0	30.0	1.402	-36.9	001.5
7	9	213.0	40.0	3.864	-27.9	358.7
8	7	207.0	32.0	3.128	-35.4	001.2
9	6	196.0	14.0	34.633	-49.2	008.6
11	6	203.0	25.0	0.480	-40.9	003.1
12	6	192.0	19.0	1.288	-47.9	015.5
13	6	214.0	30.0	1.354	-32.9	353.5
14	7	203.0	30.0	8.912	-38.2	004.8
15	7	030.0	-37.0	0.165	31.1	180.2
16	7	208.0	26.0	6.819	-38.1	357.9
17	7	214.0	21.0	0.648	-37.2	349.8
18	8	031.0	-38.0	25.951	30.1	179.7
19	7	036.0	-27.0	21.052	33.2	170.4
20	6	184.0	32.0	0.291	-41.8	028.2
21	8	035.0	-42.0	0.744	25.7	177.9
26	7	212.0	26.0	0.262	-36.0	353.8

TABLE 3
(continuation)

Site	N	Dec. °	Inc. °	Int.	VGPs	
					Lat. °	Long. °
Mean	20	207.0	29.0		-36.6	360.0
		α_{95} = 4.22 °			A_{95} = 3.81 °	
3. Lower Cretaceous						
1	9	28.0	24.0	63.067	58.6	150.6
2	8	28.0	25.0	81.672	59.0	149.7
3	8	205.0	-24.0	7.278	-60.9	334.3
4	8	204.0	-26.0	6.016	-62.4	333.9
5	7	200.0	-27.0	1.920	-65.6	338.9
6	8	20.0	36.0	1.399	69.2	147.4
7	9	23.0	17.0	7.548	59.5	162.7
8	7	198.0	-22.0	0.333	-64.8	346.9
9	8	201.0	-25.0	0.297	-64.1	339.2
10	8	209.0	-17.0	1.408	-55.4	334.8
11	7	210.0	-23.0	0.198	-56.8	329.2
Mean	11	204.0	-24.0		-61.6	335.1
		α_{95} = 3.6 °			A_{95} = 2.8 °	

overall mean direction of D = 207°, I = 29°, K = 60.7 and α_{95}=4.2°. The equivalent VGPs (Table 4) suggest an overall mean palaeomagnetic south pole of Lat. = 36.6 °S, Long.= 360.0 °E and A_{95}= 3.8 °.

TABLE 4

Stepwise unthrusting of magnetization of the Triassic and Jurassic rocks.

Fold Axis	Direction		Pole		Rotation	
Strike/Dip	Dec. °	Inc. °	Lat ° (S)	Long ° (E)	R (°)	P(°)
1. Triassic						
In situ	182.0	45.0	-33.1	32.3	7.1±7.2	-30.4±6.7
065/10	178.4	35.9	-39.7	36.4	3.9±7.0	-23.7±6.7
065/20	176.1	26.7	-45.4	39.9	1.0±6.8	-17.9±6.7
065/30	174.7	17.3	-50.5	42.7	0.0±6.7	-12.6±6.7
065/40	173.9	7.9	-55.2	45.2	0.9±6.7	-07.8±6.7
2. Jurassic						
In situ	207.0	29.0	-36.6	360.0	33.2±5.1	-19.7±5.0
250/10	203.6	22.8	-42.2	001.4	29.3±5.1	-15.7±5.0
250/20	201.4	14.6	-46.7	001.5	27.1±5.1	-11.7±5.0
250/30	200.1	07.0	-50.8	000.5	25.8±5.1	-07.7±5.0
250/40	199.8	-00.7	-54.3	357.8	25.6±5.1	-03.9±5.0

The tightest site-mean grouping of directions from the Lower Cretaceous rocks was found when the fold was restored to 80% (Table 2). This suggests that the magnetization could have been acquired during folding, i.e during Upper Cretaceous-Lower Tertiary which is the time proposed for the age of folding. Therefore directions obtained at 80% correction have been considered to be the characteristic magnetization carried by the Shabrawet Lower Cretaceous rocks. The site-mean directions and the corresponding VGPs (Table 3) yield an overall mean site direction, giving unit weight to each site, of D = 204°, I = -24° with α_{95}= 3.6° and a corresponding palaeomagnetic south pole of Lat.= 66.1°S, Long.= 335.1°E with A_{95}= 2.8°.

DISCUSSION AND TECTONIC IMPLICATIONS

Although the fold test results were not strongly significant at a 95% statistical confidence level in directions from the three folds, which could be attributed to the shallow dipping of the beds, they still suggest that the remanence is most likely to be of secondary origin. Stepwise unfolding also indicates that magnetization was probably acquired during the very latest stage of the main phase of folding in the Upper Cretaceous-Lower Tertiary (BARTOV *et al.* 1980; ALLAM and KHALIL 1988; MOUSTAFA and KHALIL 1989). The magnetization could, therefore, have been acquired due to recrystallization of haematite as a result of chemical changes probably associated folding.

The overall palaeomagentic pole computed from site mean directions from each of the three folds was compared with the pole expected for the area under study, assuming it to be a part of stable Africa during the Upper Cretaceous-Early Tertiary times (as a proposed age of magnetization). The 80 my average palaeomagnetic pole of 63.0°S Lat, 46°E Long with A_{95}= 4.3° was chosen (IRVING and IRVING 1982; PIPER 1987, 1988; BESSE and COURTILLOT 1988, 1991) as the reference pole representing the time of acquisition of the magnetization. Using the method of BECK (1980), corrected by DEMAREST (1983), rotation and flattening were then calculated for each of the three folds.

The comparison of directions from the Triassic rocks with the chosen reference pole yielded 7.1°±7.2° for the rotation about the vertical axis, i.e insignificant rotation. They also yielded -30.4°±6.7° for the rotation about the horizontal axis, which indicates substantial palaeopoleward translation.

The comparison of the overall palaeomagnetic pole computed from the Jurassic site mean directions with the reference pole yielded a significant rotation of 37.3°±5.2° about the vertical axis and -22.2°±5.1° rotation about a horizontal axis. The latter suggests a substantial south poleward translation.

When the palaeomagnetic pole from the Lower Cretaceous rocks was compared to the reference pole it yielded a significant rotation of 28°±4.6° around the vertical axis and an insignificant rotation of 1.9°±4.5° along the horizontal axis. This indicates that, unlike the results from Arif El Naga (Triassic) and Maghara (Jurassic), this result does not suggest a palaeopole translation component and the rotation around vertical axis is the only significant.

The resultant southward poleward translation of 30° for the Triassic rocks and 22° for the Jurassic rocks cannot be accommodated but due to local tectonic effects. This is due to the fact that the tectonic history of these areas, as a part from the stable north Sinai province, gives no evidence whatsoever to support the idea that the region has translated either to the north or to the south as a separate microplate. This is also evident from the fact that there is a continuity of geological formations,

since early Mesozoic age and onwards, extending from Sinai to southern Israel into Lebanon and Syria, with no clear tectonic disruption reported.

It has been known that pole translation can be interpreted as a result of normal, or reverse, faulting, which could lead to a change in the magnetic inclination (RON *et al.* 1986). This gives a clue that this component could be related to the effect of the thrusting which affected the two areas at their southern borders. The thrusting which was contemporaneously with, or soon after, the main folding (BARTOV *et al.* 1980; MOUSTAFA and KHALIL 1989), could have pulled these folds rigid blocks, towards the SE. Consequently, the beds attitude has changed from, presumably, fairly steep and symmetric on both sides of the fold to shallow, <20°, in the north and very steep or overturned in the south, close to the thrust.

An attempt to test this model for the restoration of these folds to a pre-thrusting attitude was made by applying a stepwise conventional bedding correction to the magnetization resulted from rocks of the two folds using their axes directions and proposed angles to pull the folds back to the NW. The proposed model appears to be applicable as the pole translation component becomes insignificant at an angle of 40° for the Triassic rocks and 30° for the Jurassic rocks (Table 4) when both anticlines are pulled back to the NW.

The geological applicability of the proposed model has also been tested by applying the same bedding correction used previously for the magnetization to two in-situ field readings for bedding on both sides of the Arif El Naga fold. The reading from the northern flank had an attitude of 120°/10° while the other from the southern flank had an attitude of 075°/80°. Results of the suggested stepwise unthrusting (Table 5) suggest that the Arif El Naga fold, and Maghara by implication, could have been a symmetrical anticline before thrusting with the beds on the limbs dipping between 40° and 45°.

TABLE 5

Stepwise unthrusting of the Arif El Naga anticline.

Fold	Fold axis attitude				
limb	In situ	065°/10°	065°/20°	065°/30°	065°/40°
Northern	120/10	093/18	083/27	079/37	076/46
Southern	075/80	076/70	076/60	078/51	080/41

The presence of faulting and folding (MOUSTAFA and KHALIL 1989) as well as the large scale of the Maghara fold (1500 km^2), could have led to a rotation about an inclined axis which in turn might have resulted in the combined rotation around both the horizontal and vertical axes. This might account for the remaining significant angle of rotation of 25.6°±5.1° around the vertical axis. The area, like most of the North Sinai province, is highly deformed by sets of E-W trending strike-slip faults. It has long been recognized that fault blocks in strike-slip tectonic domains must progressively rotate on vertical axes as the overall strike-slip motion continues (FREUND 1974, RON *et al.* 1984, GARFUNKEL and RON 1985).

The remaining clockwise rotation of 26° around a vertical axis of the Maghara fold could, therefore, only be related to the effect of the strike-slip faults recognized in the area. These faults could have created separate fault domains, in each of which the rocks should rotate in the same way, but rocks in different domains rotate in different ways.

The available limited picture of tectonic setting of the Shabrawet area (SAID 1962, AL-AHWANI 1982, OMRAN 1989), on the other hand, does not support rigid block rotation, instead the area is highly dissected by faults dominated by two main

sets of high angle normal faults, the older ENE—WSW which affected the Cretaceous rocks and younger trending NW—SE and exposed the Eocene rocks. The latter were rejuvenated in the late Miocene due to the opening of the Gulf of Suez (AL-AHWANI 1982). This might have risen the local stresses and deformation of the area as it becomes a part of the plate marigin between the Arabian plate and the Sinai microplate separated by the Gulf of Suez. Consequently, in order to accommodate these stress strike slip movements, probably of left lateral sense, could have occurred along the old NW—SE faults. This new movements would create separate fault domains which would cause rocks to rotate in the same sense within each of these domains and probably in different sense in the other domains. The obtained 28°±4.6° degree of rotation could therefore represent the average value of the different movements. At the moment and with the available limited structural field observations it is difficult to depict a clear tectonic setting of the area in a satisfactory way. Therefore more palaeomagnetic and field observational data are essentially required for further analysis.

SUMMARY

The studied rocks were found carrying a stable secondary magnetization, probably acquired during the late stages of the folding in the Upper Cretaceous-Lower Tertiary time. Palaeomagnetic results from the different areas suggest a chemical origin for the magnetic minerals carrying the magnetization as a result of recrystallization which could have taken place due to the folding forces. The results also throw some more light on the origin and development of these anticlines, suggesting that the folds were dragged to the SE as a result of the thrusting and that this probably took place during or soon after folding. The proposed models have been found geologically feasible and provides a simple explanation of the palaeomagnetic observations.

ACKNOWLEDGEMENTS

Measurements of the samples were carried out at the Palaeomagnetic Lab. of the Department of Geological Sciences, University of Plymouth, England. We would like to thank with gratitude Professor D. H. TARLING University of Plymouth, for giving access to use the palaeomagnetic instruments and for kind help, guidance and fruitful suggestions. Thanks are also due to Dr E. HAILWOOD Oceanography Department, University of Southampton, England, for allowing us to use the cryogenic magnetometer.

REFERENCES

AGAH A. 1981. Structural map and plate reconstruction of the Gulf of Suez-Sinai area. Rep., Conoco Oil Co., Houston, Texas, USA.

AL-AHWANI M. M. 1982. Geological and sedimentological studies of Gebel Shabrawet area, Suez Canal district. Egypt. Ann. Geol. Surv. Egypt. **12**, 305—381.

ALLAM A. M. and KHALIL H. M. 1988. Geology and stratigraphy of the Arif El-Naqa area, Sinai, Egypt. Egypt J. Geol. **32**, 199—218.

BARTOV Y., LEWY Z., STEINITZ G. and ZAK I. 1980. Mesozoic and Tertiary stratigraphy, paleogeography and structural history of the Gebel Arif en Naga area, eastern Sinai. Isr. J. Earth Sci. **29**, 114—139.

BECK M. E. JR. 1980. Paleomagnetic record of plate margin tectonic processes along the western edge of North America. J. Geophys. Res. **85**, 7115—7131.
BESSE J. and COURTILLOT V. 1988. Paleogeographic maps of the continents bordering the Indian Ocean since the Early Jurassic. J. Geophys. Res. **93**, 11,791—11,808.
BESSE J. and COURTILLOT V. 1991. Revised and synthetic apparent polar wander paths of the African, Eurasian, North American and Indian plates, and true polar wander since 200 Ma. J. Geophys.. Res. **96**, 4029—4050.
DEMAREST Jr. H. H. 1983. Error analysis for the determination of tectonic rotation from paleomagnetic data. J. Geophys. Res. **88**, 4321—4328.
DIXON J. E. and ROBERTSON A. H. F. (eds) 1984. The gelogical evolution of the eastern Mediterranean. Blackwell Sci. Publish. Oxford, 824 p.
EYAL Y. and RECHES Z. 1983. Tectonic analysis of the Dead Sea rift region since the late Cretaceous based on mesostructures. Tectonics. **2**, 167—185.
FISHER R. A. 1953. Dispersion on a sphere. Proc. R. Soc. Lond. A217, 295—305.
FREUND R. 1974. Kinematics of transform and transcurrent faults. Tectonophys. **21**, 93—134.
GARFUNKEL Z. and RON H. 1985. Block rotation and deformation by strike-slip faults 2.The properties of a type of macroscopic discontinous deformation. J. Geophys. Res. **90**, 8589—8602.
GRAHAM J.W. 1949. The stability and significance of magnetism in sedimentary rocks. J. Geophys. Res. **54**, 131—167.
IRVING E. and IRVING G. A. 1982. Apparent polar wander paths Carboniferous through Cenozoic and the assembly of Gondwana. Geophys. Surv. **5**, 141—188.
JENKINS D. A. 1990. North and Central Sinai. *In:* SAID R. (eds) The geology of Egypt. Rotterdam and Boston, Balkema, 361—380.
JENKINS D. A., HARMS J. C. and OESLEBY T. W. 1982. Mesozoic sediments of Gebel Maghara, north Sinai. Sixth E.G.P.C. Explor. Seminar Cairo. **1**, 130—158.
KIRSCHVINK J. L. 1980. The least-squares line and plane and the analysis of palaeomagnetic data. Geophys. J.R. astr. Soc. **62**, 699—718.
KRENKEL E. 1925. Geologie Afrikeas. Brontraeger, Berlin. **1**, 461p.
MCCLELLAND BROWN E. 1983. Palaeomagnetic studies of fold development and propagation in the Pembrokeshire Old Red sandstone. Tectonophys. **98**, 131—149.
MCFADDEN P. L. 1990. A new fold test for palaeomagnetic studies. Geophys. J. Int. **103**, 163—169.
MCFADDEN P. L. and JONES D. L. 1981. The fold test in palaeomagnetism. Geophys. J. R. astr. Soc. **67**, 53—58.
MOUSTAFA A. R. and KHALIL M. H. 1989. North Sinai: Structures and tectonic evolution. M.E.R.C. Ain Shams Univ. Earth Sci. Ser. **3**, 215—231.
OMRAN M. A. 1989. Geological studies in Shabrawet area. Suez Canal, Egypt. M.Sc. Thesis, Suez Canal Univ. 234 p.
PERROUD H. 1983. Palaeomagnetism of Palaeozoic rocks from the Cabo de Penas, Asturia, Spain. Gephys. J. R. astr. Soc. **75**, 201—215.
PIPER J. D. A. 1987. Palaeomagnetism and the continental crust. Open Univ. Press, Milton Keynes, 434 p.
PIPER J. D. A. 1988. Palaeomagnetic database. Open Univ. Press, Milton Keynes, 304 p.
RIVA E. T. 1986. Compressive features and wrench tectonics in western central Sinai. Eighth Explor. Sem. Cairo, November 1986.
RON H., FREUND R., GARFUNKEL Z. and NUR A. 1984. Block rotation of strike-slip faulting: structural and paleomagnetic evidence. J. Geophys. Res. **89**, 6256—6270.
RON H., AYDIN A. and NUR A. 1986. Strike-slip faulting and block rotation in the Lake Mead fault system. Geology. **14**, 1020—1023.
SAID R. 1962. The geology of Egypt. Elsev. Publish. Co. Amster., 377 p.
TARLING D. H. and SYMOND D. T. A. 1967. A stability index of remanence in palaeomagnetism. Geophys. J. R. astr. Soc. **12**, 443—448.

Manuscript received, 14 January, 1993

Acta Mineralogica-Petrographica, Szeged, XXXIV, 99—117, 1993

DOUBLE-LAYERED EQUATION OF MOTION: PLATONIC-ARCHIMEDEAN SPHERICAL CELLULAR AUTOMATA IN THE SOLUTION OF THE INDIRECT VON-NEUMANN PROBLEM ON SPHERE FOR TRANSFORMATIONS OF REGULAR TESSELLATIONS

SZ. BÉRCZI*

Department of General Technics of Eötvös Loránd University

ABSTRACT

This paper shows a method of the parallel description of transformations of a structure which involves two levels of hierarchy and its transformations concern both hierarchy levels. The method reworks the cellular automaton model, but uses it in the direction of the indirect von Neumann problem (BÉRCZI 1991).

Tabular order of the transformational relations between Platonic and Archimedean (without distinguished rotational axis) solids was given on the basis of the truncation operation 13 years ago (BÉRCZI 1980). In this paper the reformulation of the system by a cellular automata in the form of indirect von-Neumann problem (BÉRCZI 1985) solution is given.

THE TRANSFORMATIONS OF A WHOLE BY ITS PHASES

If we are not present during the transformations of an object: the WHOLE, then we need to introduce a principle to be able to describe these transformations. Step by step in time, we may observe the transformations, so we can describe the process by the sequence of the moment-observations. These moment observations are the phases of the transformational process. So the description of the process will be given in the form of the sequence of these phases.

THE TWO HIERARCHY LEVELS OF SYMMETRY

The concept of symmetry inherently involves two levels of hierarchy of the structure. Symmetry is the invariance of a WHOLE over transformations, which may exchange some of the ELEMENTS, which build up the WHOLE. So the ELEMENTs and the WHOLE form two different levels of hierarchy. If symmetry is manifested in the form of a geometrical object, then the elements, which build up the geometrical object, form a pattern. This pattern is a regular arrangement on a surface. Both the regular LOCAL arrangement of the elements, and the regular GLOBAL structure of the WHOLE are important constituents of the SYMMETRY OF THE WHOLE. Both regularities of the two hierarchy levels are used up in construc-

* H—1088 Budapest, Rákóczi út 5, Hungary (after 1-st Jan. 1994: Department of Astronomy, Eötvös University H—1083 Budapest, Ludovika tér 2.)

tion and specification of the cellular automaton model. The coherency between the two regularities makes it possible to decipher local operations of the elements from the global transformations of the whole. This problem of deciphering will be the indirect von-Neumann problem.

THE CELLULAR AUTOMATON MODEL: A TENTATIVE AXIOMATIC APPROACH

The unification of the former two structural descriptions: the TRANSFORMATIONS OF A WHOLE BY ITS PHASES (*Fig. 1*) and the SYMMETRY OF A WHOLE results in a constructive approach to build up the cellular automaton model. The

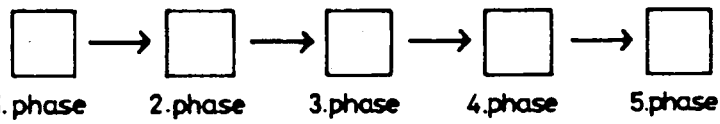

Fig. 1. The TRANSFORMATIONS BY ITS PHASES principle.

principle: TRANSFORMATIONS BY ITS PHASES gives a step by step discrete description of the transformations of the WHOLE and the ELEMENTS. The principle: SYMMETRY OF THE WHOLE gives the structural constraint of the description of transformations on two hierarchy levels: on the level of the ELEMENTS, and on the level of the WHOLE. (*Fig. 2*). So in the cellular automaton model the description of the transformations is given on both hierarchy levels in parallel form. (*Fig. 3* and *4*)

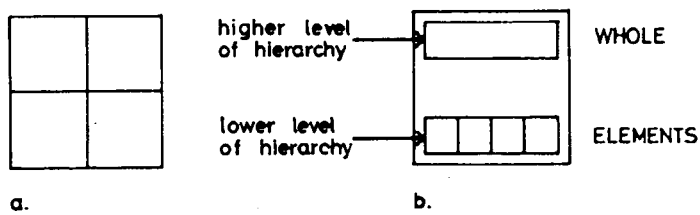

Fig. 2. The decomposition of the WHOLE, which has symmetries. **a.** The symbol shows, that elements build up the whole. **b.** The symbol shows the two hierarchy levels of the whole; used later.

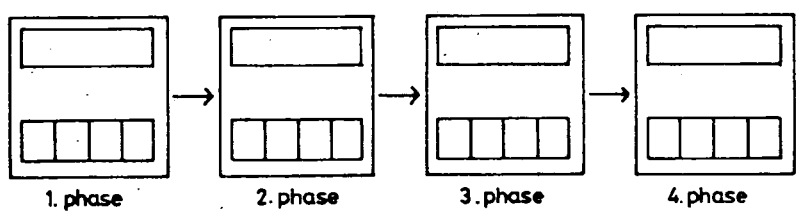

Fig. 3. The WHOLE with symmetry and so with two hierarchy levels has been substituted into the graph of the TRANSFORMATIONS BY ITS PHASES principle (*Fig. 1*) in the form of **b.** of *Fig. 2.*

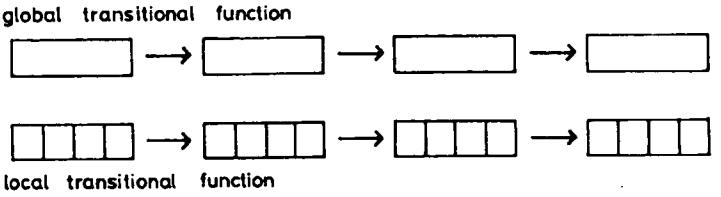

Fig. 4. Separation of phase blocks to its two parts gives the most characteristical framework of the cellular automatic description: the two parallel "equations of motion": that on the higher level of hierarchy — i.e. the GLOBAL TRANSITIONAL FUNCTION, and that on the lower level of hierarchy — i.e. the LOCAL TRANSITIONAL FUNCTION. Both functions are discrete functions in time. Detailed specifications of the model are given in *Fig. 5.*

FRAMEWORK OF THE CELLULAR AUTOMATIC SYSTEM'S DESCRIPTION

On the basis of the three introductory principles and other earlier works (i.e. VOLLMAR 1978, BÉRCZI 1991) we may summarize the sturctural characteristics and specifications of the description style of cellular automata as a framework. It is composed from two parts of the description on two hierarchy levels. The two parts are: the CELLULAR BACKGROUND, which is the structural one, and the TRANSITIONAL FUNCTION, which is the kinematical one. The two levels of hierarchy are: the LOCAL one, that of the cells, and the GLOBAL one, that of the WHOLE, the SYSTEM of the cell-mosaic itself.

The two X two (2x2) system of condiditons of description in the framework of cellular automata system suggests a matrix-summary of conditions. So first we give the tabular form (from BÉRCZI 1991) and then the Relation-table of the conditions (*Fig. 5*).

A. CELLULAR BACKGROUND

Aa. Local characteristics of the cell-mosaic system give the form of cells, their connections and neighbourhood relations (with initial condiditons)

Ab. Global characteristics of the cell-mosaic system give the enclosure of the local relations to form a whole, a surface of the cell-mosaic system

B. TRANSITIONAL FUNCTIONS

Ba. Local transitional function for cell-mosaic elements which are individual automata (this is a discrete funciton of steps in space and time)

Bb. Global transitional function for the whole surface built up by the cell-mosaic system as a whole (this function is also a discrete one consisting of the sequence of the stages of discrete transformations summarized from cellular steps)

Cellular automatic framework about description of transformations	L O C A L	G L O B A L
B A C K G R O U N D	Aa the form, the elementary neighbourhood, the connections and the initial states of cells	Ab the cell mosaic system built together from cells; a surface or spatial region with its initial parameters
T R A N S I T I O N	Ba transition of cellular states, / local transitional function/: depends on the states of neighbour cells, on the earlier state of the cell itself, and on the program written into the cell	Bb transition of the cell mosaic system /surface or spatial region/ composed of the cells: this global transitional function is summarized from the local transitions of the cells, step by step in time
H I E R A R C H Y	First, lower level of hierarchy	Second, higher level of hierarchy

Direction of construction of operation — direct von Neumann problem →

Deciphering of state changes and their description — indirect von Neumann problem ←

Fig. 5. Relation table of the specifications of the cellular automata models. Directions of the direct and indirect VON NEUMANN problems are also shown below.

DEFINITION OF THE INDIRECT VON-NEUMANN PROBLEM

If we consider the cellular automatic description of a deformational motion of a cell-mosaic-system as a new motion-description on a flexible or plastic background, then the first step is the formation and definition of the background and the second one is the formulation of transitional function. But in the cellular automaton modelling there is a double-level description, so the direction of problem formulation is open both for Ba→Bb and Bb→Ba cases. The classical way of construction and development of the cellular automaton modelling was: /1/ construction of Aa and Ab background, /2/ construction of the Ba local transitional function, /3/ deduction of the Bb global transitional function. Although iteration could happen between Ba and Bb function formulation, in the given sequence of formulation of problem solving the last step was the summary of the model. So the Ba→Bb direction of construction is characteristical to such modelling. We call this

direction of construction to the direct von NEUMANN problem. The principal aim of the construction of von Nemann's cellular automata model was to build a self-reproducing structure on the level of the global background by a global transitional function.

The direction of our efforts in problem solutions in this paper is the opposite direction in the level of transitional functions, if compared to that of von NEUMANN's problem solution. Our aim is to read out local transitional function (uniform for all cells) from the given or reconstructed global transitional function. Therefore we call our program and formulation to indirect von NEUMANN problem (Bb→Ba). *(Fig. 5)*

FEED-BACKS AND COHERENCY OF LOCAL AND GLOBAL STRUCTURE

Symmetry of the cell-mosaic background means a coherency of regularity between its local and global structure. Therefore symmetry results in simplicity in the formulation of the transitional functions in the cellular automaton model (Ba and Bb). But symmetry of the cell-mosaic structure has another benefit, too. Symmetry may make it possible to formulate easily the direct (Ba→Bb) or the indirect (Bb→Ba) program in model-construction; these transcriptions make complete the cellular automaton model. In our formulations of the indirect programs (transcriptions of the global transitional function into the local one) we shall use up these benefits of symmetry.

Global structure (background, *Fig. 6*) is a kind of feed-back of local regularity (transitional function, *Fig. 6*) into itself, if the surface is at least partly closed. Movements, which are important cellular-automatic local operations in our formulations, partly rearrange this feed-back structure, too. Movements between cells are allowed, because a degree of freedom remains to carry out it: /1/ if the surface is only partly closed, or /2/ if a regular separation-operation make cells partly and temporaly free in the temporaly and partly loosed structure. After rearranging cell-movements cells fix their new contacts. These kinds of operations are the main benefits of our modelling symmetry by cellular automata (BÉRCZI 1985).

In our paper we refer to other ones and show one such kind of model where partial and local deformations of the cells form the local operations.

THE MAPPING OF PHENOMENA IN ORDER TO SELECT THOSE WHICH NEED CELLULAR AUTOMATIC DESCRIPTION

We may construct a compositional diagram for three basic components. The components are: basic characteristics of phenomena in everyday experiences. These were the following basic characteristics: RIGID, GRANULAR-COARSE, and CRUMPLED-SOFT. Different mixing of these components in phenomena occurs in those ones which take place inside the triangle (according to the compositional regulas of VIVIANI's theorem). The mostly viable phenomena which are combined from the three basic characteristics can be found in the centre of the triangle (*Fig. 7.*): they are weighted with almost equal weights from the three components. These phenomena are: crops of plants and some parts of plants themselves, embryos, cell systems and nets, and crystal-structure rearrangements, etc.

Cellular automatic description of cell-mosaic system's deformational transformations does not fix the time-scale of the phenomena. So the same transformational process may represent a short and a very long time process. That is the case

CLASSICAL FORM OF DESCRIPTION OF TRANSFORMATIONS IN CELL-SYSTEM	SPECIFICATIONS IN THE CELLULAR AUTOMATON MODEL			
	BACKGROUND		TRANSITIONAL FUNCTIONS	
	Aa LOCAL	Ab GLOBAL	Ba LOCAL	Bb GLOBAL
SYSTEM OF REFERENCE	THE NETWORK (MOSAIC) AND SHAPE OF THE CELLS	INVARIANT PROPERTIES OF SURFACE		
INITIAL CONDITIONS	SPECIFICATIONS OF THE INITIAL VALUES OF CELL STATES	SPECIFICATIONS OF THE INITIAL PARAMETERS OF THE NETWORK		
BORDER CONDITIONS		SPECIFICATIONS OF THE TYPE OF THE SURFACE (TOPOLOGY)		
FEEDBACK INVOLVED IN STRUCTURE		DETERMINED BY RETURNING BANDS OF CELLS ON THE SURFACE	DETERMINED BY NEIGHBOURHOOD EFFECTS OF CELLS	
EQUATIONS OF MOTION			TRANSITIONS OF STATES OF CELLS DEPEND ON CELL INTERACTIONS	TRANSITIONS OF THE WHOLE SURFACE SUMMED UP FROM CELL-TRANS.

Fig. 6. Feedbacks appear on two hierarchy levels and in two types of specifications in the cellular automaton model. (with black frame). Feedback in the global background is resulted in by the enclosure of the surface into itself (or with a BORN-KRÁMÁN boundary condition).

with our crystal structures during crystallization, or recrystallization under high pressure. Different final products of the process can be found in different truncated stages but the reconstruction of the transformational sequence can be considered as a short term transformation during the development of an individual, (an entity of a mineral,) and at the same time it can be considered as a stage of transformational process which resulted in reaching of different final stages of the process modelled by the cellular automatic description. So our first example will show the cellular automatic description of truncation of Platonic and Archimedean solids and tesselations: it is partly a summary of earlier papers (BÉRCZI 1979, 1980, 1991).

EVOLUTIONARY SERIES FROM MULTITUDE.

Where can be found a community of the same type of structures in order to select a representative series for the development and evolution of the structure of

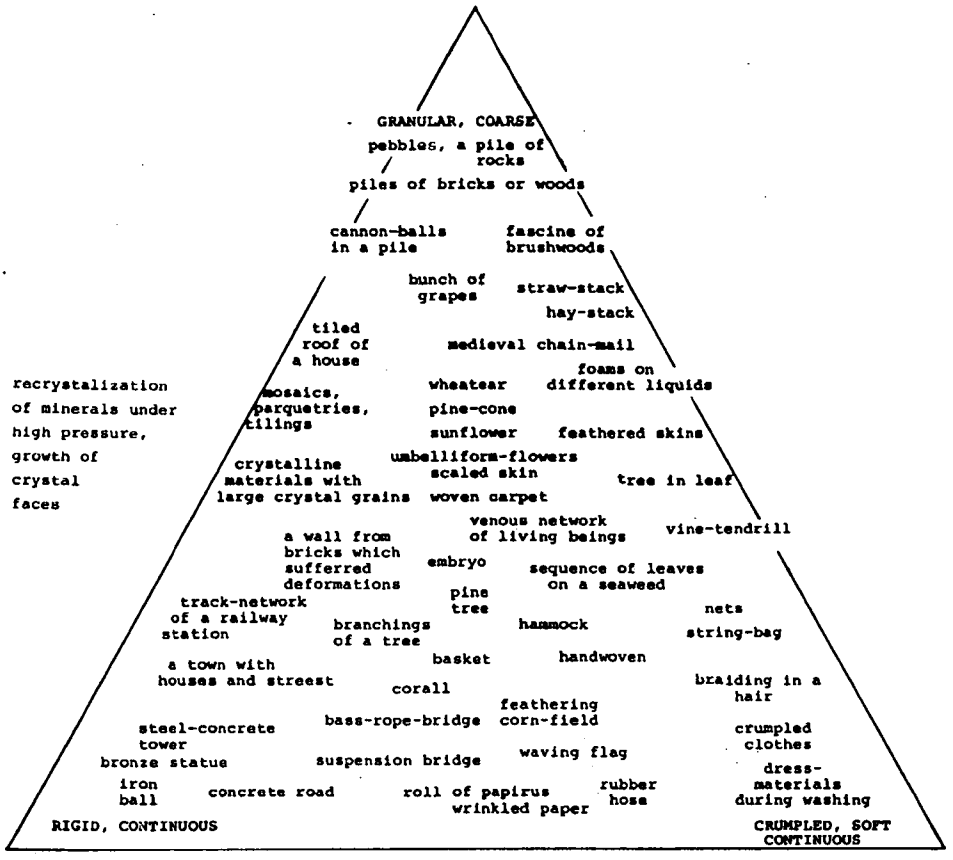

Fig. 7. Mapping of phenomena (different structures) according to three basic characteristics: RIGID, GRANULAR-COARSE and CRUMPLED-SOFT. The problem shown in this paper can be found in the center of this map, signed by a dot. Other related problems can be found in frame.

such type? Because the description: CHANGES BY THE PHASES needs such a community as a background of the phenomena to model the evolutionary events. Individuals in the community grow with different speeds, so in a community (or multitude) we can find representatives from different periods of the life-stage of individual structures. At one moment these individuals of such multitude represent a stage of an evolutionary or developmental sequence (depending on the time scale to be considered). Such multitude for example can be an open or globular cluster of stars, or a forest of trees. Observing the characteristics of the elements (the wholes, the individuals) of the multitude, a sequence of representative individuals can be selected from the multitude, they can be arranged into an evolutioary series according to these time dependent characteristics. This sequence (or chain) of the whole (individuals) gives a discrete description about the stages of transformations of the structure type, so in this form the principle of CHANGES BY THE PHASES of transformations was used on the multitude. The principle of selection of EVOLUTIONARY SERIES FROM MULTITUDE is an important tool, when we intend to formalize the abstract way of the foundation of cellular automatic description of

wholes. (*Fig. 8.*) A further principle is necessary, however, if we want a next step to the double-layered description of transformations. This principle has been detailed earlier: the SYMMETRY OF THE WHOLE, which implies two layered structure of the whole.

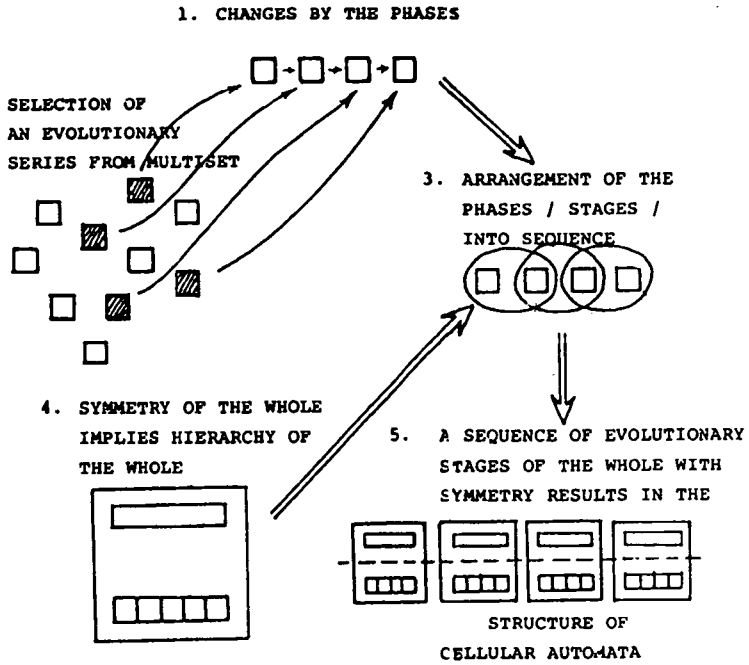

Fig. 8. The summary of principles which were necessary to the foundation of cellular automata description of the state changes of a whole with symmetry. The steps of the using of these principles in solving a problem can be given as follows: /1/ I can describe kinematics by CHANGES BY THE PHASES of a whole. /2/ Because of evolutionary events on individual wholes I can select a series of wholes from a multiset to describe the evolutionary steps. /3/ I can arrange them into a sequence. /4/ If the wholes are with symmetry, than they have two layers of hierarchy in their structure. /5/ Then cellular automata decomposition of the evolutionary sequence is possible.

THE "ACTORS" OF OUR MODEL: THE PLATONIC AND ARCHIMEDEAN SOLIDS

The basic process to be studied here by cellular automata description is the hypothetical changes of faces on crystal. But the same process advances when recrystallization happens under high pressure: there the coordination numbers change because of different compressibility of different ion-balls. We shall see that this second type of transformation is a higher dimensional equivalent "truncation" problem, as the first one. Both cases can be used in formulating the most simple cellular automata model, in crystallography.

Transformation of a spherical cellular system is a common phenomenon in development of embryonal structures too. These transformations may be formulated according to different languages of descriptions. Among the most simple cases of such transformations there are those which preserve some properties of the initial cellular arrangement. One form of initial simplicity of cellular arrangements is the symmetry. Now we study those spherical cell-arrangements which

have symmetries that of the Platonic solids. We do not distinguish solids (which are covered by regular faces) and spherical tessellations (which are the corresponding cellular mosaics on the circumscribed spheres by central projection of the former solids).

Platonic solids are covered by congruent regular polygons of the same kind, while Archimedean solids are covered by 2 or 3 types of such regular polygons. Symmetry of these solids means regularity of not only the covering polygons, but the uniformity of the vertex configurations, too. This uniformity of the vertices allows a simple naming of these solids according to the polygons meeting at a vertex (listed in a given circulating order around a vertex). These are the STEINER symbols: the cube is named (4,4,4), the octahedron is (3,3,3,3) according to Steiner's terminology, (where numbers mean the sides of a regular polygon meeting at a vertex). The solids involved in our problem-solving are given in *Fig. 9.* Those solids, which traditionally are also Archimedean solids, and can be

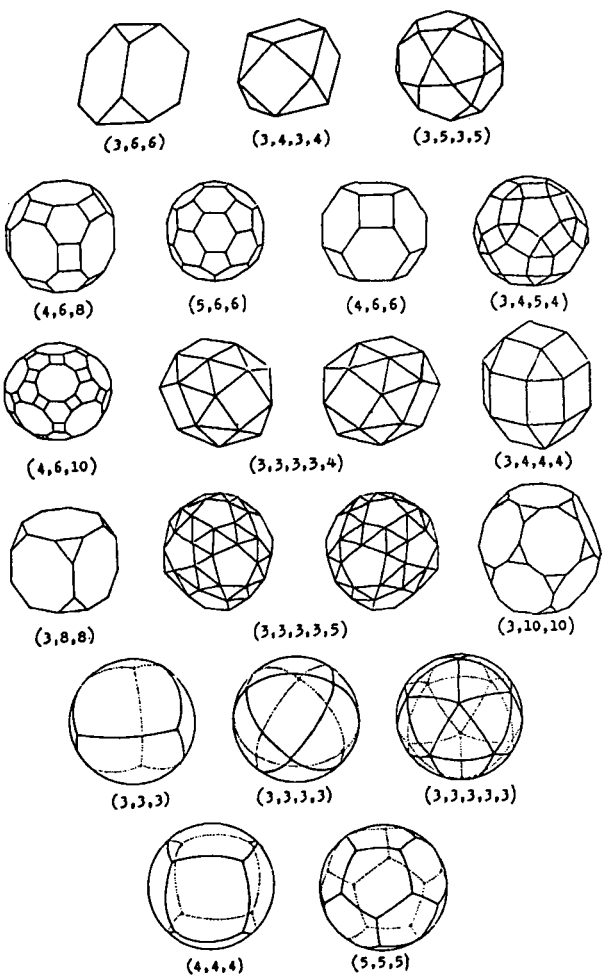

Fig. 9. The complete set of Archimedean solids (upper four rows) and Platonic solids (in their spherical tessellation form, lower two rows) which were arranged in a periodic table according to a cellular automatic operation: by truncation.

given by Steiner symbols, but has distinguished rotational axis, do not take part in our transformational system (*Fig. 10*). These prisms and antiprisms can not involved into a sequence where solids are listed according to a coherent transformational operation on their faces (on sphere on cells): this operation is the truncation.

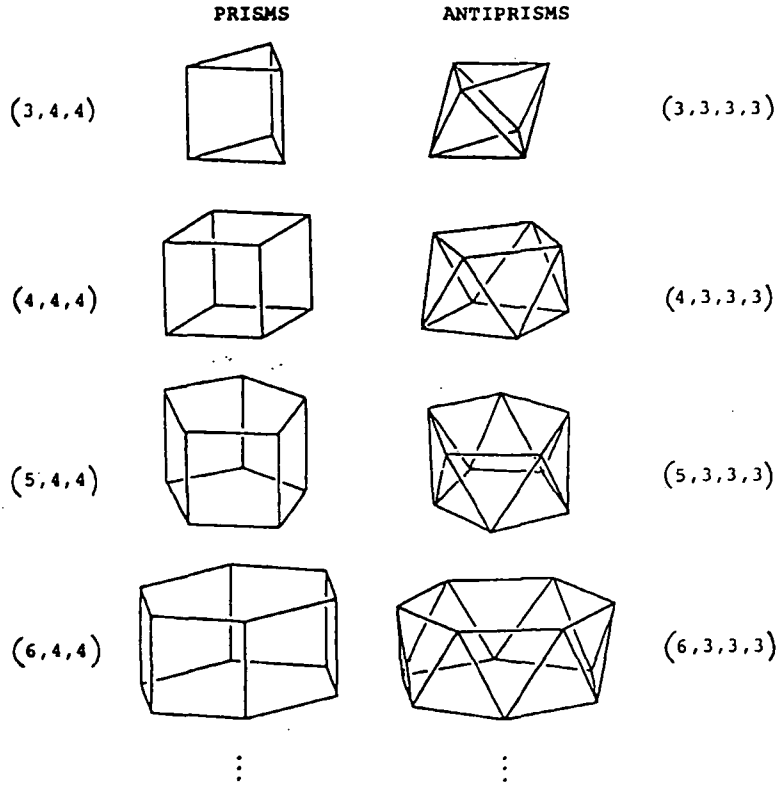

Fig. 10. The complete set of those Archimedean solids, which were not involved in the periodic table, because they have distinguished rotational axis (except (3,3,3,3) and (4,4,4), which are regular solids).

FORMULATION OF TRUNCATION AS CELLULAR AUTOMATIC OPERATION

The members of the complete set of regular and semiregular cellular arrangements on sphere (*Fig. 11*) were considered as stages of tranformational sequences, where the transformation was generated by an operation: the truncation (BÉRCZI 1980.). This truncation changes the cellular surface of a Platonic or Archimedean solid (or spherical mosaic) but does not change the symmetry group of the solid. The concept of truncation has a visually imaginable meaning for solids: the pyramids at vertices of regular solids are cut leaving a face on the place of the vertex: the base of pyramid. The cutting plane is perpendicular to the radius vector coming from the center of the regular solid to the vertex. Advanced truncation cuts truncated pyramids. In the spherical case truncation means: blowing up of initial vertex "points" of a regular spherical tessellation. In both variants of coordinate

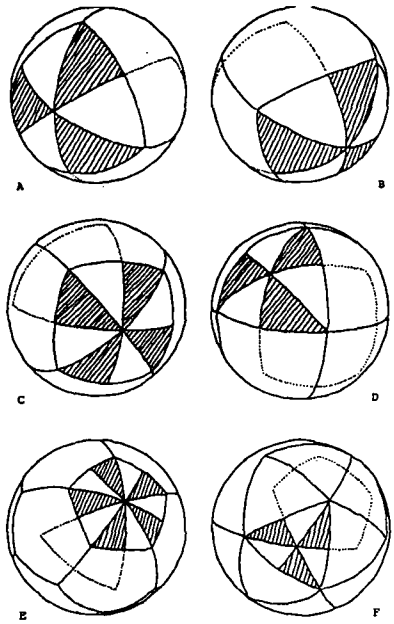

Fig. 11. Faces of dual regular solids are different regular-face-forming blocks of fundamental regions in the spherical tessellation of fundamental regions of tetrahedral- (A,B,), octahedral-(C,D,), and icosahedral- (E,F,) groups. A third kind of block-forming should result in rombohedral faces: these solids are also missing from the periodic table.

systems (solid-representation or spherical representation) three different stages with equal edge-lengths for all faces appear, when trucation started from a regular solid and advanced till the reaching of the dual solid of the initial one. The two closing regular (Platonic) solids in the truncational sequence flanks three Archimedean solids as stages of truncation operation. It is shown for the case of cube-octahedron sequence in *Fig. 12 and 13.*

The definition of the indirect von Neumann problem (implicit formulation: BÉRCZI 1980, 1985, explicit formulation: BÉRCZI 1991.) allows an easy formulation of the truncational transformations (*Fig. 14*). Let us consider the simple truncational sequences as global transitional functions with 5 stages (steps) for solids. *(Fig. 15)* Then the local transitional functions are the blowing up sequences for vertices (or complementary equivalents: the truncational sequences of initial faces or polygons (or cells)). These formulations — the global and local transitional functions — were given parallel for the higher dimensional case of the transformations for spatial cube-tessellation (BÉRCZI 1980.). This was the first implicit formulation of the Platonic-Archimedean Spherical Cellular Automata (PASCA). *(Fig. 16)*

EXTENSIONS OF PASCA: THE PERIODIC TABLE AND HIGHER DIMENSIONAL DEVELOPMENTS

Fitting together the corresponding PASCA sequences of the three 3D spherical symmetry groups (terahedral, octahedral, icosahedral) and also to planar and hyperbolic tessellations, a periodic table was given, as a summary of the deduction system built by truncation. (*Fig. 17*, BÉRCZI 1980) .This Periodic Table of Platonic

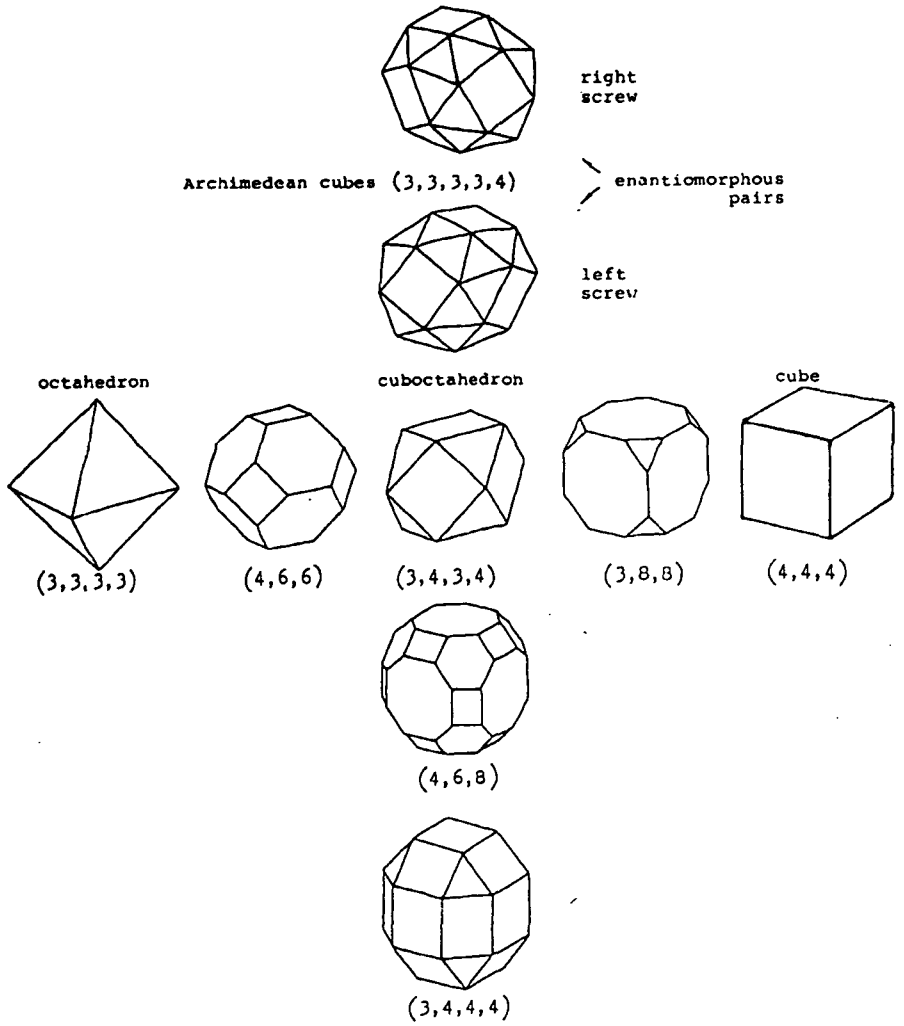

Fig. 12. Truncations in the octahedron-cube (hexahedron) system. The two Platonic solids close the simple truncation sequence. Halfway between them, the cuboctahedron is the generator of the complex truncation sequence (below (3,4,3,4)), and the snub-truncated enantiomorphous pairs (above (3,4,3,4)). The simple truncation sequence is considered to be the global transitional function in *Fig. 14.*

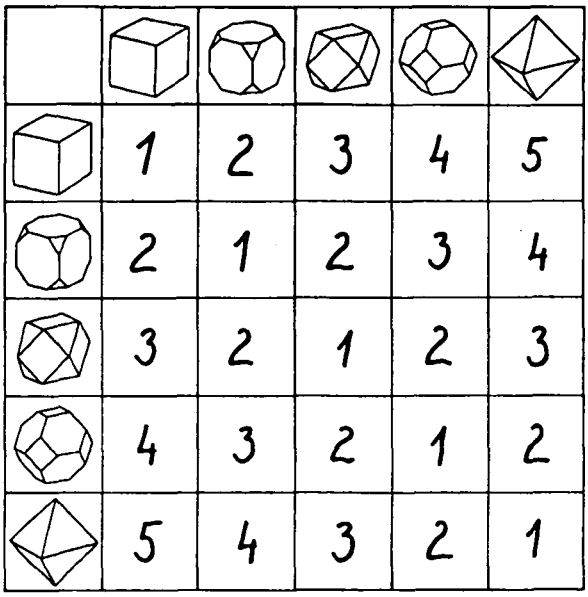

Fig. 13. Truncational distance matrix of the cube-octahedron sequence. Numbers mean the number of steps between the solids of a column and a row. Identical step is 1, without further truncation.

and Archimedean Solids and Tessellations shows the price payed for the ordered arrangement of solids given in *Fig. 9.* Some of the structures occurs more than once. But, on the other hand, the functional aspect of the relations between solids arises the source of simplicity: it is both in symmetry of initial conditions (Sphere, symmetric mosaic), and in formulation of the operation. Indirect von Neumann problems can be formulated and solved for the first cases when symmetry reduces the number of states of cells to small numbers. (*Fig. 18*)

SUMMARY

A classical problem of the functional arranging of regular and semi-regular (Platonic and Archimedean) solids (and tessellations) was solved and tabularly formulated by a cellular automatic operation using up the framework of the indirect von Neumann problem. (*Fig. 19*) The cellular transformation were double-terminated by regular dual-solids; therefore these arrangements of cells seemed more like a wave-motion of a global state of the spherical surface between opposite wave-formations. But the method and the approach to the problem may be useful, when more complex cellular states and arrangement are to be discerned and described.

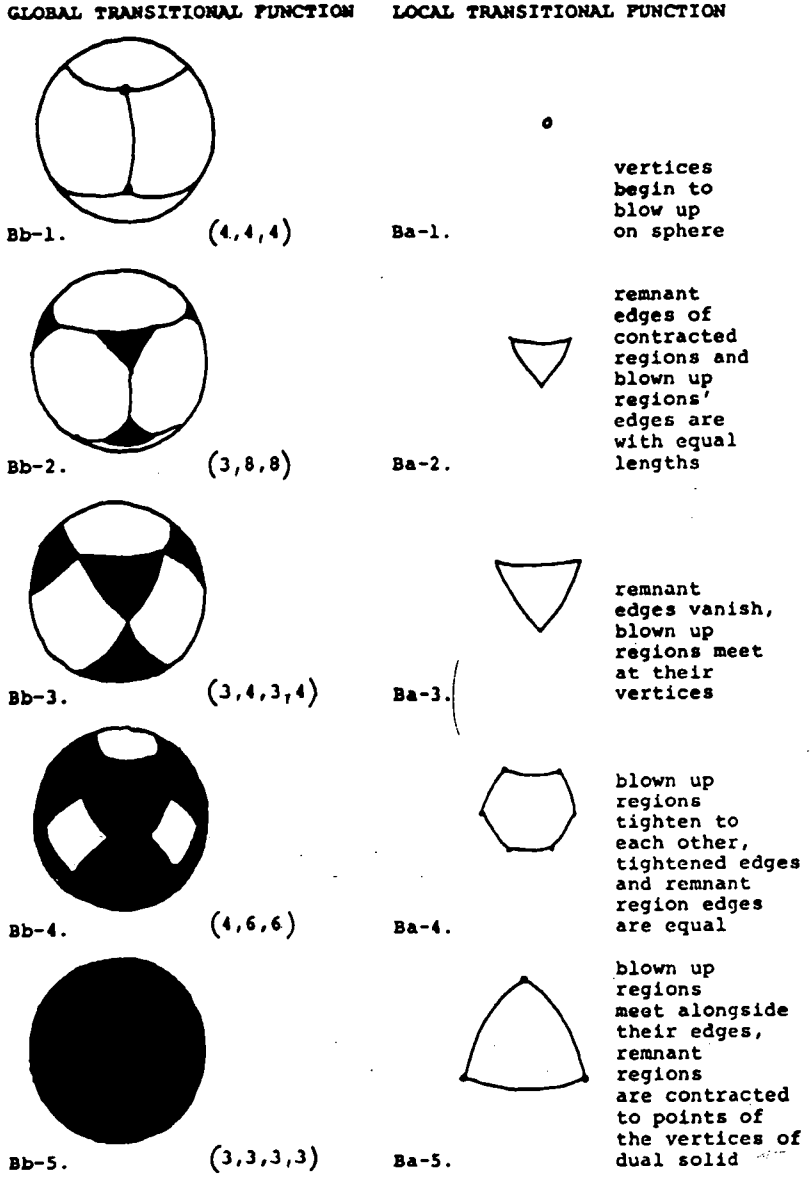

Fig. 14. The global (left column) and the local (right column) transitional function in the cellular automatic formulation of the truncational transformation between duals of regular solids.

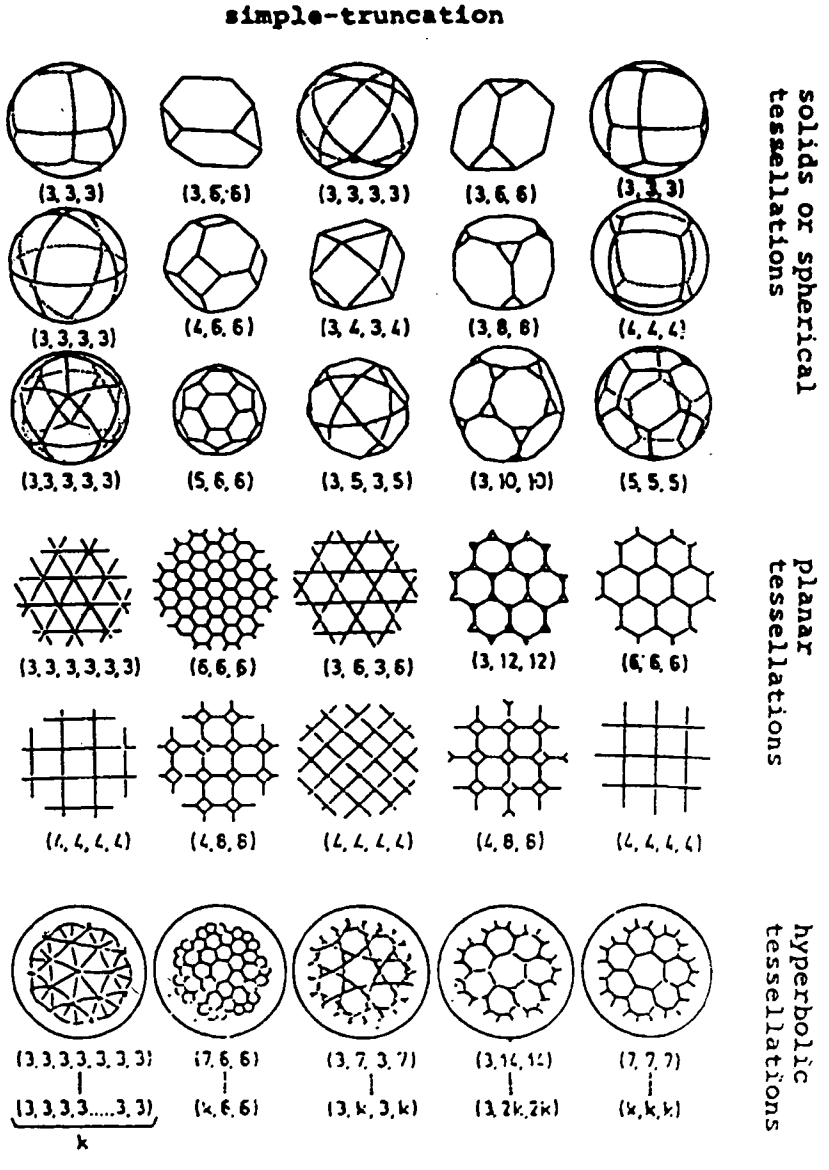

Fig. 15. One direction of extension of the ordering benefits for simplicity and comprehensive role of cellular automatic representation of the simple truncation sequence is to all regular solids (or spherical tessellations) and planar and hyperbolic tessellations. (BÉRCZI 1979.) The other direction of extension of the principle is to higher dimensional cases of regular solids and tessellations. *Fig. 14.* and *Fig. 16.* show, that the local transitional function in D dimension is the global transitional function in D-1 dimensions. Both extensions shown here prove that truncation operation in such a cellular automatic formulation is a comprehensive principle in deduction of regular solids and tessellations in any dimensions.

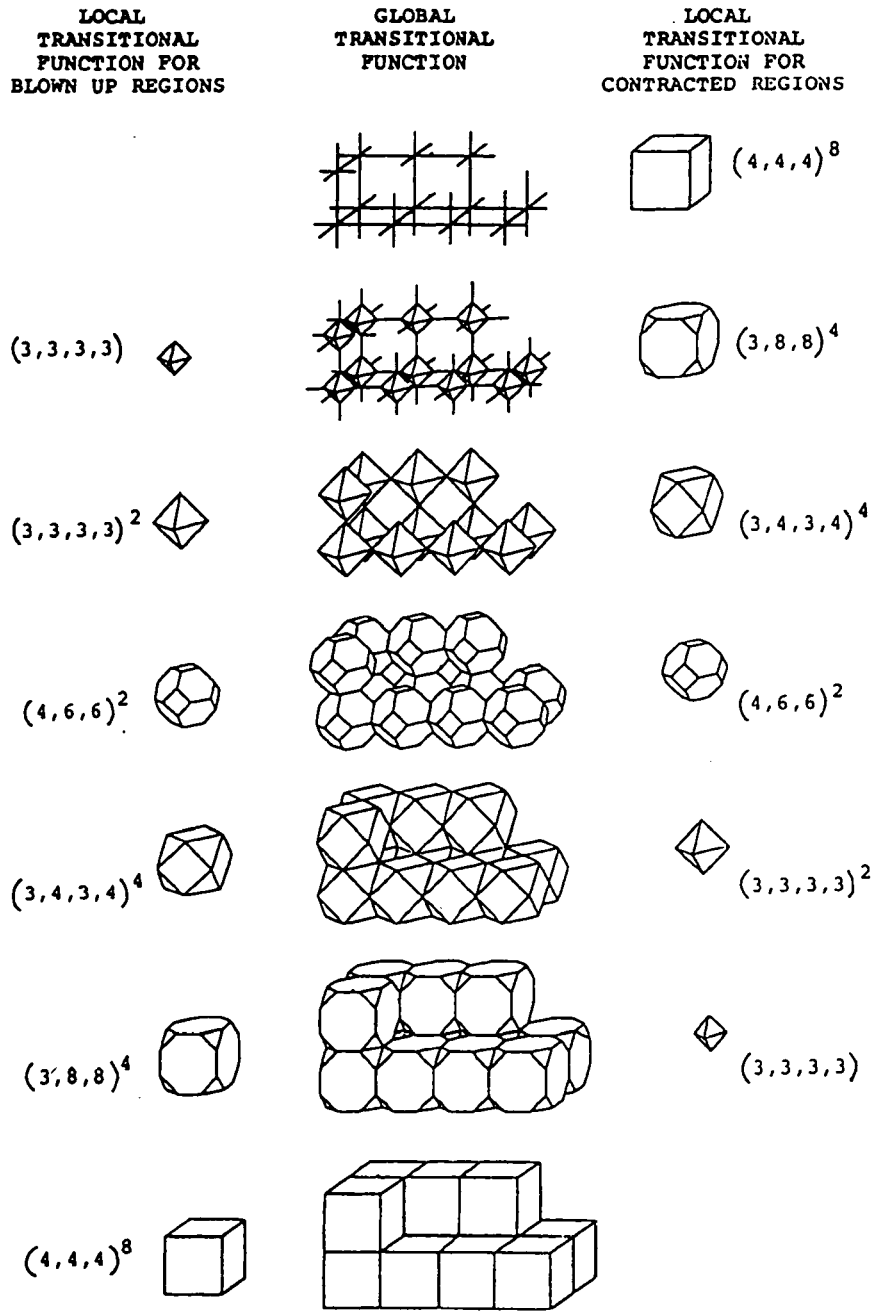

Fig. 16. Simple truncational sequence of spatial tessellation $(4,4,4)^8$ in cellular automatic formulation (BÉRCZI 1979, 1980).

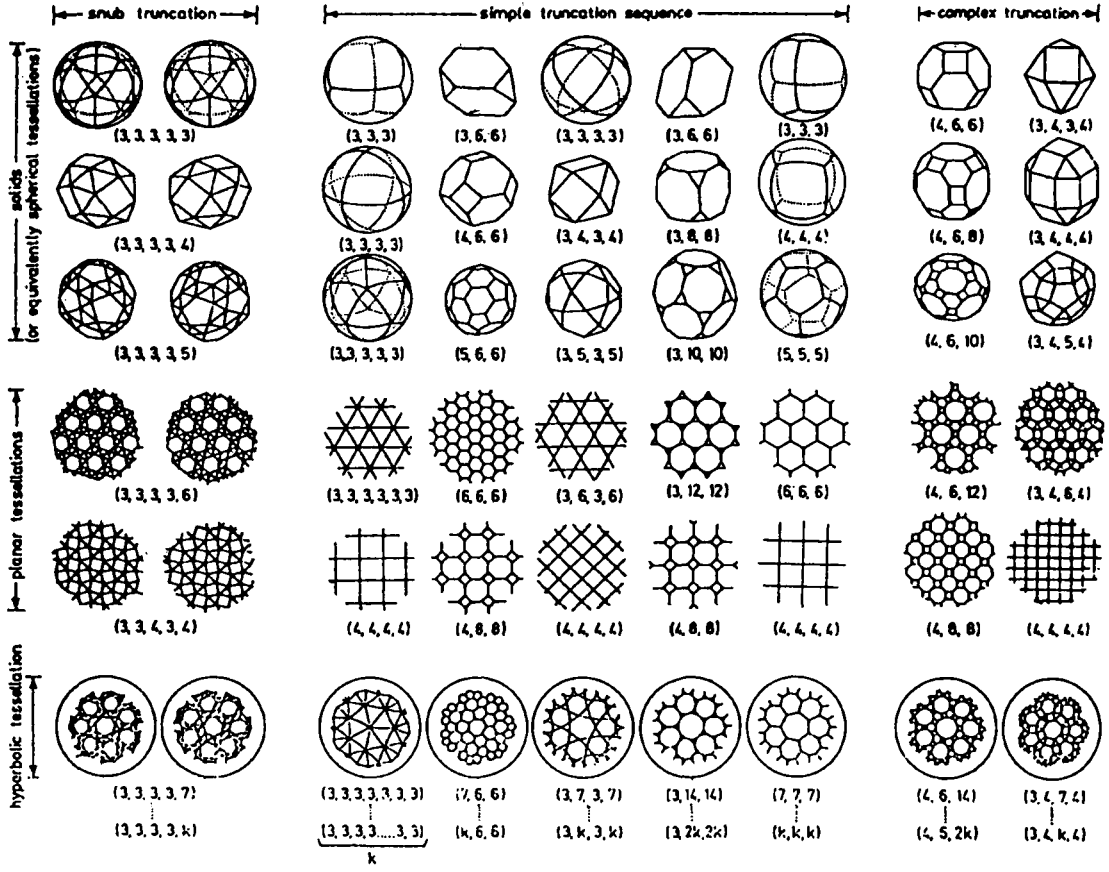

Fig. 17. The periodic table of Platonic and Archimedean solids and tessellations, or the spherical-, planar-, and hyperbolic tessellations. Regular solids are represented by their spherical tessellations for the sake of emphasis: they are the generators for semi-regular ones. (BÉRCZI 1979, 1980)

Two simple cellular automata mosaic systems with global symmetry	Type of operation	Number of cell-types / i.e. that of the local transitional functions/	Number of different "steps" /i.e. the state-ABC of local trans.func./	Type of the global symmetry of the surface
/Bérczi, 1985./ FIBONACCI	one unit sliding of cells	1	2	cylindrical
/this paper/ PLATONIC-ARCHIMEDEAN	blowing up or shrinking of cells	2	1	spherical

Fig. 18. Comparison of the characteristical features of the two cellular mosaic automata system models worked out in the form of indirect von Neumann problem by the author. Global symmetry not only reflects the global boundary condition and the form of the surface but means the form of feedback-directions by the local transitional function.

REFERENCES

BÉRCZI SZ. (1979): A platoni és archimédeszi testek és mozaikok periódusos rendszere. Középiskolai Matematikai Lapok. **1979/10**. 193—199.

BÉRCZI SZ. (1980): The Periodic System of Platonic and Archimedean Solids and Tessellations. Acta Geologica Acad. Sci. Hung. **23**, /1-4/, 184—200.

BÉRCZI SZ. (1985): Symmetries in the Plant Surface Lattice Systems: Development of Fibonacci Numbered Structure in a Cellular Automaton Model. (Lect. in Conf. on Intuitive Geometry, Balatonszéplak, 1985.)

BÉRCZI SZ. (1991): Platonic-Archimedean Cellular Automata. (In: Symmetry and Topology in Evolution. B. LUKÁCS, SZ. BÉRCZI, I. MOLNÁR, GY. PAÁL, Eds. 111—116. MTA-KFKI-1991-32/C. Budapest.

VOLLMAR R. (1982): Sejtautomata algoritmusok. Műszaki K. Budapest.

Manuscript received, 31 August, 1992

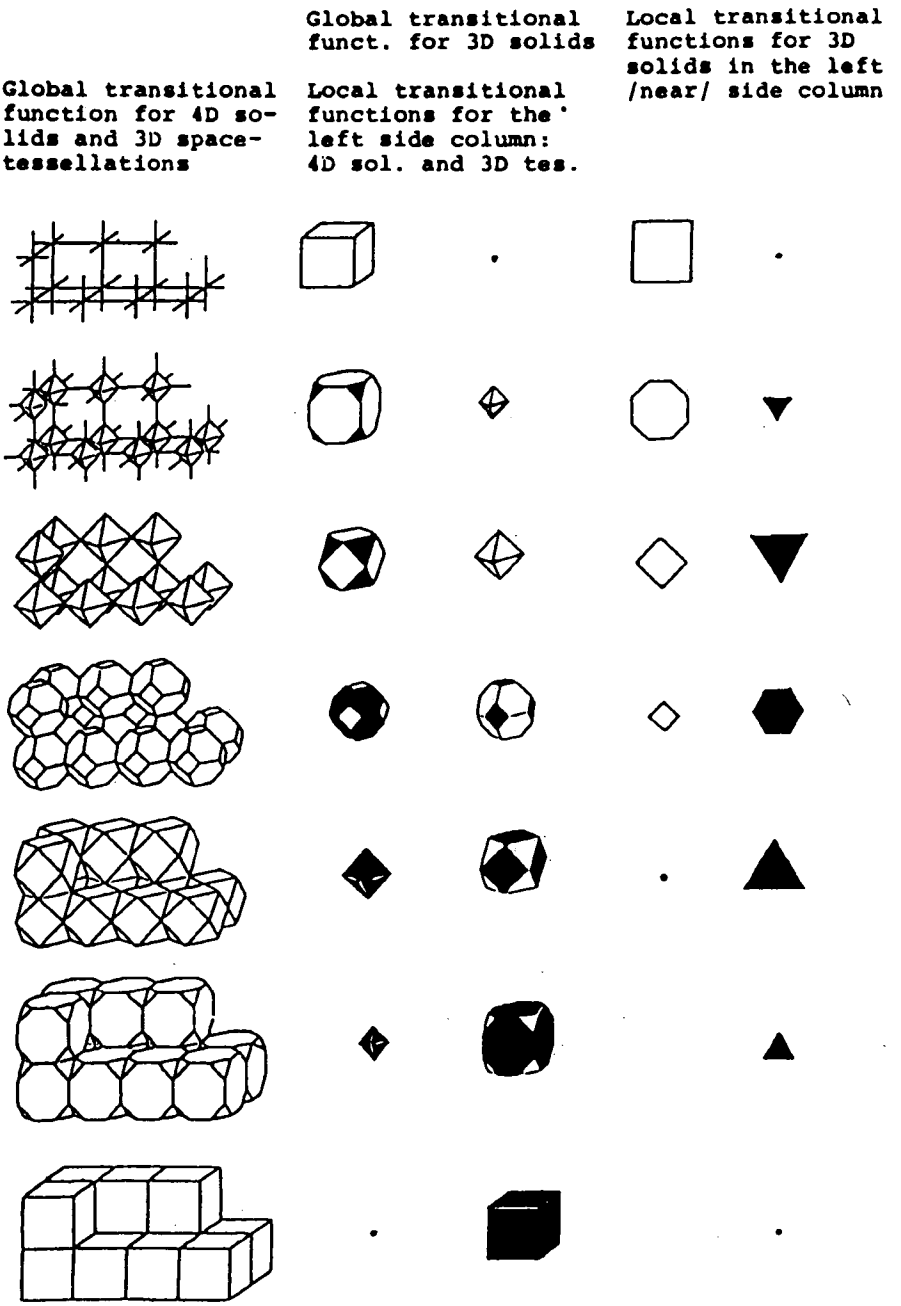

Fig. 19. Depending on the dimensions of the space where the problem is composed the truncation sequences may serve both as local and as global transitional functions, as shown here for three layers of construction.